Transient Analysis of Hydride Fueled Pressurized Water Reactor Cores

by

Jarrod Michael Trant

B.S Mechanical Engineering
U.S. NAVAL ACADEMY, 2002

SUBMITTED TO THE DEPARTMENT OF NUCLEAR ENGINEERING IN PARTIAL FULLFILLMENT OF THE REQUIREMENTS FOR THE DEGREE OF

MASTER OF SCIENCE IN NUCLEAR ENGINEERING
AT THE
MASSACHUSETTS INSTITUTE OF TECHNOLOGY

SEPTEMBER 2004

Signature of Author:_____
Department of Nuclear Engineering
August 25, 2004

Certified By:_____
Neil E. Todreas
KEPCO Professor of Nuclear Engineering, Professor of Mechanical Engineering
Thesis Supervisor

Read By:_____
Pavel Hejzlar
Principal Research Scientist
Thesis Reader

Accepted By:_____
Jeffrey A. Coderre
Chairman, Department Committee on Graduate Students

Transient Analysis of Hydride Fueled Pressurized Water Reactor Cores

by

Jarrod Michael Trant

Submitted to the Department of Nuclear Engineering
on August 25, 2004 in partial fullfillment of the
requirements for the Degree of Master of Science in
Nuclear Engineering

ABSTRACT

This thesis contributes to the hydride nuclear fuel project led by U. C. Berkeley for which MIT is to perform the thermal hydraulic and economic analyses. A parametric study has been performed to determine the optimum combination of lattice pitch, rod diameter, and channel shape—further referred to as geometry—for maximizing power given specific transient conditions for pressurized water reactors (PWR) loaded with either UO_2 or $UZrH_{1.6}$ fuel. Several geometries have been examined with the VIPRE subchannel analysis tool along with MATLAB scripts previously developed to automate VIPRE execution. The transients investigated were a large break loss of coolant accident (LBLOCA), an overpower transient, and a complete loss of flow accident. The maximum achievable power for each geometry is defined as the highest power that can be sustained without exceeding any of the steady state or transient limits. The limits were chosen based on technical feasibility and safety of the reference core and compared with the final safety analysis report (FSAR) of the reference core, the South Texas Project Electric Generating Station (STPEGS), whenever possible. This analysis was performed for two separate pressure drop limits of 29 and 60 psia for both a square array with grid spacers and a hexagonal array with wire wraps.

The square core geometry sustaining the highest power (4820.0 MW) for both the hydride and oxide fueled has a pitch of 9.0 mm and a rod diameter of 6.5 mm and was limited by the complete loss of flow accident. Both of these maximum power geometries occurred at the 60 psia pressure drop case. The maximum power of the 29 psia pressure drop case (4103.9 MW) for both fuel types occurred at a pitch of 9.7 mm and a rod diameter of 6.5 mm. The maximum power for the hexagonal arrayed cores occurred at the same hydrogen to heavy metal ratio as the square cores. The hydride fueled core power (5123.2 MW) was limited by the overpower transient while the oxide fueled core power (4996.1 MW) was limited by the overpower transient. The pressure drop constraint was not limiting for either fuel type for either pressure drop case for the wire wrapped cores.

Thesis Supervisor: Neil E. Todreas
Title: KEPCO Professor of Nuclear Engineering, Professor of Mechanical Engineering

ACKNOWLEDGEMENTS

The author would like to thank Professor Todreas, Dr. Hejzlar, and Professor Greenspan of U. C. Berkeley for their guidance and patience. It was my honor to work with Carter Shuffler, Jon Malen, Stu Blair, and Jacapo Sacheri who made valuable contributions to this work.

TABLE OF CONTENTS

LIST OF FIGURES

LIST OF TABLES

1 INTRODUCTION

1.1 MOTIVATION TO INVESTIGATE HYDRIDE FUELS FOR LIGHT WATER REACTORS

The addition of solid hydride atoms into the fuel matrix will allow for the optimal neutron spectrum while using relatively small volume fraction of water. This is due to the fact that the concentration of hydrogen atoms in the fuel is comparable to that in liquid water in an LWR core. This will result in the volume of water being dependant only on cooling needs. Thus a current core could be retrofitted to allow a higher total power than current LWR cores or new cores could be built with smaller volumes with the same core power. Along with these advantages thorium fuel matrices allow for an even higher heavy metal loading. This combined with the higher fuel-to-water volume ratio of the hydride cores will allow new and retrofitted cores to be designed to have a significantly higher energy generation per core loading and significantly longer core life than the corresponding oxide fueled cores. The final outcome of using hydride fuels versus oxide fuels is expected to be improved resource utilization, reduced waste, improved economics, improved proliferation resistance and improved safety.

The potential list of LWR improvements due to using solid hydrides as one of the core constituents are as follows [1]:

- Increasing the core life, discharge burnup, total energy generated per fuel load and the capacity factor of LWR's. Expected outcomes are reduction of the fuel cycle cost and cost of electricity (COE) along with increased fuel utilization, reduction in the amount and toxicity of high-level waste, and improved proliferation resistance.
- Reducing the volume of the core and pressure vessel for a given power LWR's, or increasing the power level of a given volume core, thus reducing the COE.
- Increasing the capability of LWR's to recycle commercial plutonium and to dispose of military plutonium.

- Increasing the capability of LWR's to utilize thorium.
- Improving the safety of LWR's, due to the inherent negative temperature reactivity effect of hydride fuel and, in BWR's, also due to reduction of the negative void reactivity coefficient.
- Reducing the heterogeneity of BWR cores and the negative void coefficient of these cores so as to simplify the fuel assembly design and the reactor control system, thereby improving the BWR economics.

1.2 PREVIOUS WORK

Previous aspects of this study determined the design variables for safe hydride cores that would lead to an optimized core given the advantageous characteristics of hydride fuel over oxide fuel, given nominal full power conditions [2]. The fuel type previously considered was U-$ZrH_{1.6}$.

1.3 GOALS OF THIS WORK

The overall hydride feasibility study will examine the thermal-hydraulics, fuel cycle, economics, safety, material, and reactor physics of both PWR and BWR designs. Provided this study produces favorable results, further materials research will be conducted as a follow-on project. This specific assessment will determine the design margins for specific transient operations of the optimized hydride and oxide fueled cores.

This assessment will be performed for a square array with grid spacers for both hydride and oxide fueled cores for two separate pressure drop limits. The maximum achievable power of these cores will be compared to the reference oxide fueled core power of 3800 MW_{th}. In addition to this the single highest power hydride fueled core will be compared to the single highest power oxide fueled core for:

- Minor Backfit: Minor backfit of existing LWRs seeks to limit the plant modifications required for conversion to hydride fuel use by maintaining the existing fuel assembly and control rod configurations within the pressure vessel

(i.e., maintaining the same pitch and rod number in the core). In this case, upgrades to the steam generators and high pressure turbine will be required to accommodate higher powers;

- Major Backfit: Major backfit of existing LWRs does not limit the design space. The layout of hydride fuel in the core can therefore assume any combination of lattice pitch, rod diameter, and channel shape, further referred to throughout this report as a design or geometry. Note that in addition to upgrades of components on the steam side of the plant, modifications to the reactor vessel head and core internals will also be necessary.

The transient analyses to be performed include a loss of coolant accident (LOCA), an overpower transient, and a loss of flow accident (LOFA). While both PWR and BWR cores are to be addressed in the hydride fuel study as a whole, this assessment will only address PWR's. In order to verify the data, the reference core transient results will be benchmarked against the known results of the reference core as shown in the South Texas Project Electric Generating Station (STPEGS) Final Safety Analysis Report (FSAR) [3] whenever possible.

Also included in this work is an analysis of wire wrapped hexagonal arrayed cores. The hexagonal wire wrapped cores will be investigated in the same manner as the square cores for steady state, LOCA, and overpower conditions.

2 NOMINAL FULL POWER METHODOLOGY

2.1 NOMINAL FULL POWER METHOD

The approach used by our Hydride Group, referred to as the nominal full power method, is a two-step process. The first step is a steady state parametric analysis. The second step is a transient analysis of specific core geometries of interest. Many equations, terms, and factors used in the analysis of a reactor core for both steady state and transient operations are proprietary in nature, such as MDNBR correlations. Others are specific to certain cores, such as transient behavior. In this study we analyze multiple core geometries based on the South Texas reference core. The nominal full power method uses the values obtained from the reference oxide core geometry and operating conditions as the limit when no other limits are available.

2.1.1 STEADY STATE ANALYSIS

The first step of the steady state analysis is to determine a range of viable core geometries for steady state operations. This parametric study was previously performed by J. Malen for steady state conditions [2]. Initially this approach adopted four criteria as the limiting steady state criteria, as shown in table 2.1

Table 2.1: Initial Steady State Core Limiting Conditions

Limiting Criteria	Value	Source
MDNBR	*2.17*	Steady State Reference Core
Core Pressure Drop	*28.9 / 60.0 psia*	Steady State Ref. Core / Pump Limitations
Hydride Fuel Centerline Temperature / Oxide Average Fuel Temperature	*1382 °F / 2552 °F*	Hydride Fission Gas Release / Oxide Fission Gas Release
Flow Velocity	*8 m/s*	Team Judgement [2]

Any core geometry that exceeded one of the limits was considered unacceptable and its power was reduced to within acceptable margins.

The reference core geometry and nominal full power operating conditions are shown in table 2.2.

Table 2.2: Reference Core Geometry and Operating Conditions

Parameter	Symbol	Value
OPERATING CONDITIONS		
Thermal Power	$\dot{Q}_{ref}$	*3800 MW_T*
Core Enthalpy Rise	Δh	*204 kJ/kg*
Peak to Average Power	$F_{q'}$	*1.65*
Inlet Temperature	T_{inlet}	561.2 F *[294 C]*
System Pressure	p	2250 psia *[15.5 MPa]*
GEOMETRY		
Pitch	P_{ref}	0.4959" *[12.6 mm]*
Diameter	D_{ref}	0.3742" *[9.5 mm]*
Pitch-to-Diameter Ratio	P/D	1.326
Number of Heated Rods	N_{ref}	50956
Cross Sectional Flow Area of Heated Channels	A_{core}	87.07 ft^2 *[8.089 m^2]*
Active Fuel Length	L_h	168" *[4.26 m]*
Assembly Length	L_{ass}	181.1" *[4.599 m]*
Grid Spacer Thickness	t_{grid}	0.0197" *[0.5mm]*

The previous power and burnup analysis [2] detailed a parametric study covering a wide range of rod diameters from 6.5 mm to 15 mm and pitch to diameter ratios (P/D) ranging from 1.07 to 1.54. As previously outlined the achievable power for each hydride and

oxide fueled core geometry was that which met each of the four constraints outlined in table 2.1. This provided the maximum achievable power for each core geometry at the reference operating conditions.

2.1.1.1 Further Steady State Work

Further steady state work performed by C. Shuffler [4] replaced the generic velocity limit by a series of more complex rod vibrations limits. Also, initial economic and core physics work showed that the upper range of rod diameters was unnecessary and the range of the study was adjusted to encompass a range of rod diameters from 6.5 mm to 12.5 mm. This new range of geometries and initial steady state constraints provide the initial conditions for the second phase of the nominal full power method, the transient analysis. The rod vibrations limits will be applied separately by C. Shuffler [4].

2.1.2 TRANSIENT ANALYSIS

The second step in the nominal full power method is a transient analysis. The transients to be considered for this study include a loss of coolant accident (LOCA), an overpower transient, and a loss of flow accident (LOFA). The LOCA and overpower transient will each yield the maximum achievable power for the given condition over the entire range of geometries. The maximum achievable power for each of these two transients as well as the initial steady state maximum power will be compared and the minimum power at each geometry will be obtained. These values are then also compared to the rod vibration limits [4] to yield the maximum achievable power for the complete steady state, LOCA, and overpower limits. This data will then be used by C. Shuffler to determine the most economical hydride and oxide cores.

The LOFA transient will then be applied to the most economic cores to verify that they meet the LOFA constraints. This limited assessment of core geometries for the LOFA is necessitated by the fact that there exists no method for determining the viability of specific core geometries without performing a complicated full core analysis. Any of the cores investigated that do not meet the LOFA constraints will be adjusted. These final cores will be the most economic cores based on all previously mentioned steady state and transient limits.

The nominal full power method will be performed for both hydride and oxide fuel for both the 29.0 and 60 psia pressure drop cases. The maximum achievable power of these cores will be compared to the reference oxide fueled core power of 3800 MW_{th} as well as comparing the single highest power hydride fueled core to the single highest power oxide fueled cores over the geometry range. In addition the two fuel types will be compared at each pressure drop case over the range of P/D ratios but at the reference oxide core pitch (12.98 mm) in order to cover a small scale backfit of existing core designs.

2.1.2.1 Loss of Coolant Accident

The first transient to be considered is the loss of coolant accident (LOCA). There are two types of LOCA events that could be considered. The large break LOCA (LBLOCA) is an ANS condition IV transient, while the small break LOCA is an ANS condition III transient. The large break LOCA, being more restrictive, will be considered here.

A full scale LOCA evaluation over the entire design range is impractical. However, using the methodology of Catton, et.al [5] will allow use of the clad temperature history of the reference core as the bounding criteria for the entire range of geometries.

2.1.2.2 Overpower Transient

The second transient to be considered is an overpower transient. There are two ANS Condition II overpower transients which are considered in the South Texas Project Electric Generating Station (STPEGS) Final Safety Analysis Report (FSAR).

The first event is concerned with a main steam line break at power. The second event is rod bank withdrawal at power and the limit challenged is the minimum departure from nucleate boiling ratio (MDNBR).

The main steam line break overpower transient is constrained by the plant's 22.45 kW/ft linear heat rate limit. The rod withdrawal transient is limited by the 18% limit. This 18% overpower limit equates to a 16.03 kW/ft linear heat rate. Therefore, when considering a generic overpower transient, the 16.03 kW/ft limit will be breached prior to the 22.45 kW/ft limit. Therefore, the rod withdrawal will be treated here to cover both overpower

transients over the entire geometry range. The limiting condition will be defined as the MDNBR of the reference core for this overpower transient.

2.1.2.3 Loss of Flow Accident

The third transient, the loss of flow accident, also consists of two categories, the complete loss of flow (CLOFA) and the partial loss of flow accident (PLOFA). The complete loss of flow is more limiting and will be considered here. The CLOFA is an ANS Condition III transient; however, in this paper as well as in the STPEGS FSAR the Condition II limits will be applied.

As with the LOCA, the CLOFA is a complicated transient which is highly dependant upon core geometry. Unlike the loss of coolant accident, there exists no method for determining the viability of specific core geometries without performing a complicated full core analysis.

As such, the LOFA will not be examined over the entire range of geometries. Instead the output from the steady state, overpower, and LOCA analysis will be used in an economic study performed by C. Shuffler to determine the most economical hydride cores. These specific cores will then be analyzed for the CLOFA. This will provide the most economical hydride and oxide cores for both pressure drop cases for the steady state, overpower, LOCA, and LOFA limits.

This complete nominal full power methodology is outlined in figure 2.1.

Figure 2.1: Complete Nominal Full Power Methodology Outline

1. Initial steady state maximum achievable power as determined by J. Malen [2]
2. Revised steady state maximum achievable power as determined by C. Shuffler [4]
    - Replaces the generic flow velocity limit with a more specific set of rod vibrations criteria
    - Adjusts the range of rod diameters due to initial physics and economic concerns
3. Perform overpower transient analysis
    - Determines the maximum achievable power considering an overpower transient
4. Perform LOCA anlaysis
    - Determines the maximum achievable power considering a LOCA
5. Specify the most economic cores, as determined by C. Shuffler [4]
    - Based on all previous work as well as physics limitations and other economic constraints
6. Perform LOFA analysis on specified economically desirable core geometries
7. Repeat previous steps for both oxide and hydride cores for both pressure drop cases
8. Make final comparison to determine the optimal hydride core geometry considering all outlined steady state, transient, and economic constraints

2.2 TRANSIENT METHODOLOGY

The first step in analyzing each transient involves applying the relevant transient to the reference core geometry. The overpower and LOFA transients use the MDNBR of the reference core under each condition as the limiting criteria. The LOCA uses the clad temperature history of the reference core as the limiting criterion.

Applying the LOFA and overpower transient to the reference core will provide the Safety Analysis Limit MDNBR ($MDNBR_{S.A.L., REF}$) as shown in figure 2.2. This Safety Analysis Limit MDNBR will be the minimum MDNBR for all cores for the specific transient before applying the "Margin for Transients".

Figure 2.2: Separated Components of Margin for MDNBR

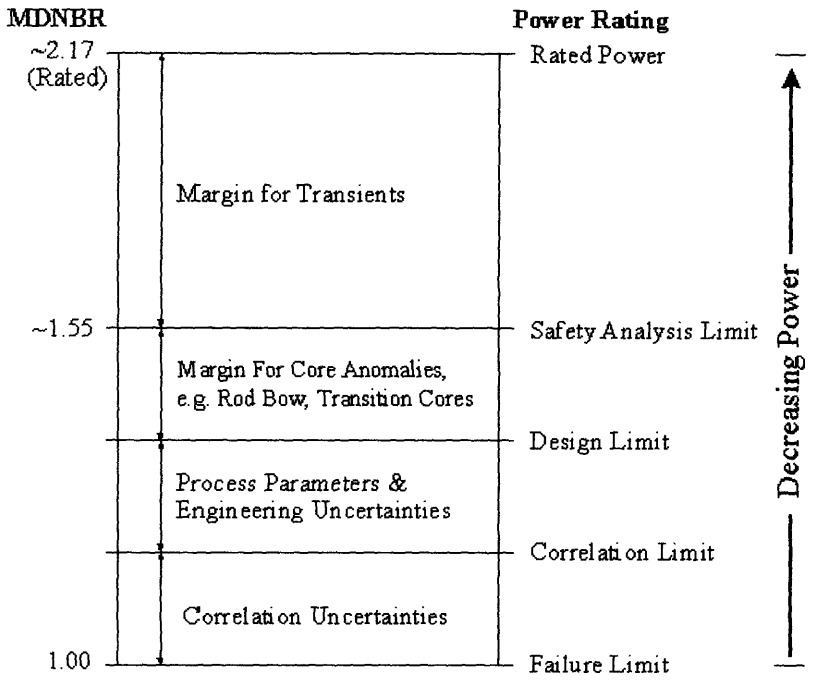

First, the overpower transient will be carried out in a similar manner as the steady state analysis. The maximum power will be determined over the entire geometry range such that the Safety Analysis Limit MDNBR ($MDNBR_{S.A.L}$) of each core does not go below that of the reference core as well as meeting the other steady state limits (flow velocity, pressure drop, and fuel centerline temperature).

The LOCA will then be applied to the reference core to determine the clad temperature over time of the reference core during a LOCA. The LOCA will then be applied to the results from the overpower analysis. Any core geometry whose clad temperature exceeds temperature of the reference core cladding at any time will have its power reduced until it no longer exceeds the reference clad temperature. This will determine the maximum power over the entire range of geometries for steady state, overpower, and LOCA conditions.

Lastly, the LOFA transient will be applied to the most desirable core geometries as determined by the previous analyses along with an economic analysis.

The power and flow history during the LOFA will be determined using RELAP and will be used as the input to VIPRE to determine the time step where the MDNBR is lowest.

Using the coast down values provided by RELAP the power and flow will be determined such that they meet they Safety Analysis Limit MDNBR of the reference core. This will then yield the Rated Power for this core geometry under LOFA conditions.

However, as the steady state power is decreased due to LOFA limitations, the mass flowrate will also be lowered, in order to maintain constant enthalpy rise across the core. The flow coastdown rate, however, is dependent up not only the core geometry but the initial mass flow rate as well. This is demonstrated in Appendix B. This makes it necessary to iterate between the flow coastdown value obtained from RELAP and the steady state power (and thus flow) obtained from VIPRE until the coastdown value and power yield the same flow that value within 1%.

This iteration provides a final maximum power and flow for each geometry such that they meet all the limits as previously proscribed in the steady state approach as well as the new $MDNBR_{S.A.L., REF}$ limit from the LOFA transient analysis.

This final Rated Power yields the maximum achievable power of the each core, considering both steady state, overpower, LOCA, and LOFA conditions.

2.3 Maximum Power Methodology Comparison

The purpose of this analysis is to compare two approaches for steady-state T-H analysis. The first approach is the nominal full power approach as used in our hydride fuel project [2]. The second is a quasi-transient approach as used by the Annular Fuel group at MIT [6].

The approach used by our Hydride Group adopts as the initial limiting steady state MDNBR the value resulting from the selected core (South Texas) at its nominal full power conditions, which corresponds to the Rated Power as previously shown in figure 2.2. The Annular Group uses a quasi-transient approach that determines an MDNBR value based on applying the margin for transients (18% overpower, 5% underflow and $2^{o}C$ higher than nominal coolant inlet temperature) to reference core conditions. This

MDNBR value is approximately 1.55. This assumed core condition corresponds approximately to the Safety Analysis Limit Power also shown in figure 2.2. The Annular Group then compares the MDNBR values of various core geometries under this quasi-transient condition to the Safety Analysis Limit MDNBR of their reference core. The quasi-transient method is an approximation providing an allowance for all transients and thus has a lower MDNBR limit than the nominal full power method.

The nominal full power method uses the actual power of the reference core to determine the Rated Power MDNBR, again referring to figure 2.2. The VIPRE code determined this MDNBR value to be approximately 2.17 for the South Texas core. This was confirmed through correspondence between Jon Malen and Mitch Nissley (an industry contact at Westinghouse). The nominal full power method then compares the MDNBR values of various core geometries under nominal full power conditions to the Rated Power MDNBR of the reference core.

All values of MDNBR for both the nominal full power method and the quasi-transient method are obtained by performance of a VIPRE thermal hydraulic analysis of the selected cores at their respective initial conditions.

It must be noted that both methods rely upon a future detailed transient analysis of specific cores. The quasi-transient method, however, provides for an initial assessment of transient results. The nominal full power method requires both an initial steady state analysis and a general transient assessment as outline in section 2.1.

2.3.1 COMPARISON METHODOLOGY

In order to compare the two methods numerically both the quasi-transient method and the nominal full power method were used to determine a Rated Power (figure 2.1) of each core.

First, the quasi-transient Safety Analysis Limit Power (figure 2.1) was determined by using the relevant inlet mass flux and temperature values as presented in table 2.1 in the VIPRE thermal hydraulic code and varying the core linear heat rate until the MDNBR constraint of 1.55 was reached as shown in columns (a) and (c). The 18% overpower, 5% underflow and 2°C higher inlet temperature conditions was then removed from the quasi-

transient input conditions to determine the Rated Power for the cores of columns (b) and (d). The resultant quasi-transient Rated Power MDNBR for these cores (columns (b) and (d)) is also shown in table 2.3 (The resulting power levels from this approach appear in table 2.5).

Table 2.3: Quasi-Transient Method Input Variables

	Hydride Core (Safety Analysis Power) **(a)**	Hydride Core (Rated Power) **(b)**	Annular Core (Safety Analysis Power) **(c)**	Annular Core (Rated Power) **(d)**
G_{in} (Mlbm/hr-ft^2) *[Mg/s]*	2.450 *[15.52]*	2.579 *[16.34]*	2.47 *[14.97]*	2.597 *[15.761]*
T_{in} (^{o}F) *[^{o}C]*	564.8 *[296]*	561.2 *[294]*	562.46 *[294.7]*	558.86 *[292.7]*
MDNBR	1.55	*2.32*	1.55	2.26

Note: Hydride Core refers to the Hydride Group reference oxide core (South Texas). Annular Core refers to the Annular Group reference solid fuel core (Seabrook).

It must be mentioned that the MDNBR value for each core at the Rated Power as determined by the quasi-transient method (2.32 and 2.26) is higher than the limits discussed previously of 2.17 for each core. This is because these Rated Power MDNBR and power values were backed out of the Safety Analysis values with an MDNBR value of 1.55. This MDNBR is an approximate value only and cannot be more exact without more information from the industry. Thus the Rated Power MDNBR values may exceed the previously mentioned values, indicating that this Safety Limit MDNBR is most likely conservative.

Next the Rated Power of each core was determined using the nominal full power method. The input values for the nominal full power method are the reference values for each core (South Texas and Seabrook, respectively). It is important to note that no Safety Analysis Limit Power was determined for the nominal full power method. As outlined in section 3.1.2 of the projects power and burnup analysis [2] as well as previously in this work

these values will be determined later through a series of transient analyses. The input conditions for the nominal full power method for each core are presented in table 2.4. Since this study uses the reference core geometries and initial conditions, when the nominal full power method is applied to each core the MDNBR will be the Rated Power MDNBR as is shown. (The resulting power levels from this approach appear in table 2.6)

Table 2.4: Nominal Full Power Method Input Variables

	Hydride Core (Safety Analysis Power) **(a)**	Hydride Core (Rated Power) **(b)**	Annular Core (Safety Analysis Power) **(c)**	Annular Core (Rated Power) **(d)**
G_{in} (Mlbm/hr-ft^2) *[Mg/s]*	*	2.942 *[18.627]*	*	2.942 *[18.627]*
T_{in} (^{o}F) *[^{o}C]*	*	561.2 *[294]*	*	558.86 *[292.7]*
MDNBR	*	2.17	*	2.17

***To Be Determined through transient analyses**

Throughout the analysis a constant vessel outlet temperature for each core was maintained during normal operation. The Hydride Group reference vessel outlet temperature was held at 624.8 ^{o}F *[329.4 ^{o}C]*. This value has been confirmed through email contact with Hans Garkisch as the correct vessel outlet (before uprating) at the design and operating conditions used for this reference case. The Annular Group reference vessel outlet temperature was held at 619.0 ^{o}F *[326.1 ^{o}C]*, as confirmed by Pavel Hejzlar.

2.3.2 RESULTS

The Safety Analysis Limit Power and Rated Power determined for each core using the quasi-transient method are listed in table 2.5. Recall here that the quasi-transient method is applied using the Safety Analysis Limit MDNBR, which for this study had a value of 1.55. This provides the Safety Analysis Limit Power for each core as previously described, shown in columns (a) and (c) of table 2.5. The 18% overpower, 5% underflow and 2°C higher inlet temperature were then removed to determine the Rated Power for each core as determined by the quasi-transient method, as shown in columns (b) and (d).

Table 2.5: Quasi-Transient Method Power Results

	Hydride Core (Safety Analysis Power) **(a)**	Hydride Core (Rated Power) **(b)**	Annular Core (Safety Analysis Power) **(c)**	Annular Core (Rated Power) **(d)**
Power (kW/ft-rod) *[MW]*	5.435 *[3933.6]*	4.606 *[3333.6]*	6.215 *[3800]*	5.266 *[3220]*

It must be emphasized again that the exact value for the Safety Analysis Limit MDNBR is not known. The value of 1.55 is an approximate value only and cannot be more exact without more information from the industry. Also, this quasi-transient method is not exact itself, but is an indicator of whether or not the core will be in a safe condition during transient operations. A more exact answer would require an in-depth transient analysis using such codes as RELAP and VIPRE.

The Rated Power determined for each core using the nominal full power method is listed in table 2.6.

Table 2.6: Nominal Full Power Method Power Results

	Hydride Core (Safety Analysis Power)	Hydride Core (Rated Power)	Annular Core (Safety Analysis Power)	Annular Core (Rated Power)
Power (kW/ft-rod) *[MW]*	*	5.327 *[3800.0]*	*	5.574 *[3411.0]*

***To Be Determined through transient analyses**

The Rated Power of the Hydride Group reference core and the Annular Group reference core as determined separately by each method and the percent power difference between each method is compared in table 2.7.

Table 2.7: Rated Power Comparison

	Hydride Core (Nom. Full Power)	Hydride Core (Quasi-Trans)	Annular Core (Nom. Full Power)	Annular Core (Quasi-Trans)
Power (kW/ft-rod) *[MW]*	5.327 *[3800.0]*	4.606 *[3333.6]*	5.574 *[3411.0]*	5.266 *[3220.0]*
Percent Difference	12.3%		5.6%	

2.3.3 DISCUSSION OF RESULTS

The difference between the Rated Power for the Hydride Group core as determined by the nominal full power method and the quasi-transient method is 12.3%. The difference between the Rated Power for the Annular Group core as determined by the nominal full power method and the quasi-transient method is 5.6%.

This shows that the difference in Rated Power between the two methods is approximately 6-12 %. This is an acceptable margin considering that the actual Safety Analysis Limit MDNBR of 1.55 is only an approximation. The values of the power as obtained by the

nominal full power method are known to be correct in this case because the actual full power values of the selected plant cores were used. However, changing the Safety Analysis Limit MDNBR would affect both the Rated Power and the Safety Analysis Limit Power as obtained from quasi-transient method. Thus a more exact value would give less of a margin between the two methods, as it would correspond to the actual Safety Analysis limit used in the actual core, just as the nominal full power method uses the Rated Power of the actual core. Also, the nominal full power method requires future input of more exact transient information.

2.3.4 FURTHER COMPARISON

In order to further verify these results over the range of geometries of interest for the Hydride Project, two additional Hydride Core geometries were compared using the previously detailed methodology. One is a relatively loose geometry of P/D = 1.52 and the other is a tight geometry of P/D = 1.13. Both of these geometries are based on a 60 psia pressure drop limited core design as detailed in reference [2]. The relevant inlet mass flux, temperature, and MDNBR values are presented in table 2.8, along with the rod diameter of each core. The Safety Analysis Power values after matching the MDNBR of 1.55 are again shown in columns (a) and (c). The resultant quasi-transient Rated Power MDNBR for these hydride core geometries (columns (b) and (d)) is also shown in table 2.8. (The resulting power levels from this approach appear in table 2.10.)

Table 2.8: Quasi-Transient Method Input Variables, Variable Geometry

	P/D = 1.52 (Safety Analysis Power) **(a)**	P/D = 1.52 (Rated Power) **(b)**	P/D = 1.13 (Safety Analysis Power) **(c)**	P/D = 1.13 (Rated Power) **(d)**
G_{in} (Mlbm/hr-ft^2) *[Mg/s]*	1.414 *[11.161]*	1.3437 *[10.603]*	3.550 *[16.524]*	3.3723 *[15.698]*
T_{in} (^{o}F) *[^{o}C]*	564.8 *[296]*	561.2 *[294]*	564.8 *[296]*	561.2 *[294]*
Diameter (inches) *[mm]*	0.3264 *[8.290]*	0.3264 *[8.290]*	0.5377 *[13.658]*	0.5377 *[13.658]*
MDNBR	1.55	*2.21*	1.55	*2.58*

The input conditions for the nominal full power method for each core geometry are presented in table 2.9. These values are as determined in reference [2]. (The resulting power levels from this approach appear in table 2.11.)

Table 2.9: Nominal Full Power Method Input Variables, Variable Geometry

	P/D = 1.52 (Safety Analysis Power) **(a)**	P/D = 1.52 (Rated Power) **(b)**	P/D = 1.13 (Safety Analysis Power) **(c)**	P/D = 1.13 (Rated Power) **(d)**
G_{in} (Mlbm/hr-ft^2) *[Mg/s]*	*	1.4587 *[10.935]*	*	3.7872 *[16.749]*
T_{in} (^{o}F) *[^{o}C]*	*	561.2 *[294]*	*	561.2 *[294]*
MDNBR	*	*2.17*	*	*2.51*

***To Be Determined through transient analyses**

2.3.4.1 Results

The Safety Analysis Limit Power and Rated Power determined for each core geometry using the quasi-transient method are listed in table 2.10. Recall here that the quasi-transient method is applied using the Safety Analysis Limit MDNBR, which for this study had a value of 1.55. This provides the Safety Analysis Limit Power for each core as previously described, shown in columns (a) and (c) of table 2.8. The 18% overpower, 5% underflow and 2°C higher inlet temperature were then removed to determine the Rated Power for each core as determined by the quasi-transient method, as shown in columns (b) and (d).

Table 2.10: Quasi-Transient Method Power Results, Variable Geometry

	P/D = 1.52 (Safety Analysis Power) **(a)**	P/D = 1.52 (Rated Power) **(b)**	P/D = 1.13 (Safety Analysis Power) **(c)**	P/D = 1.13 (Rated Power) **(d)**
Power (kW/ft-rod) *[MW]*	3.5263 *[2552.3]*	2.988 *[2163.0]*	8.343 *[3778.9]*	7.070 *[3202.4]*

The Rated Power determined for each core geometry using the nominal full power method is listed in table 2.11.

Table 2.11: Nominal Full Power Method Power Results, Variable Geometry

	P/D = 1.52 (Safety Analysis Power) **(a)**	P/D = 1.52 (Rated Power) **(b)**	P/D = 1.13 (Safety Analysis Power) **(c)**	P/D = 1.13 (Rated Power) **(d)**
Power (kW/ft-rod) *[MW]*	*	3.0821 *[2330.8]*	*	7.5437 *[3416.7]*

***To Be Determined through transient analyses**

The Rated Power of each of the two core geometries as determined separately by each method and the percent power difference between each method is compared in table 2.12.

Table 2.12: Rated Power Comparison, Variable Geometry

	P/D = 1.52 (Nom. Full Power)	P/D = 1.52 (Quasi-Trans)	P/D = 1.13 (Nom. Full Power)	P/D = 1.13 (Quasi-Trans)
Power (kW/ft-rod) *[MW]*	3.0821 *[2330.8]*	2.988 *[2163.0]*	7.5437 *[3416.7]*	7.070 *[3202.4]*
Percent Difference	7.2%		6.3%	

2.3.4.2 Discussion of Results

The difference between the Rated Power for the wide core (P/D = 1.52) as determined by the nominal full power method and the quasi-transient method is 7.2%. The difference between the Rated Power for the tight core (P/D = 1.13) as determined by the nominal full power method and the quasi-transient method is 6.3%.

This shows that the difference in Rated Power between the two methods is approximately 6-7 %. When compared to the difference range of 6-12% determined from the Hydride and Annular Group reference cores this shows that for extreme P/D ratios the difference is in the lower range of values. This is still an acceptable margin considering the previously discussed assumptions. Primarily that the most relevant of these assumptions being that the nominal full power method requires further transient analysis to be performed.

2.3.5 Final Maximum Power Methodology Comparison

The percent difference in the predicted maximum achievable power between our hydride groups' nominal full power method given initial steady state constraints and the annular groups quasi-transient method was approximately 6-12%. However, the nominal full power method also relies upon further transient work being performed.

Table 2.13 shows the same two hydride fueled square core geometries, one relatively loose and one relatively tight, that were previously investigated. The quasi-transient method rated power is the same as previously displayed. However, the nominal full power method now includes the final transient results presented in chapter 7.

Table 2.13: Final Maximum Power Methodology Comparison

	P/D = 1.52 (Nom. Full Power) (incl. Transients)	P/D = 1.52 (Quasi-Trans)	P/D = 1.13 (Nom. Full Power) (incl. Transients)	P/D = 1.13 (Quasi-Trans)
Power (kW/ft-rod) *[MW]*	3.119 *[2262.0]*	2.988 *[2163.0]*	6.756 *[3060.0]*	7.070 *[3202.4]*
Diameter (inches) *[mm]*	0.3264 *[8.290]*	0.3264 *[8.290]*	0.5377 *[13.658]*	0.5377 *[13.658]*
Percent Difference	4.4%		4.7%	

The initial percent difference was 7.2% and 6.3%, respectively. The maximum achievable power of both geometries was lowered due to the transient analyses for the nominal full power method. Previously, the nominal full power method predicted higher powers than the quasi-transient method for both cores. However, following the transient analyses, the nominal full power method predicts a lower power for the tighter core. The percent difference in predicted maximum power did decrease for both geometries to 4.4% and 4.7%, respectively.

This demonstrates that both methods will provide reasonably similar values for maximum achievable power.

3 LOSS OF COOLANT ACCIDENT

3.1 REGULATORY REQUIREMENTS

Federal regulations as described in 10CFR50.46 [7] outline two types of LOCA events. The large break LOCA (LBLOCA) is an ANS condition IV incident (limiting faults). The second is a small break LOCA and is an ANS condition III incident (infrequent faults). The large break LOCA, being more restrictive, will be considered here.

The limiting conditions in a LBLOCA as detailed in 10CFR50.46 are as follows:

1. The calculated peak fuel element clad temperature is below the requirement of 2,200°F.
2. The amount of fuel element cladding that reacts chemically with water or steam does not exceed 1 percent of the total amount of Zircaloy in the reactor.
3. The clad temperature transient is terminated at a time when the core geometry is still amenable to cooling. The localized cladding oxidation limits of 17 percent are not exceeded during or after quenching.
4. The core remains amenable to cooling during and after the break.
5. The core temperature is reduced and decay heat is removed for an extended period of time, as required by the long-lived radioactivity remaining in the core.

Evaluating each of these criteria is beyond the scope of this study; however, with some specific assumptions this transient can be analyzed. The LBLOCA will be analyzed based on the methodology of Catton, et.al [5]. This methodology calculates the peak clad temperature during the LOCA. According to the South Texas Project Electric Generating Station (STPEGS) Final Safety Analysis Report (FSAR) the 2200 °F temperature limit will cover both the first and second criteria. The third, fourth, and fifth criterion primarily concern reflooding the core following the accident and can be accommodated with an emergency core cooling system or some other system currently in use.

3.2 METHODOLOGY

The clad temperature over time was calculated for both hydride and oxide fuel for both pressure drop cases is based on equation (1).

$$T_{clad,final} - T_{clad,initial} = aq' - \left(T_{PCT,BD} - \overline{T_S}\right)\left(1 - \frac{1}{1.09 + 0.9 \cdot m \cdot \tau}\right) + \Delta T_r + \frac{K}{U_R^n}\left(T_r - \overline{T_s}\right) \quad \textbf{(3.1)}$$

$T_{clad,final} - T_{clad,initial}$ = heating from stored energy + blowdown cooling + decay heat refill heating + decay heat and reflood cooling

where $T_{clad,final}$, $T_{clad,initial}$, $T_{PCT,BD}$, $\overline{T_s}$, ΔT_r, and T_r are the final clad temperature, the intitial clad temperature, the peak clad temperature during the blowdown, the average coolant saturation temperature, the change in clad temperature during refill, and the clad temperature at the end of refill and the terms a and K are constants. The term U_R^n represents the core reflood rate and the terms m and τ are given as follows:

$$m = \left(\frac{\overline{h} \cdot A_{surf}}{(\rho \cdot c_p \cdot V)_{Fuel}}\right) \quad \textbf{(3.2)}$$

$$\tau = (t_{MCT,BD} - t_{PCT,BD}) \quad \textbf{(3.3)}$$

where $\overline{h}$, A_{surf}, ρ_f, $c_{p,f}$, V_f, $t_{MCT,BD}$, $t_{PCT,BD}$ are the average coolant heat transfer coefficient, surface area of the rod, density, specific heat, and volume of the fuel, time to the minimum clad temperature during the blowdown, and the time to the peak clad temperature during blowdown.

While it is possible through use of a comprehensive thermal hydraulics code, such as RELAP, to determine the refill and reflood time for each core geometry, this is not

practical for our scooping study of the entire four hundred point parametric range. However, using the temperature history of the clad for the reference oxide core as the bounding criterion for all core geometries ensures that none of the cores will exceed any of the regulatory limits. This reduces equation (3.1) to the following.

$$T_{clad,final} - T_{clad,initial} = aq' - \left(T_{PCT,BD} - \overline{T_S}\right)\left(1 - \frac{1}{1.09 + 0.9 \cdot m \cdot \tau}\right) + \Delta T_{DH} \qquad \textbf{(3.4)}$$

where ΔT_{DH} is the change in clad temperature due to decay heat over the given time range. This term is comprised of the last three terms in equation (3.1), excluding the cooling effects of the refill and reflood. The complete derivation of equation (3.4) is contained in Appendix C. This exclusion will cause the reference core clad temperature to exceed the 2200 °F temperature limit. However, use of equation (3.4) will yield a reference core clad temperature history as an upperbound limit against which both hydride and oxide fuel geometries will be compared.

The sequence of events for the LBLOCA is taken from the STPEGS FSAR [3] and is shown in table 3.1 and figure 3.1. The relevant conditions for the reference core for the LBLOCA from the STPEGS FSAR [3] and are shown in table 3.2, as well as the conditions for the hydride and oxide cores, for comparison.

Table 3.1: Reference Core Sequence of Events for a LBLOCA

SEQUENCE OF EVENTS	
Event	**Time**
Peak Clad Temperature During Blowdown	*4 seconds*
Minimum Clad Temperature During Blowdown	*14 seconds*
End of Blowdown	*24.9 seconds*
Bottom of Core Recovery	*32.7 seconds*

The sequence of events is relevant in that it gives a reference time scale over which to compare the temperature values.

Table 3.2: Reference Core Operating Conditions for a LBLOCA

Parameter	Symbol	Reference Oxide Core	Hydride Cores	Oxide Cores
OPERATING CONDITIONS				
Thermal Power	$\dot{Q}_{ref}$	*3853 MW_T*	*VARIES*	*VARIES*
Average Linear Heat Rate	$\overline{q'}$	*5.3 kW/ft*	*VARIES*	*VARIES*
Peak Linear Heat Rate	q'_{peak}	*13.523 kW/ft*	*VARIES*	*VARIES*
Axial Peaking Factor	F_{axial}	*1.65*	*1.65*	*1.65*
Total Peaking Factor (Axial and Radial)	F_{total}	*2.55*	*2.55*	*2.55*
THERMAL HYDRAULIC PARAMETERS				
Parameter	**Symbol**	**Reference Oxide Core**	**Hydride Cores**	**Oxide Cores**
Fuel Thermal Conductivity	k_{fuel}	*3.6 W/m-K*	*17.6 W/m-K*	*3.6 W/m-K*
Fuel Density	ρ_{fuel}	*1.04E+4 kg/m^3*	*8.26E+3 kg/m^3*	*1.04E+4 kg/m^3*
Fuel Specific Heat	$c_{p,fuel}$	*350 J/kg-K*	*497 J/kg-K*	*350 J/kg-K*
Volumetric Heat Capacity	$c_{p,fuel} * \rho_{fuel}$	*3.67E+6 $J/K\text{-}m^3$*	*4.10E+6 $J/K\text{-}m^3$*	*3.67E+6 $J/K\text{-}m^3$*
Gap Thermal Conductivity	k_{gap}	*0.31 W/m-K*	*35 W/m-K*	*35 W/m-K*
Clad Thermal Conductivity	k_{clad}	*13 W/m-K*	*13 W/m-K*	*13 W/m-K*

Figure 3.1 shows the limiting LBLOCA for STPEGS, from the FSAR.

Figure 3.1: South Texas FSAR Limiting Clad Temperature for LBLOCA

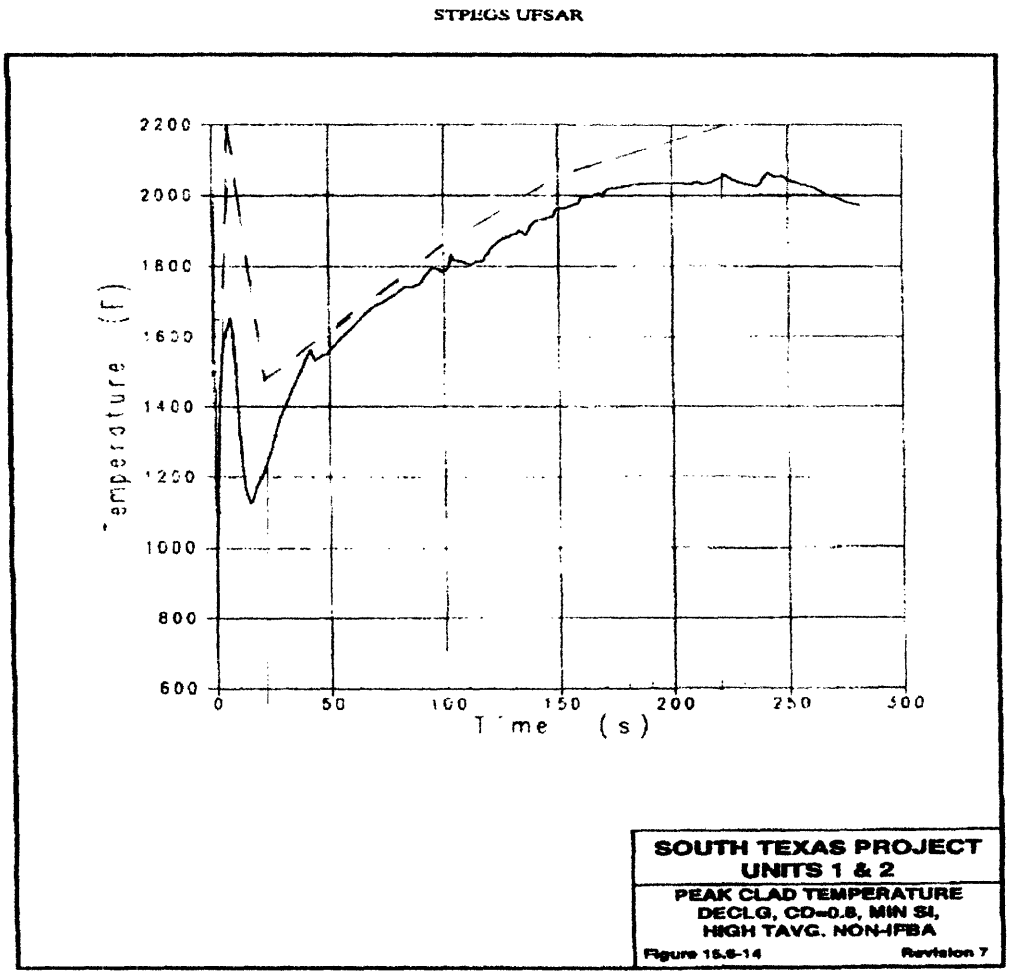

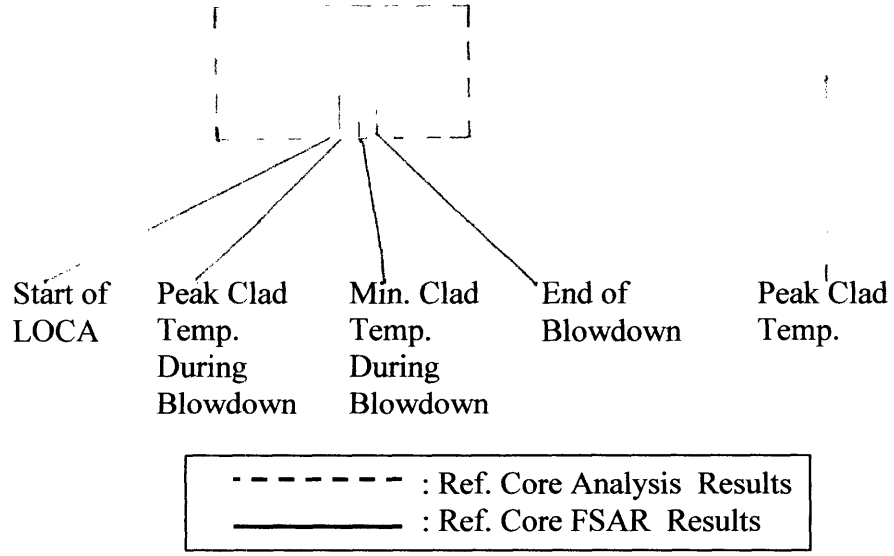

This shows the initial spike in clad temperature followed by a significant cooldown due to the blowdown. Then comes a sharp temperature increase due to decay heat following the end of the blowdown. This figure also shows that the peak clad temperature occurs approximately 220 seconds into the transient. The dashed line represents the reference core clad temperature history calculated with equation (3.4). The behavior of the calculated curve is similar to the FSAR curve, but higher in value. This demonstrates how the calculated value will be used as an upper bound.

3.2.1 TAU FACTOR SENSITIVITY

Referring again to equation (3.4), each of the terms is either known or can be calculated, with the exception of the time term, τ. As shown in equation (3.3) and figure 3.1, τ is the difference in time between the peak and minimum clad temperatures during blowdown. The peak clad temperature during blowdown is based on the fuel time constant, equation (3.5).

$$\tau_{fuel} = \frac{m_{fuel} \cdot c_{p,fuel}}{h_{cool} \cdot A_{surf}} \tag{3.5}$$

where m_{fuel}, h_{cool}, A_{surf} are the mass of the fuel, coolant heat transfer coefficient, and surface area of the fuel for heat transfer. At reference conditions and geometry the oxide and hydride fuel time constants are approximately 0.16 and 0.18 seconds, respectively. However, during the blowdown the coolant heat transfer coefficient is lower and the fuel time constants are higher, as shown in table 3.3.

Table 3.3: Reference Core Geometry Fuel Time Constants

Conditions	Reference Oxide Core	Reference Hydride Core
Steady State	*0.156 s*	*0.175 s*
LBLOCA	*6.67 s*	*7.5 s*

As shown in figure 3.1, the peak clad temperature during blowdown for the reference oxide core occurs at approximately 5 seconds.

The minimum temperature during blowdown occurs at approximately 15 seconds for the reference core so that tau for the reference core geometry is 10 seconds. The time to the minimum temperature during blowdown ($t_{MCT,BD}$) is based on two factors, the first being the time duration of the blowdown, and the second being the linear heat rate. The blowdown duration will remain fairly constant at around 25 seconds regardless of the core geometry, since it is limited by the critical velocity at the break location. A higher linear heat rate will cause a faster temperature increase due to decay heat, and thus reverse the clad temperature decrease curve faster as the blowdown cooling lessens.

Any value of tau that is greater than that of the reference oxide core will cause a lower clad temperature at the end of the blowdown. However, a smaller tau will increase the clad temperature. In order to determine the effect of a decrease in tau, a 25% variation was applied to tau in order to show the sensitivity of the hydride fueled core clad temperature at the end of the blowdown due to this potential variation in tau. Figure 3.2 shows this sensitivity for the rod diameter of 12.5 mm, over all P/D values. This geometry was chosen because it is the most sensitive to changes in tau. This figure will also bound the potential variation for the oxide fueled cores, since the primary variation in tau is due potential variation in the time to minimum clad temperature during blowdown ($t_{MCT,BD}$). As previously discussed, the time to the minimum temperature during blowdown ($t_{MCT,BD}$) varies with linear heat rate, regardless of fuel type. At the most sensitive geometry, the temperature at the end of blowdown changed by a maximum of 30 degrees Fahrenheit, while in most locations the change was less. The average increase in the clad temperature at the end of blowdown over all geometries was only 15 degrees Fahrenheit. This demonstrates that it is reasonable to assume that if the value of tau varies from the nominal value of 10 seconds the resulting variation in clad temperature at the end of blowdown is minor. It is relatively constant compared to the reference core value of 10 seconds for the oxide fuel and 7.5 seconds for the hydride fuel.

Figure 3.2: Sensitivity of End of Blowdown Temperature to 25% Increase in Tau Factor Value

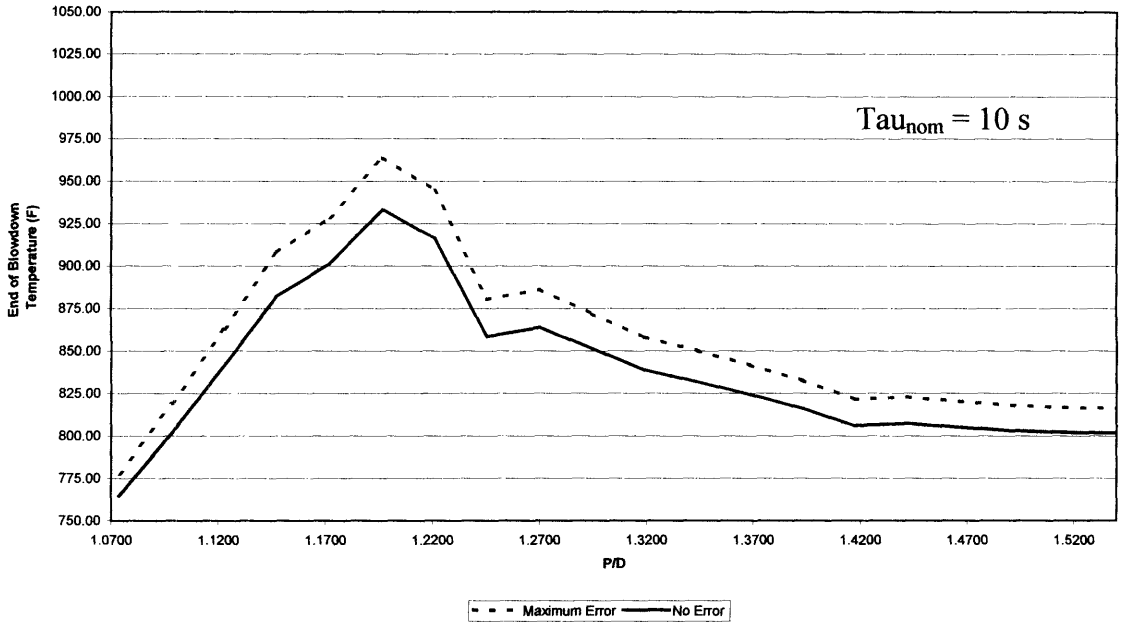

3.3 RESULTS

As previously stated this LBLOCA study assesses clad temperature following a large break loss of coolant accident. The bounding criterion for this study is the temperature history of the cladding of the reference oxide core determined using parameters from the STPEGS FSAR.

While the results for each of the two hundred geometries investigated for both the oxide and hydride fueled cores for both pressure drop cases over the entire 220-second time frame are available, displaying all of them for each case would be unwieldy and unintelligible. Thus, figure 3.3 shows the reference oxide core clad temperature and the most limiting clad temperature at each pitch-to-diameter ratio for the hydride cores for the 60 psia pressure drop limit, with the reference oxide core in black. Figure 3.4 shows the same information for the 29 psia pressure drop case.

Figure 3.3: Clad Temperature during LBLOCA for Hydride Fuel; 60 psia pressure drop

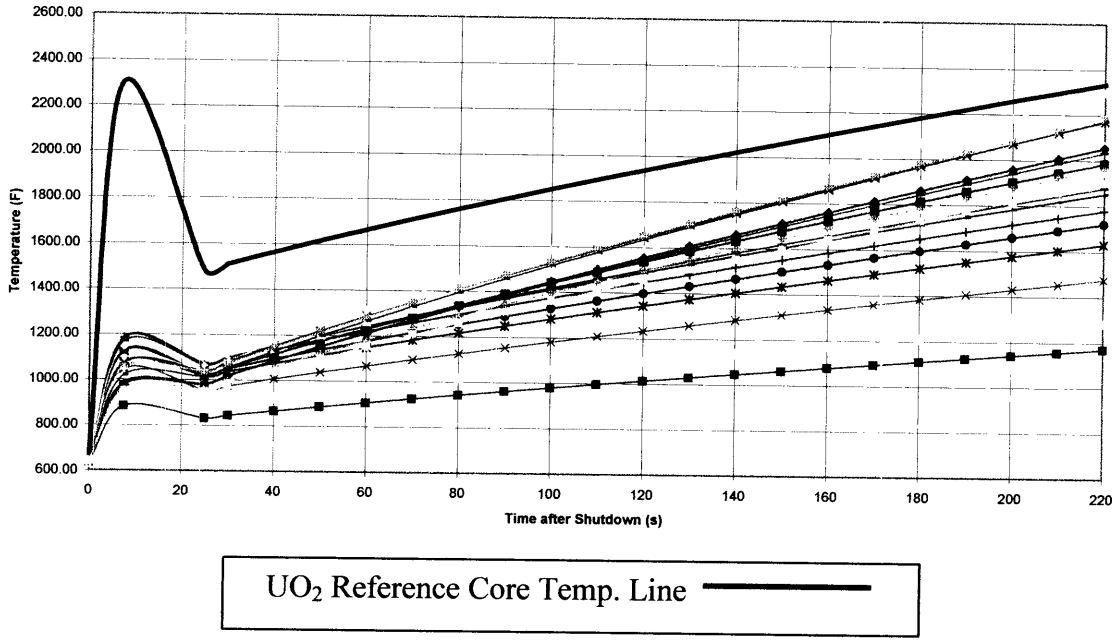

Figure 3.4: Clad Temperature during LBLOCA for Hydride Fuel; 29 psia pressure drop

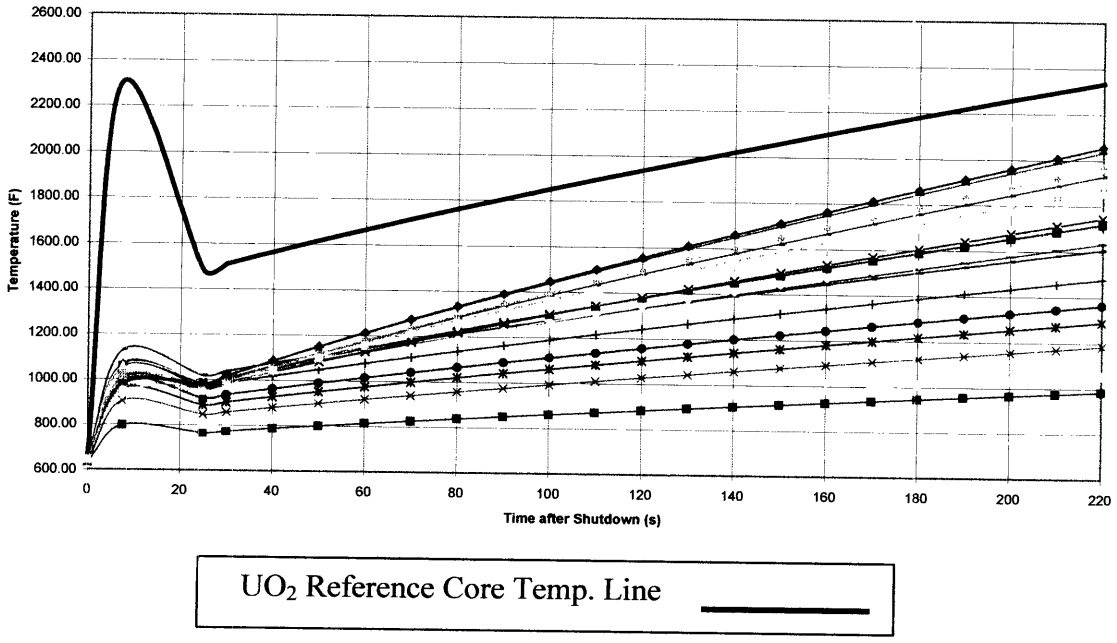

Notice that over the 220 seconds required to quench the reference core none of the hydride core clad temperatures exceed the bounding value of the reference oxide clad temperature.

However, thirty-eight oxide fueled cores do exceed the reference geometry oxide temperature during the time interval of interest for the 60 psia pressure drop case. Figure 3.5 shows the highest of these thirty-eight cases. Figure 3.6 shows the clad temperature history for the oxide fueled cores at 29 psia pressure drop, demonstrating that only one oxide core exceeds the bounding temperature for this pressure drop condition. This is due to the lower pressure drop limit. This lower limit limits many of the oxide cores that were at a higher power for the higher pressure drop case.

Figure 3.5: Clad Temperature during LBLOCA for Oxide Fuel; 60 psia pressure drop

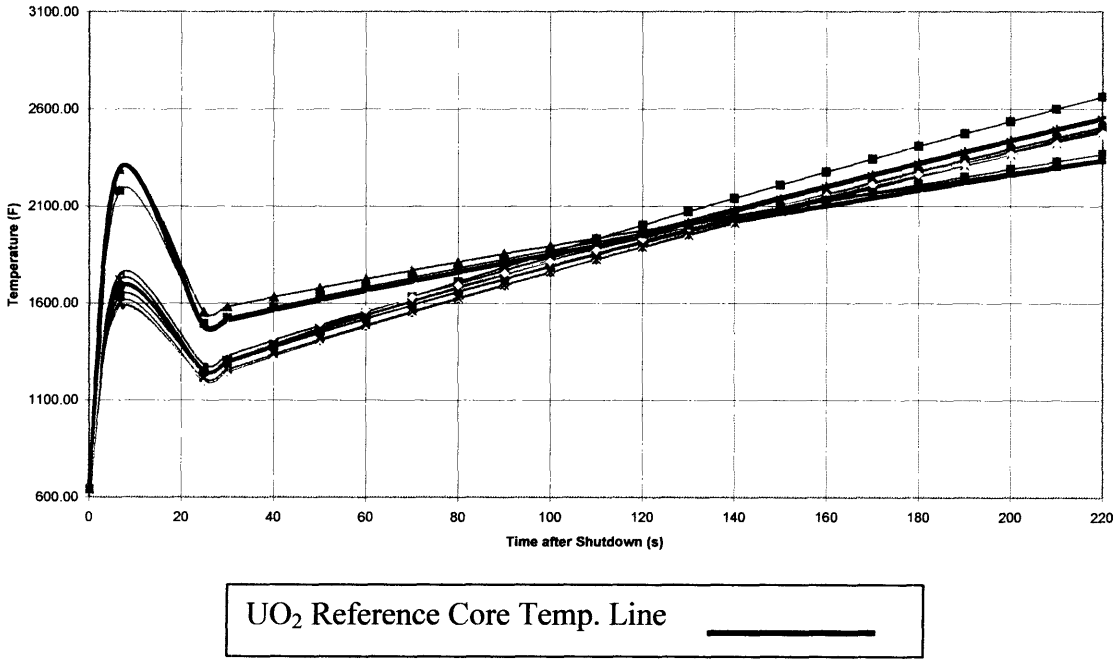

Figure 3.6: Clad Temperature during LBLOCA for Oxide Fuel; 29 psia pressure drop

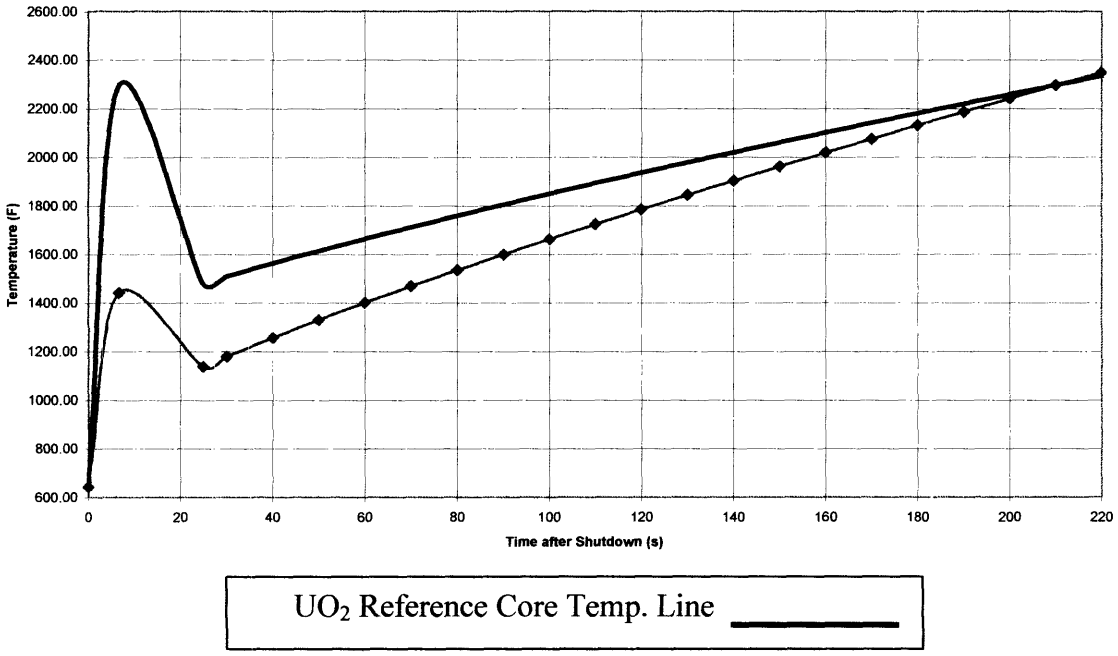

3.3.1 Discussion of Hydride Fueled Core Results

3.3.1.1 60 psia Pressure Drop Case

At 220 seconds the reference core clad temperature is 2335 °F. While none of the hydride core clad temperatures exceed this temperature within the 220 seconds, seven cores exceed it within the next 80 seconds (300 seconds total). However, each of these cores has a greater pitch-to-diameter ratio than that of the reference core. Therefore, the refill and reflood times of these cores should be equal to or less than the reference core. Thus, these cores are not limited by the LBLOCA. Every core with a smaller P/D than the reference core does not exceed 2335 °F until 300s or later, thus giving them 80+ seconds more to reflood compared to the reference core geometry.

Figure 3.7 shows the final clad temperature for the hydride fueled cores over the entire geometry range. Notice that for every geometry the hydride clad temperature is below the final reference oxide core clad temperature of 2335 °F. The loss of coolant accident is not limiting at any core geometry for the hydride fueled cores at 60 psia pressure drop.

Figure 3.7: Hydride Fueled Clad Temperature at 220s, 60 psia pressure drop

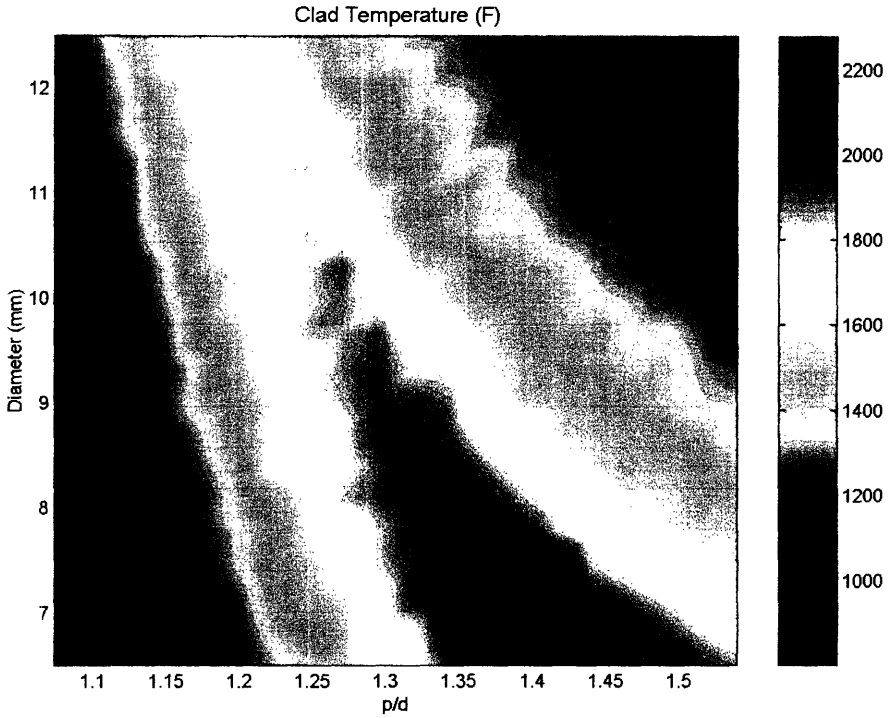

Since the LBLOCA imposes no power penalty on the hydride cores for 60 psia pressure drop, the maximum power hydride core (5458.5 MW) remains at a P/D of 1.42with a rod diameter of 6.82 mm, as was determined from the initial steady state analysis [4]. Figure 3.8 shows the Rated Power of each hydride core given the steady state limits (MDNBR, pressure drop, fuel centerline temperature, and flow velocity) and LOCA limits. Figure 3.8 shows the ratio between the rated power shown in figure 3.7 and the reference oxide core power of 3800 MW_{th}. Figures 3.9 shows the ratio between the linear heat rate and number of rods for the rated power in figure 3.7 and the linear heat rate and number of rods for the reference oxide core, respectively. In both figure 3.8 and 3.9 the solid black line represents where the ratio is equal to one.

Figure 3.8: Hydride Core Rated Power Given SS and LOCA Limits, 60 psia pressure drop

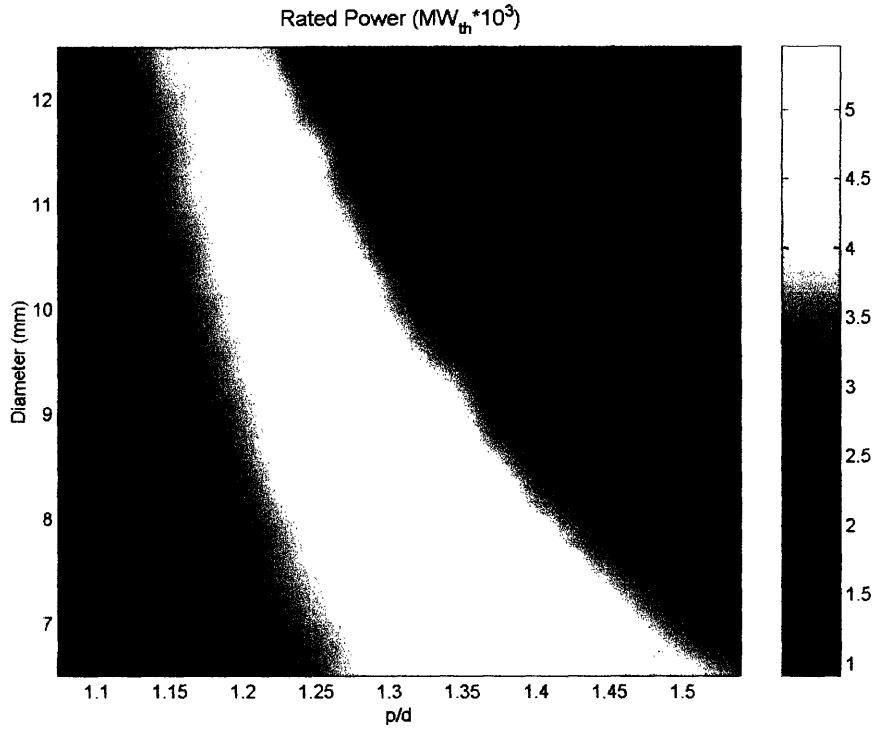

Figure 3.9: Ratio of Hydride Core Rated Power Given SS and LOCA Limits to Reference Oxide Core Power, 60 psia pressure drop

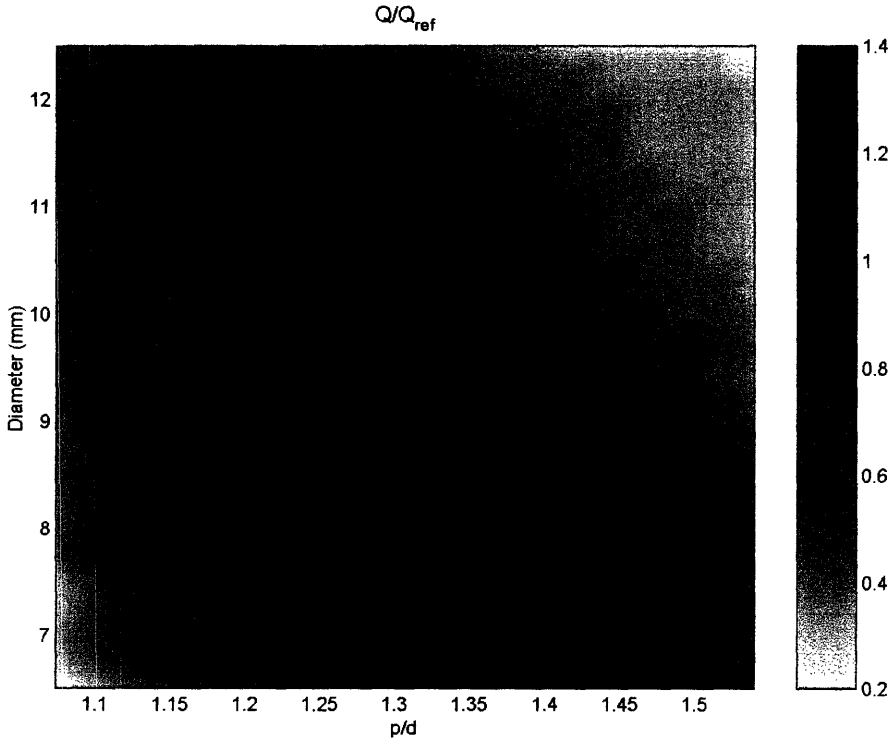

Figure 3.10: Ratio of Hydride Core Linear Heat Rate and Number of Rods Given SS and LOCA Limits to Reference Oxide Core, 60 psia pressure drop

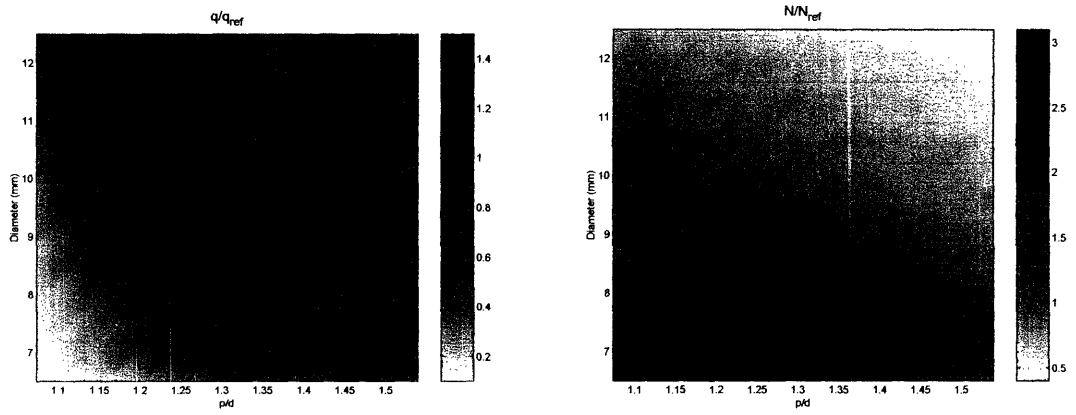

3.3.1.2 29 psia Pessure Drop Case

The results for the hydride cores at 29 psia pressure drop are similar to the results for the 60 psia pressure drop case.

Figure 3.11 shows the final clad temperature for the hydride fueled cores over the entire geometry range. Notice that for every geometry the hydride clad temperature is below the final reference oxide core clad temperature of 2335 °F. The loss of coolant accident is not limiting at any core geometry for the hydride fueled cores at 29 psia pressure drop.

Figure 3.11: Hydride Fueled Clad Temperature at 220s, 29 psia pressure drop

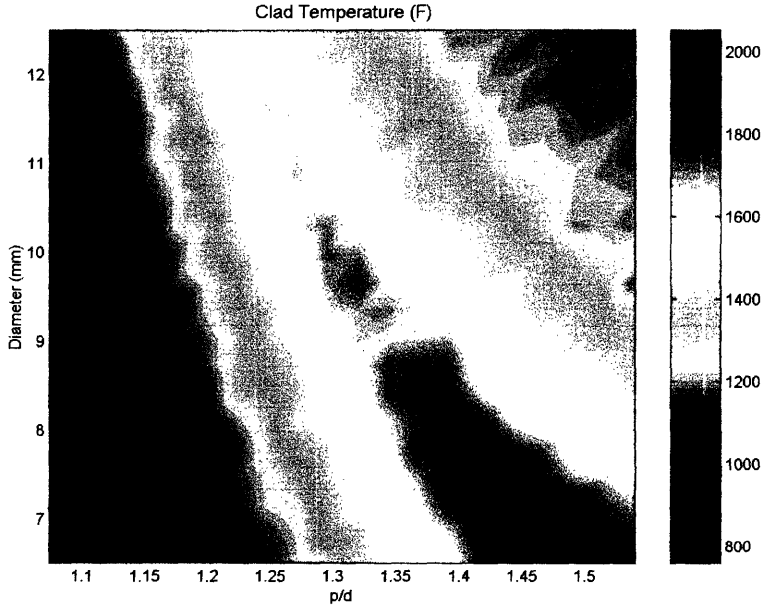

Since the LBLOCA imposes no power penalty on the hydride cores at 29 psia pressure drop, the maximum power hydride core (4245 MW) remains at a P/D of 1.49 with a rod diameter of 6.5 mm [4]. Figure 3.12 shows the Rated Power of each hydride core given the steady state limits (MDNBR, pressure drop, fuel centerline temperature, and flow velocity) and LOCA limits. Figure 3.13 shows the ratio between the rated power shown in figure 3.12 and the reference oxide core power of 3800 MW_{th}. Figure 3.14 shows the ratio between the linear heat rate and number of rods for the rated power in figure 3.12 and the linear heat rate and number of rods for the reference oxide core, respectively. In both figure 3.13 and 3.14 the solid black line represents where the ratio is equal to one.

Figure 3.12: Hydride Core Rated Power Given SS and LOCA Limits, 29 psia pressure drop

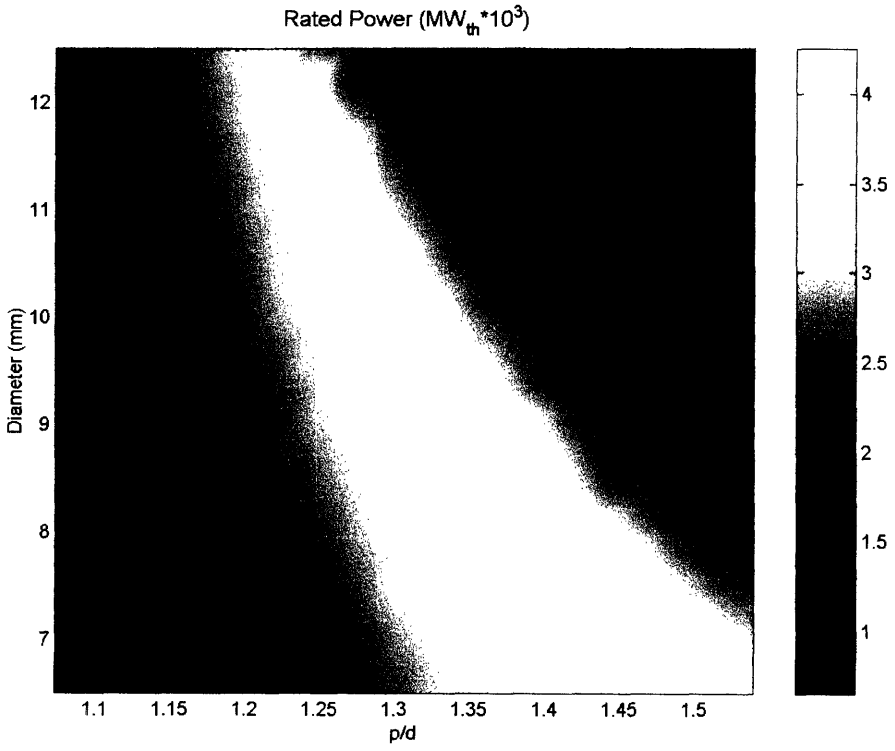

Figure 3.13: Ratio of Hydride Core Rated Power Given SS and LOCA Limits to Reference Oxide Core Power, 29 psia pressure drop

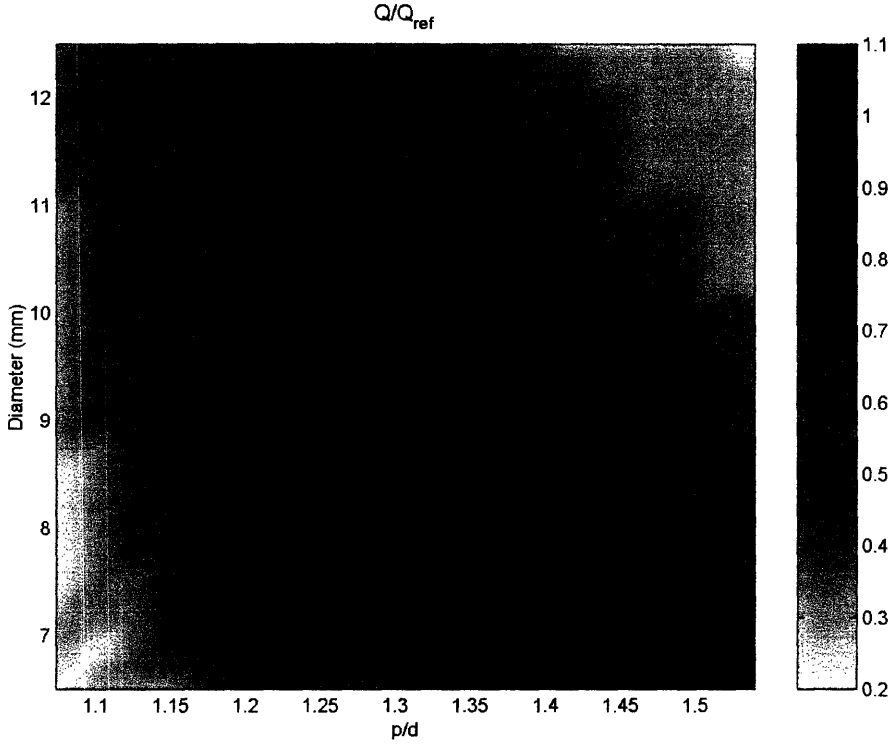

Figure 3.14: Ratio of Hydride Core Linear Heat Rate and Number of Rods Given SS and LOCA Limits to Reference Oxide Core, 29 psia pressure drop

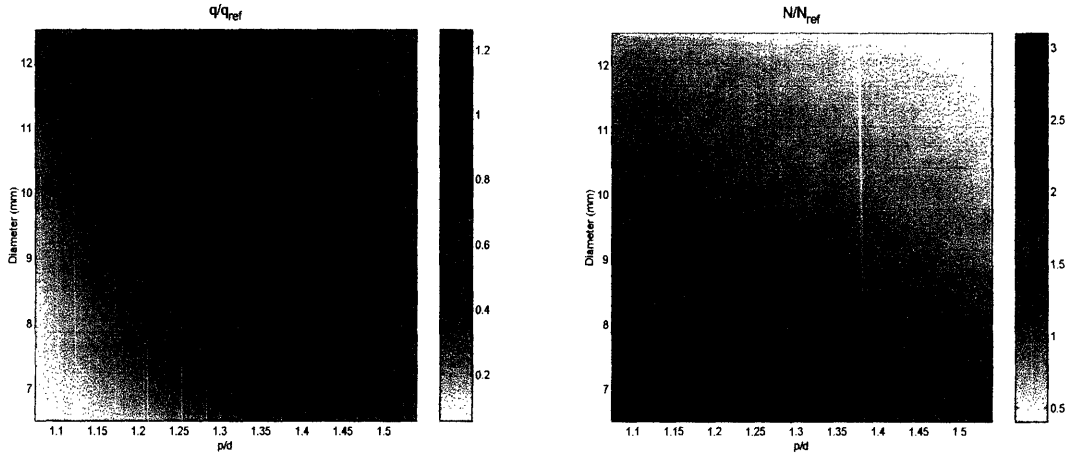

3.3.2 Discussion of Oxide Fueled Core Results

3.3.2.1 60 psia Pressure Drop Case

As previously stated, multiple oxide cores exceed the temperature limit established by the reference oxide core clad temperature time history. In order to reduce these temperatures to below the bounding temperature established by the reference oxide core, the power of each of these cores must be lowered until it falls below the temperature limit. After adjusting the power of each of these cores and reevaluating the time history of these high temperature cores against the reference core limit a new temperature profile is established. Figure 3.15 shows the final, adjusted, clad temperature for the oxide cores at 60 psia pressure drop.

Figure 3.15: Clad Temperature at 220s during LBLOCA for Oxide Fuel After Power Reduction, 60 psia pressure drop

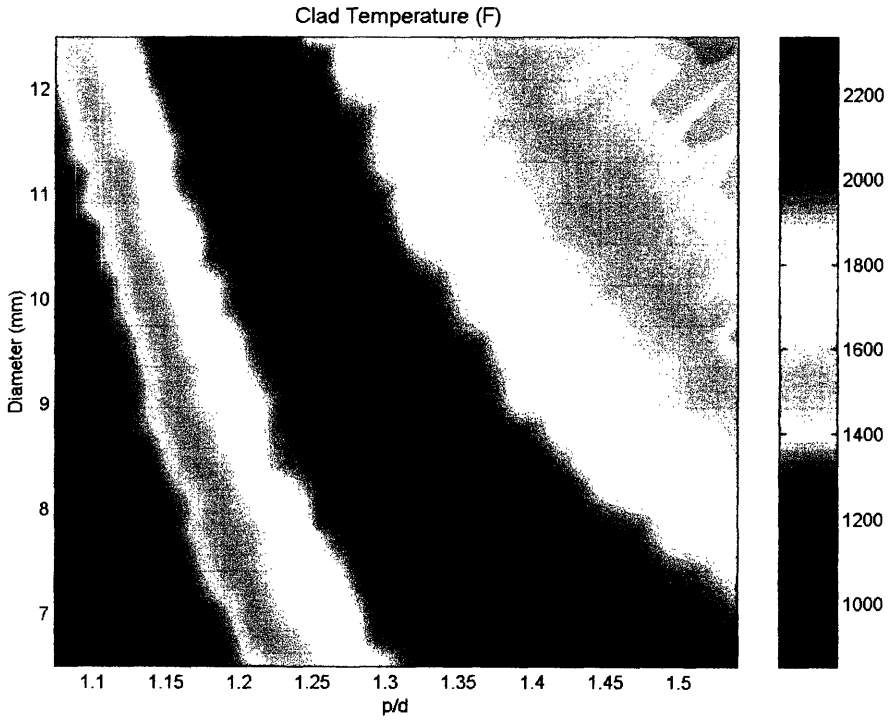

Figure 3.16 shows the Rated Power of each oxide core given the steady state limits (MDNBR, pressure drop, fuel centerline temperature, and rod vibrations) and LOCA

limits. The maximum power oxide core (4990.0 MW) is at a P/D of 1.39 with a rod diameter of 6.5 mm.

Figure 3.16: Oxide Core Rated Power Given SS and LOCA Limits, 60 psia pressure drop

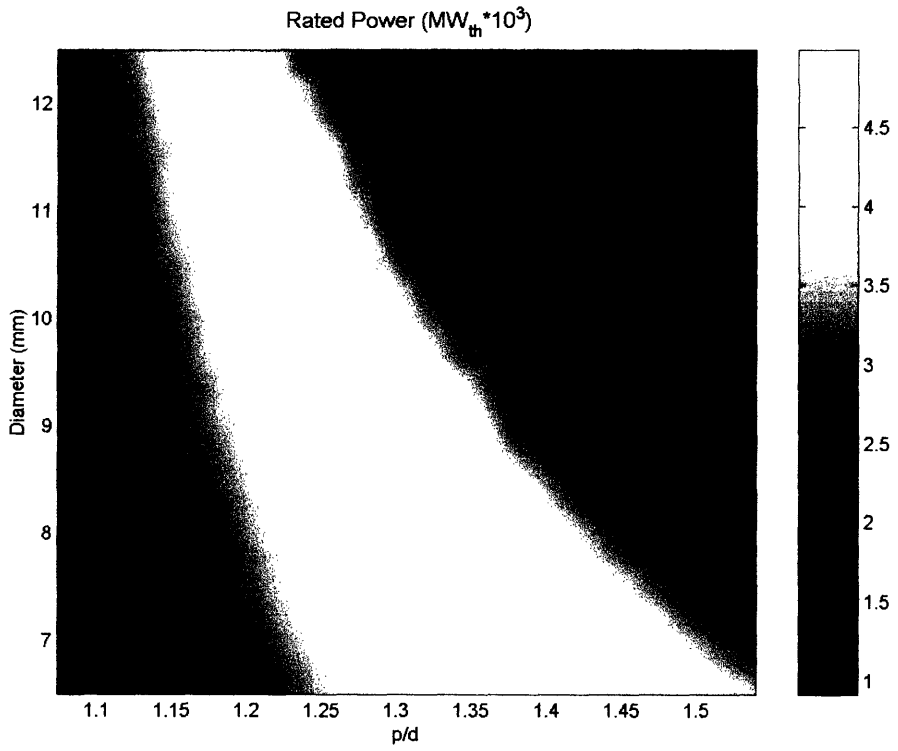

Figure 3.17 shows the ratio between the rated power shown in figure 3.17 and the reference oxide core power of 3800 MW_{th}. Figures 3.18 shows the ratio between the linear heat rate and number of rods for the rated power in figure 3.12 and the linear heat rate and number of rods for the reference oxide core, respectively. In both figure 3.17 and 3.18 the solid black line represents where the ratio is equal to one.

Figure 3.17: Ratio of Oxide Core Rated Power Given SS and LOCA Limits to Reference Oxide Core Power, 60 psia pressure drop

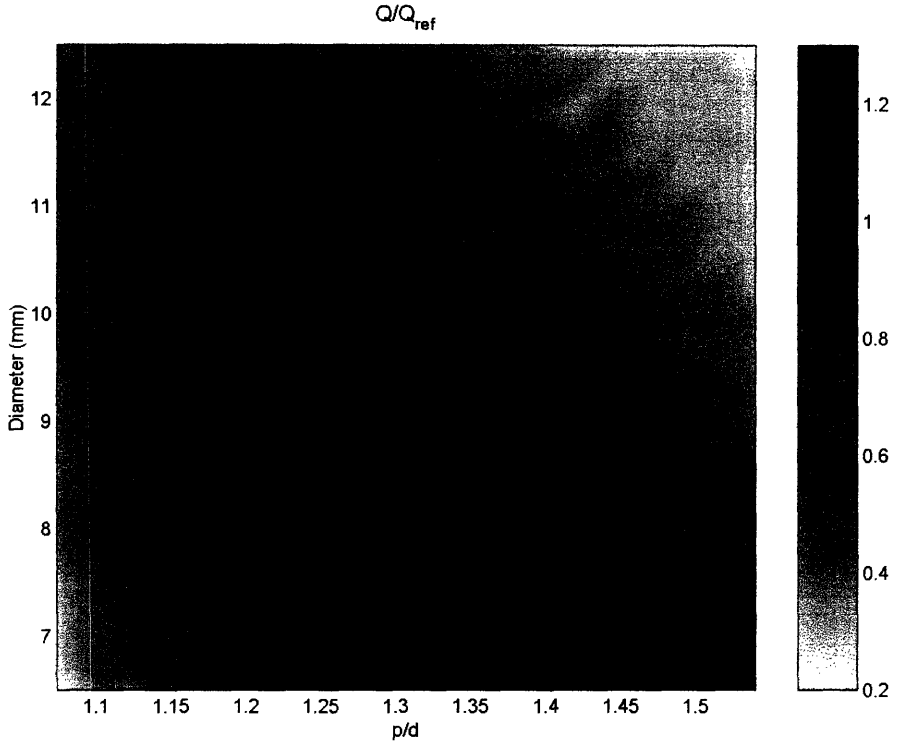

Figure 3.18: Ratio of Oxide Core Linear Heat Rate and Number of Rods Given SS and LOCA Limits to Reference Oxide Core, 60 psia pressure drop

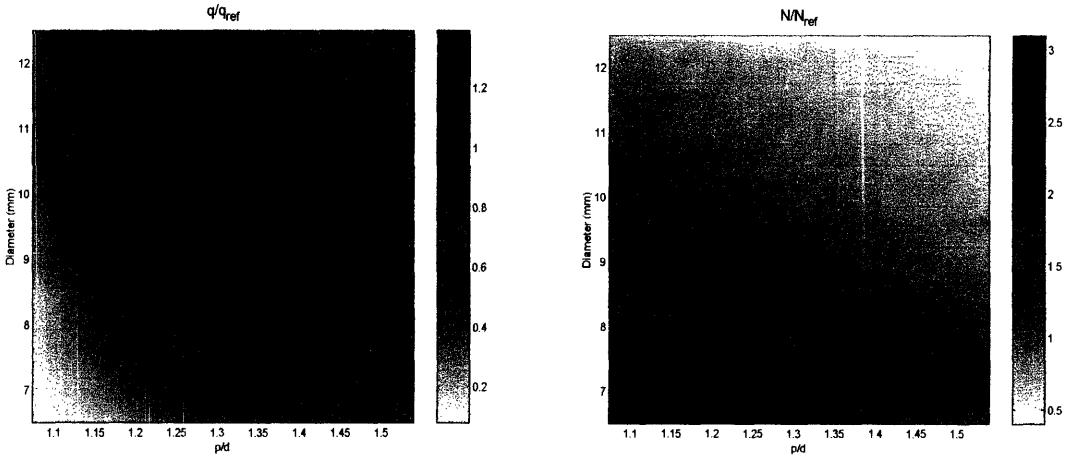

Comparing the final rated power of each hydride and oxide fueled core over the geometry ranges for which the oxide was limited for the 60 psia pressure drop case yields figure

3.19. Each value greater than one shows the locations where the hydride fueled core has a greater power than an oxide fueled core with the same geometry.

Figure 3.19: Ratio of Rated Power Given SS and LOCA Limits, Hydride to Oxide

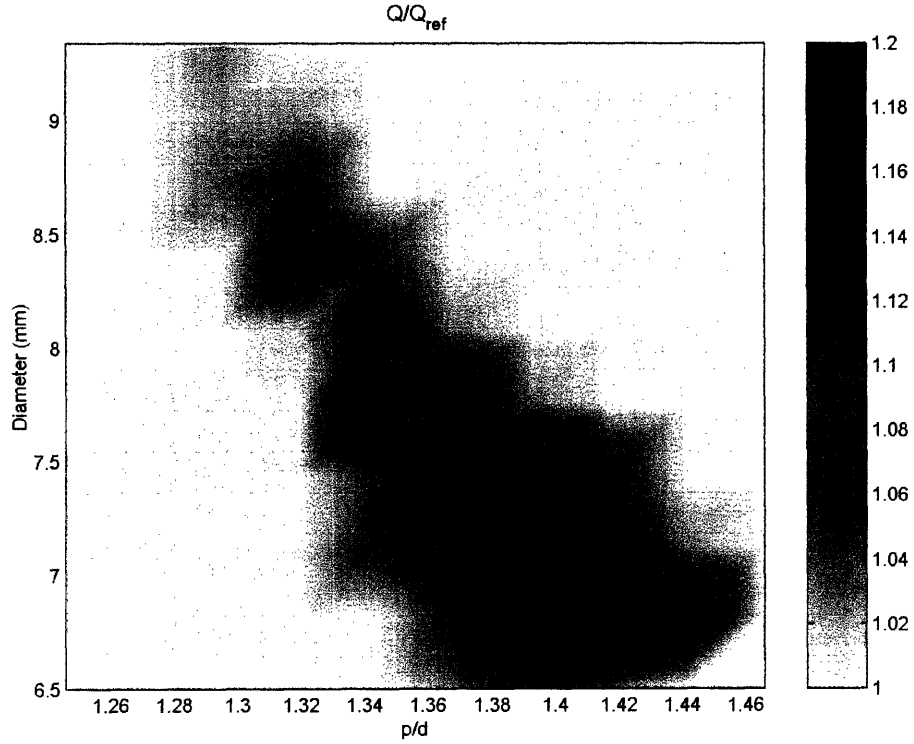

3.3.2.2 29 psia Pressure Drop Case

The results for the oxide cores at 29 psia pressure drop are similar to the results for the 60 psia pressure drop case. However, only one oxide cores exceeded the temperature limit established by the reference oxide core clad temperature time history. As with the 60 psia pressure drop case, the power of this core was reduced. After adjusting the power of this core and reevaluating the time history against the reference core limit a new temperature profile is established, mostly similar to the steady state profile. Figure 3.20 shows the final, adjusted, clad temperature for the oxide cores at 29 psia pressure drop.

Figure 3.20: Clad Temperature at 220s during LBLOCA for Oxide Fuel After Power Reduction, 29 psia pressure drop

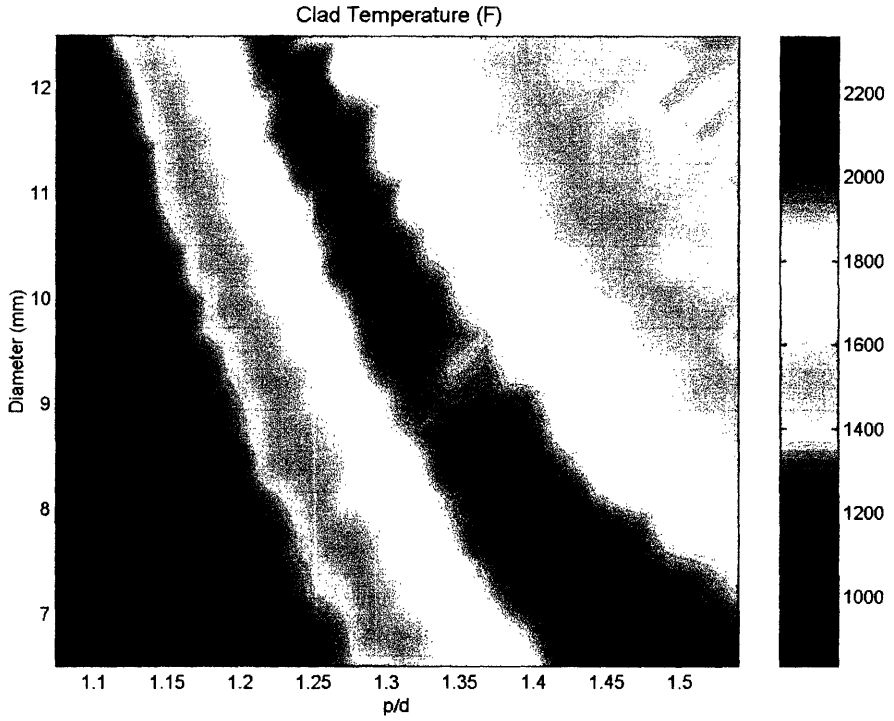

Figure 3.21 shows the Rated Power of each oxide core given the steady state limits (MDNBR, pressure drop, fuel centerline temperature, and rod vibrations) and LOCA limits. The maximum power oxide core (4202.8 MW) is at a P/D of 1.49 with a rod diameter of 6.5 mm.

Figure 3.21: Oxide Core Rated Power Given SS and LOCA Limits, 29 psia pressure drop

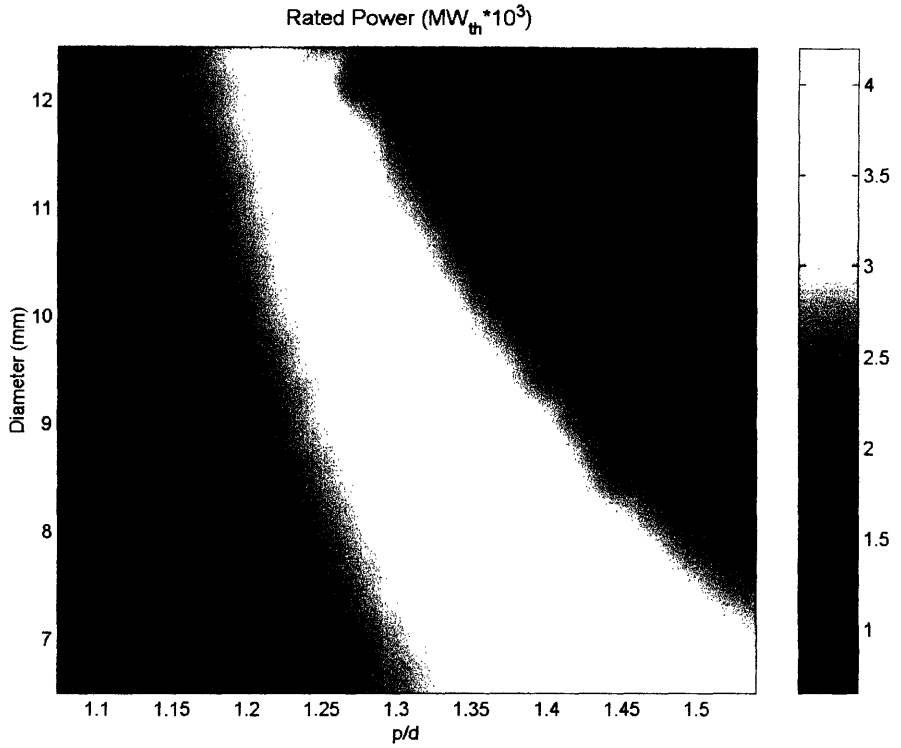

Figure 1.22 shows the ratio between the rated power shown in figure 1.21 and the reference oxide core power of 3800 MW_{th}. Figures 1.23 shows the ratio between the linear heat rate and number of rods for the rated power in figure 1.21 and the linear heat rate and number of rods for the reference oxide core, respectively. In both figure 1.22 and 1.23 the solid black line represents where the ratio is equal to one.

Figure 3.22: Ratio of Oxide Core Rated Power Given SS and LOCA Limits to Reference Oxide Core Power, 29 psia pressure drop

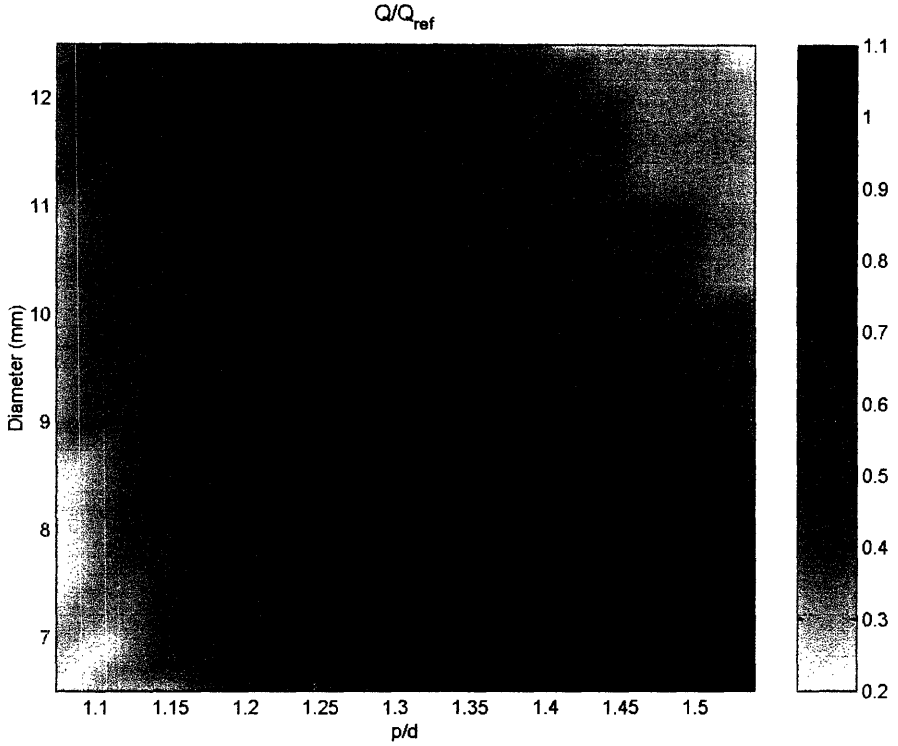

Figure 3.23: Ratio of Oxide Core Linear Heat Rate and Number of Rods Given SS and LOCA Limits to Reference Oxide Core, 29 psia pressure drop

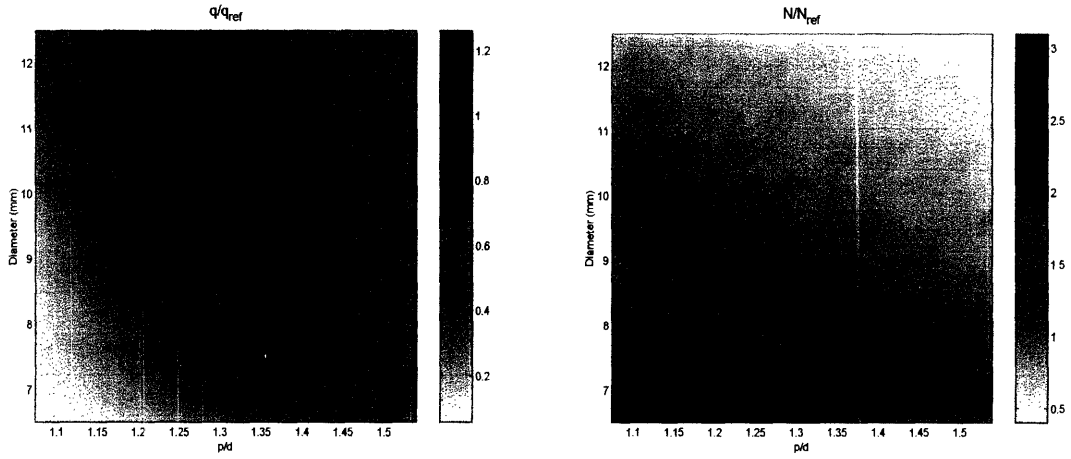

Comparing the final rated power of each hydride and oxide fueled core over the entire geometry range for the 29 psia pressure drop case yields nearly identical values. Since

only one oxide core power is limited, and only by 1.6%, this is the only geometry where the hydride fuel has a higher power than the oxide.

3.4 FACTORS AFFECTING CLAD TEMPERATURE TIME HISTORY

In order to understand the clad temperature history curves presented in figures 3.3 through 3.6, it is necessary to examine the factors that affect them. While both the hydride and oxide cores have a lower peak clad temperature during blowdown ($T_{PCT,BD}$) than the reference oxide core, the clad temperature behavior over time does vary between geometries and fuel types. Also the slope of each line varies. The clad temperature for some of the hydride and oxide cores increase faster than the reference oxide core and some slower. This slope also appears to be independent of the starting temperature.

As previously shown in equation (3.4), there are three terms that affect the clad temperature over time. The first is the stored energy redistribution that occurs in the first few seconds of the transient based on the fuel time constant. The second is the cooling that occurs during the blowdown. The last term is the heat up over time due to decay heat. Throughout this portion of the analysis the 60 psia pressure drop limit is used. However, the use of this limit is irrelevant when analyzing behavior. The actual values are differenct for each pressure drop case, but the behavior of the clad temperature history curves are the same.

$$T_{clad,final} - T_{clad,initial} = aq' - \left(T_{PCT,BD} - \overline{T_S}\right)\left(1 - \frac{1}{1.09 + 0.9 \cdot m \cdot \tau}\right) + \Delta T_{DH} \qquad \textbf{(3.4)}$$

$$T_{clad,final} - T_{clad,initial} = \begin{matrix}\text{heating}\\ \text{from}\\ \text{stored}\\ \text{energy}\end{matrix} + \begin{matrix}\text{blowdown}\\ \text{cooling}\end{matrix} + \begin{matrix}\text{decay}\\ \text{heat}\\ \text{refill}\\ \text{heating}\end{matrix}$$

3.4.1 STORED ENERGY REDISTRIBUTION

The peak clad temperature during blowdown ($T_{PCT,BD}$) is defined as the average temperature of the rod upon redistribution of the stored energy, which occurs with the characteristic time constant of the fuel shortly after the initiation of the LOCA. Recalling equation (3.4), the stored energy term is comprised of the linear heat rate and a constant, a. Equation (3.6) gives the average fuel temperature based on the steady state operating peak linear heat rate, neglecting the stored energy in the thin clad.

$$\overline{T}_{fuel} = \frac{q'}{\pi}\left(\frac{1}{8 \cdot k_{fuel}} + \frac{1}{D_{gap} \cdot h_{gap}} + \frac{t_{clad}}{D_{clad} \cdot k_{clad}} + \frac{1}{D_{rod} \cdot h_{cool}}\right) + T_{cool} \qquad \textbf{(3.6)}$$

where D_{gap}, D_{clad}, t_{clad}, h_{cool}, and T_{cool} are the mean gap diameter, mean clad diameter, clad thickness, coolant heat transfer coefficient, and coolant temperature at the axial location of the peak clad temperature. Now, if we take $\overline{T}_{fuel}$ as $T_{c,final}$ and $T_{c,initial}$ as T_{cool} then the constant coefficient, a, is as follows.

$$a = \frac{1}{\pi}\left(\frac{1}{8 \cdot k_{fuel}} + \frac{1}{D_{gap} \cdot h_{gap}}\right) \qquad (3.7)$$

3.4.1.1 Comparing Oxide Reference Core to Hydride Cores

When comparing the reference geometry oxide core to the reference geometry hydride core only the gap heat transfer coefficient and the fuel thermal conductivity are different, as shown previously in table 3.2. The difference in gap conductivity is due to the use of liquid metal bonding, vice the helium filled gap of the reference oxide core.

Comparing the fuel and gap terms in equation (3.7) for each fuel at the reference geometry yields the following results, shown in table 3.4.

Table 3.4: Stored Energy Redistribution Terms, Oxide vs. Hydride

Parameter	Reference Oxide Core	Reference Hydride Core
Fuel Term $\left(\frac{1}{8 \cdot k_{Fuel}}\right)$	$0.041\frac{m-K}{W}$	$0.007\frac{m-K}{W}$
Gap Term $\left(\frac{1}{D_{Gap} \cdot h_{Gap}}\right)$	$0.011\frac{m-K}{W}$	$0.00036\frac{m-K}{W}$

Since both the fuel and gap term are lower for the hydride fuel, the peak clad temperature during blowdown of the hydride reference core should be lower than the oxide case, which it is. The peak clad temperature during blowdown for the reference hydride core is about 46% lower that for the reference oxide core, as shown in table 3.5.

Table 3.5: Initial Pin Temperature due to Stored Energy Redistribution, Oxide vs. Hydride

Parameter	Reference Oxide Core	Reference Hydride Core
TPCT,BD	2231.6 oF	994.0 oF
Difference	$\left(\frac{2691\ .3R - 1453\ .7R}{2691\ .3R}\right) = 0.46 = 46\,\%$	

The use of a liquid metal gap vice a helium gap provides for part of the lower temperature, but the majority of the initial temperature decrease between oxide and hydride cores comes from the increased thermal conductivity of the hydride fuel.

3.4.1.2 Variable Geometry

When comparing cores with the same fuel but of variable geometry and linear heat rates the fuel term and the gap term can be ignored. The contribution from the gap is minimal, as shown in table 3.4 and can be neglected, despite the variable gap diameter. Also, since

each core has the same enthalpy rise, inlet temperature, and axial power profile, the coolant temperature will be the same.

That leaves the linear heat rate, which obviously must be accounted for, and the clad and coolant terms. The clad term however, has the clad thickness in the numerator and the clad diameter in the denominator. These two terms are both proportional to the rod diameter and thus to each other and cause the clad term to be constant with changing geometry, as shown in equation (3.8).

$$Clad\_Term = \frac{t_{clad}}{D_{clad} \cdot k_{clad}} \alpha \frac{D_{rod}}{D_{rod} \cdot k_{clad}} \alpha \frac{1}{k_{clad}} \qquad \textbf{(3.8)}$$

Table 3.6. shows that the fuel term is comparable to the coolant term for the hydride fuel, but not for the oxide fuel.

Table 3.6: Stored Energy Redistribution Terms

Parameter	Reference Oxide Geometry	Reference Hydride Geometry
Fuel Term $\left(\frac{1}{8 \cdot k_{ZrH}}\right)$	$0.041\frac{m-K}{W}$	$0.007\ \frac{m-K}{W}$
Coolant Term $\left(\frac{1}{D_{rod} \cdot h_{cool}}\right)$	$0.003\frac{m-K}{W}$	$0.003\ \frac{m-K}{W}$
Coolant Heat Transfer Coefficient (h_{cool})	4.08E+4 $\frac{W}{m^2-K}$	4.08E+4 $\frac{W}{m^2-K}$

The coolant term, as shown in table 3.6, is inversely proportional to rod diameter. Also, as shown in equation (3.6), the stored energy redistribution is proportional to the linear heat rate. Thus, for the hydride fuels, the coolant term will be more significant for smaller rod diameters and become less so as the rods increase in size. However, the linear heat rate is not proportional to just rod diameter. This makes it necessary to

evaluate the initial temperature over the entire parametric range in order to fully understand the stored energy contribution to the LOCA temperature, for hydride fuels.

Thus, for the oxide fuels, the initial temperature will be proportional to the linear heat rate, while for the hydride fuel it will be proportional to the linear heat rate and inversely proportional to the rod diameter.

Figures 3.24 and 3.25 provide the ratio of the average linear heat rate over the entire geometry range for the hydride and oxide cores for the 60 psia pressure drop limit, respectively, to the reference oxide core linear heat rate. The solid black line represents where the ratio is equal to one.

Figure 3.24: Ratio of Hydride Core Linear Heat Rate Given SS and LOCA Limits to Reference Oxide Core Linear Heat Rate, 60 psia pressure drop

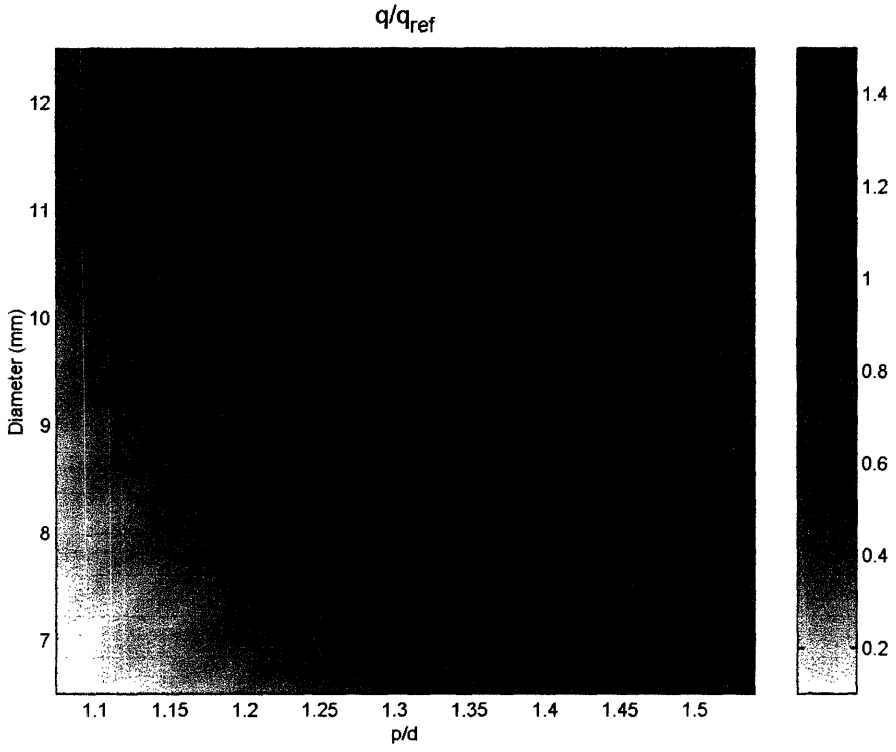

Figure 3.25: Ratio of Oxide Core Linear Heat Rate Given SS and LOCA Limits to Reference Oxide Core Linear Heat Rate, 60 psia pressure drop

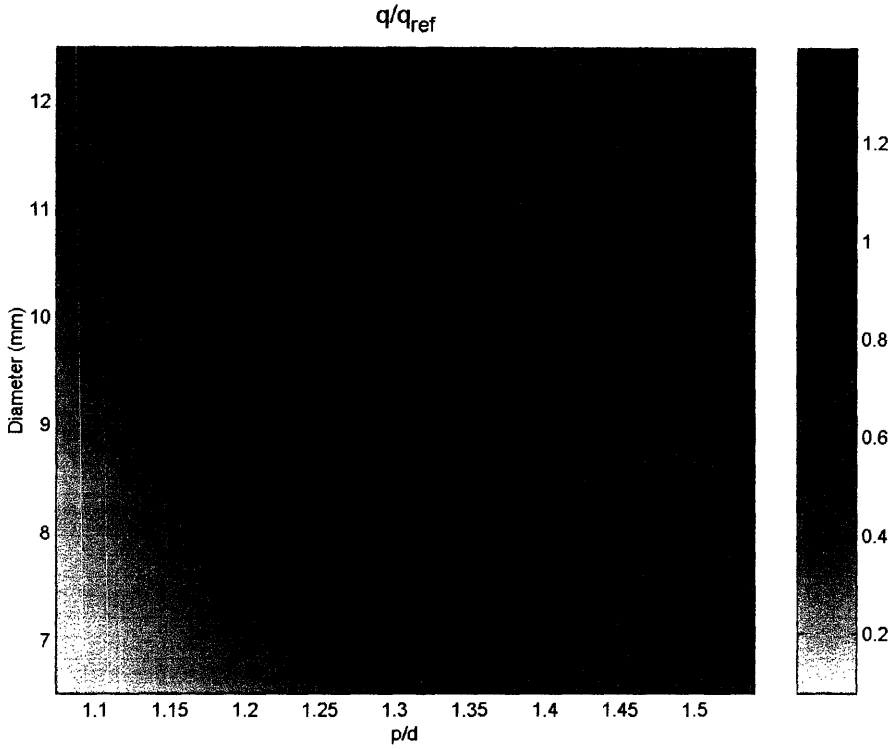

For both fuels the linear heat rate is the highest for the large rod diameters and smaller P/D ratios. The coolant term however is inversely proportional to the rod diameter. Thus, for the hydride fuels, the coolant term is less significant at larger rod diameters. The peak clad temperature during blowdown for hydride and oxide fuels, including all terms, is shown in figure 3.26 and 3.27, respectively.

Figure 3.26: Peak clad temperature during blowdown Due to Stored Energy for Hydride Cores, 60 psia pressure drop

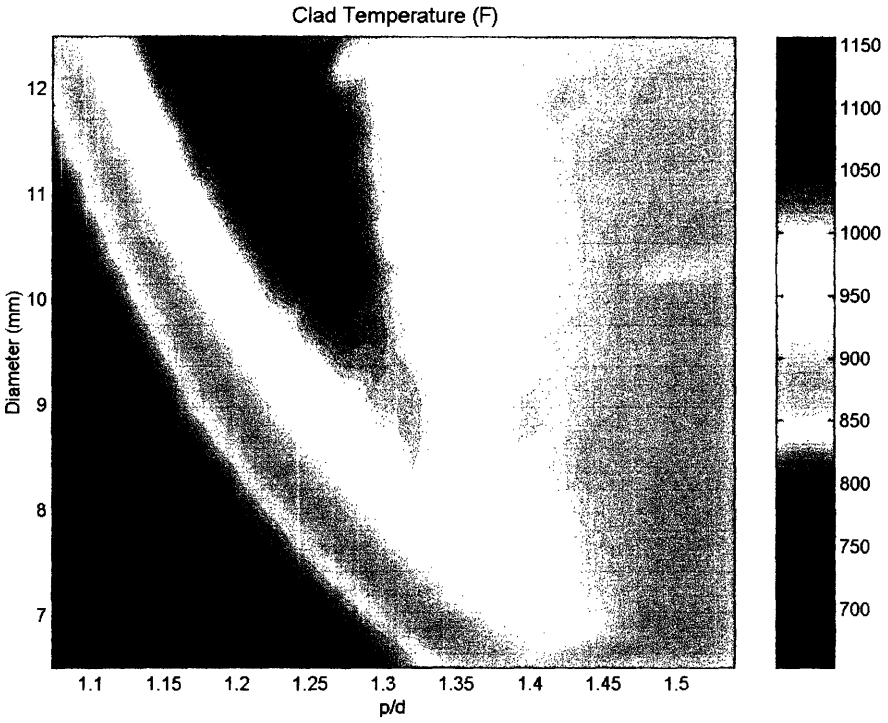

Figure 3.27: Peak clad temperature during blowdown Due to Stored Energy for Oxide Cores, 60 psia pressure drop

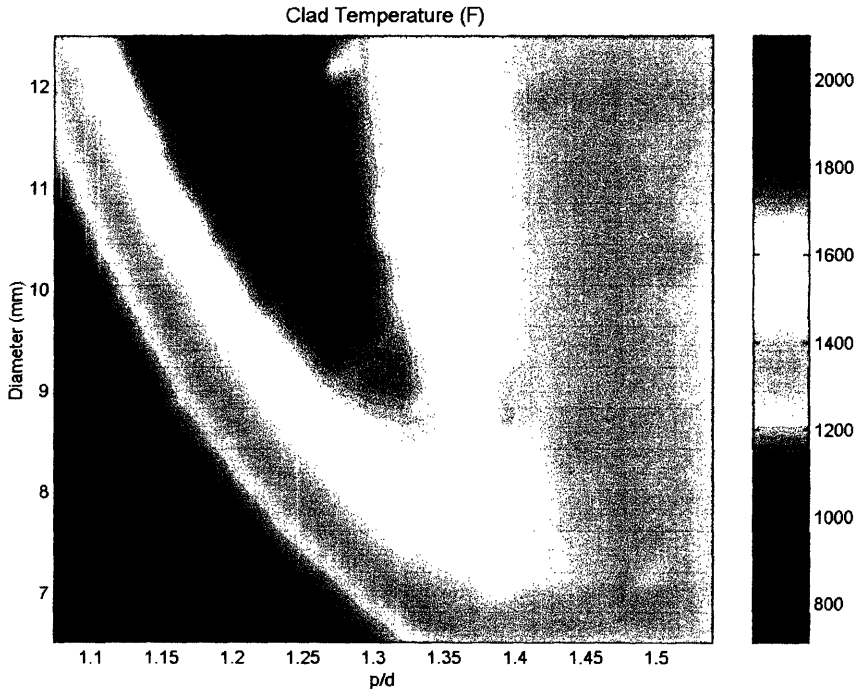

The peak clad temperature during blowdown is proportional to the linear heat rate but is skewed further towards small rod diameters than the linear heat rate alone for the hydride fuel. The highest initial temperature for the hydride fuel is 1036 °F and occurs at a P/D of 1.27 for a rod diameter of 10.3 mm. This is also the geometry with the highest linear heat rate of 6.02 $\frac{kW}{ft}$. The highest initial temperature for the oxide fuel is 2151 °F and occurs at a P/D of 1.22 for a rod diameter of 11.87 mm. Again this is also the geometry with the highest linear heat rate of 7.42 $\frac{kW}{ft}$. Thus, the stored energy and peak clad temperature during blowdown are primarily dependant upon the steady state linear heat rate for both oxide and hydride fuels.

3.4.2 BLOWDOWN COOLING

Following the initial peak in clad temperature due to stored energy redistribution, the clad will be cooled due to the coolant volume flashing to steam and increasing in velocity as it escapes the primary system. Recalling the blowdown cooling term from equation (3.4), as well as equations (3.2) and (3.3), we have the following:

$$\Delta T_{BD} = \left(T_{PCT,BD} - \overline{T_S}\right)\left(1 - \frac{1}{1.09 + 0.9 \cdot m \cdot \tau}\right) \tag{3.9}$$

$$m = \left(\frac{\bar{h} \cdot A_{surf}}{\left(\rho \cdot c_p \cdot V\right)_{Fuel}}\right) \tag{3.2}$$

$$\tau = \left(t_{MCT,BD} - t_{PCT,BD}\right) \tag{3.3}$$

where ΔT_{BD} is the decrease in clad temperature due to the blowdown.

3.4.2.1 Comparing Oxide Reference Core to Hydride Cores

As previously discussed, the time term, τ, is relatively constant for both hydride and oxide over the entire range of geometries. Also, due to the constraint of a constant inlet

and outlet enthalpy, axial power profile, and system pressure, the average coolant saturation temperature will also be the same, regardless of geometry or fuel. Thus, when comparing the reference geometry oxide core to the reference geometry hydride core only the peak clad temperature during blowdown and the term, m, will vary.

As discussed in the stored energy redistribution section, the initial peak clad temperature is higher for the reference oxide core than for the reference hydride core by 46%. The blowdown heat transfer coefficient is dependant upon the coolant properties during blowdown, which are independent of both fuel and geometry. For the reference geometry the surface area of the rod and the fuel volume are the same. Therefore, equation (3.2) can be reduced to the following proportionality for the oxide and hydride fuel of the same geometry.

$$m\alpha\left(\frac{1}{(\rho \cdot c_p)_{Fuel}}\right) \tag{3.10}$$

The product of density and heat capacity is known as the volumetric heat capacity with units of $\frac{W}{m^3 K}$, as shown in equation (3.11).

$$\text{Volumetric Heat Capacity} = c_{p,fuel} \cdot \rho_{fuel} \tag{3.11}$$

As shown previously in table 3.2, the heat capacity of the hydride fuel is higher than the oxide but the density is lower. The volumetric heat capacity of each fuel is shown in table 3.7.

Table 3.7 Blowdown Cooling Terms, Oxide vs. Hydride

Parameter	Reference Oxide Core	Reference Hydride Core
Volumetric Heat Capacity	3.67E+6 $\frac{W}{m^3 K}$,	4.10E+6 $\frac{W}{m^3 K}$.

A higher volumetric heat capacity will cause the decrease in clad temperature during blowdown for the reference hydride core cladding to be lower than that of the reference oxide core. The blowdown cooling of the clad for the reference hydride core is approximately 5 times lower that for the reference oxide core, as shown in table 3.8.

Table 3.8: Clad Cooling Due to Blowdown, Oxide vs. Hydride

Parameter	Reference Oxide Core	Reference Hydride Core
ΔT_{BD}	931.8 °F	170.2 °F

The greater blowdown cooling is due to the compounded effect of the higher peak clad temperature during blowdown of the oxide core and the lower volumetric heat capacity of the oxide fuel.

3.4.2.2 Variable Geometry

When comparing cores of the same fuel type but with various geometries and linear heat rates the time and coolant terms will still be constant. In addition the volumetric heat capacity will also be the same. However, the peak clad temperature during blowdown ($T_{PCT,BD}$), as used in equation (3.9), will still vary with linear heat rate, as outlined in the stored energy redistribution section. Also, the term m will vary inversely with rod diameter due to the surface area of the rod and fuel volume terms, as shown in equation (3.12).

$$m\alpha\left(\frac{A_{surf}}{(V)_{Fuel}}\right)\alpha\frac{D_{rod}}{D_{rod}^2}\alpha\frac{1}{D_{rod}} \tag{3.12}$$

As the rod diameter increases the cooling effect of the blowdown will decrease. The blowdown cooling effect is proportional to linear heat rate and inversely proportional to rod diameter.

However, the linear heat rate is not proportional to just rod diameter. This makes it necessary to evaluate the change in clad temperature due to blowdown over the entire parametric range in order to fully understand its contribution to the LOCA temperature, as shown in figure 3.28 and 3.29.

Figure 3.28: Change in Clad Temperature Due to Blowdown Cooling for Hydride Cores, 60 psia pressure drop

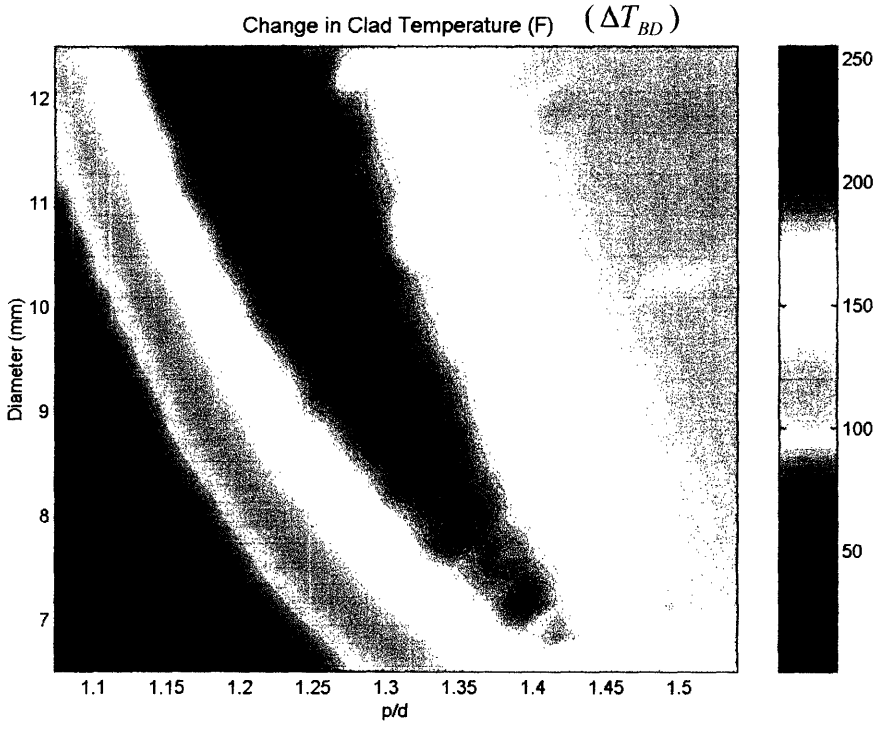

Figure 3.29: Change in Clad Temperature Due to Blowdown Cooling for Oxide Cores, 60 psia pressure drop

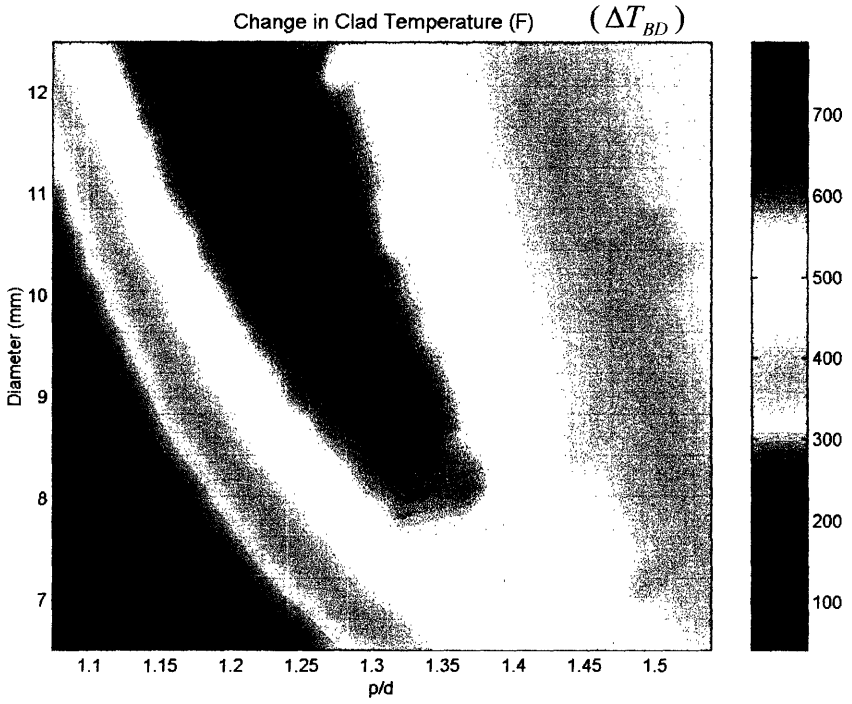

Thus, comparing figures 3.26 and 3.27 to figures 3.28 and 3.29, respectively, the highest cooling occurs where the peak clad temperatures during blowdown were initially the highest. Also notice the significantly higher blowdown cooling for the oxide cores when compared to the hydride cores of the same geometry. This is due to the volumetric heat capacity of each fuel, as discussed previously. Figures 3.30 and 3.31 show the clad temperature at the end of the blowdown for the hydride and oxide fuels for the 60 psia pressure drop limit. The profile is much more evenly distributed than the peak clad temperatures during blowdown, with the highest temperatures being in the region of highest linear heat rate where the high peak clad temperatures during blowdown dominate. However, in the region of lower linear heat rate and high diameter (upper right), the blowdown cooling was less significant and thus the temperature of that region relative to the others went up.

Figure 3.30: Clad Temperature at the End of Blowdown for Hydride Cores, 60 psia pressure drop

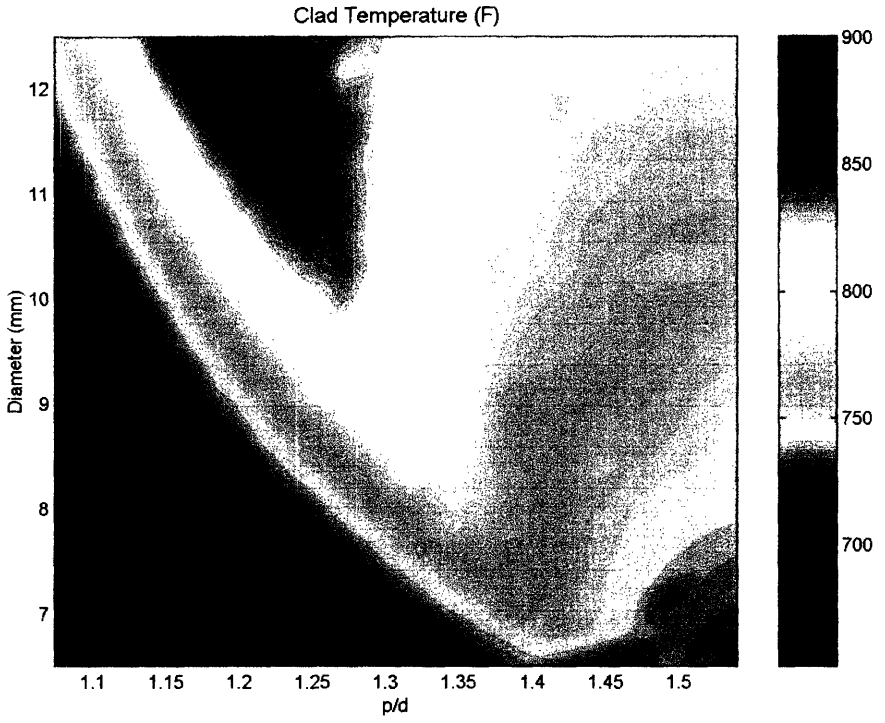

Figure 3.31: Clad Temperature at the End of Blowdown for Oxide Cores, 60 psia pressure drop

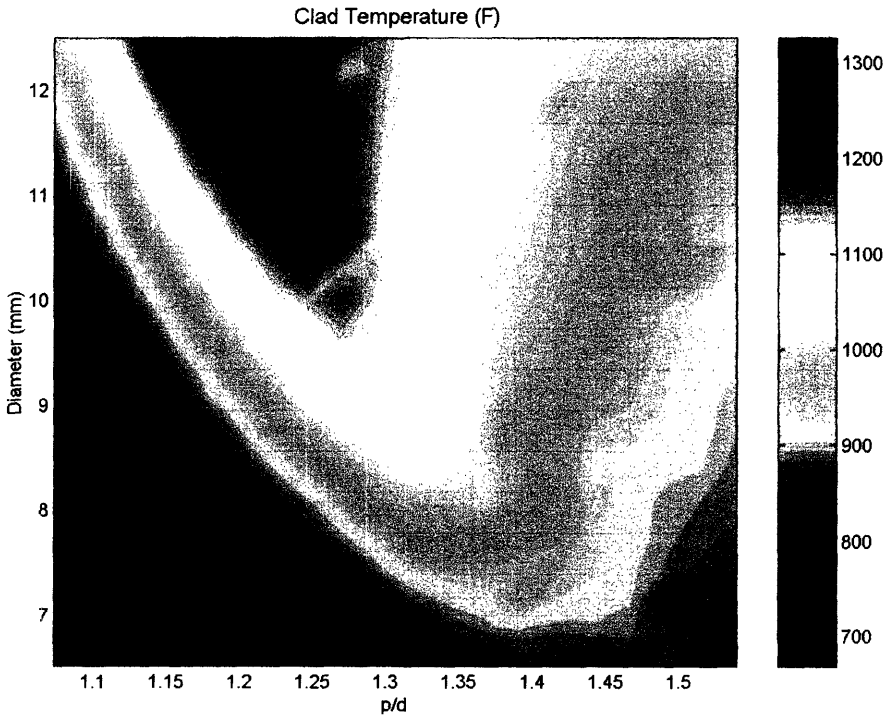

3.4.3 DECAY HEAT ADDITION (LOCA TEMPERATURE SLOPE)

After the stored energy is redistributed and the blowdown is complete, decay heat continues to heat the fuel and thus the clad. Assuming operation has been at a constant core power for at least one year, equation (3.13) gives the change of temperature in the clad due to decay heat addition over time, t, in seconds.

$$\Delta T_{DH} = \frac{(0.0825)t^{0.8}\dot{Q}_{SS}}{c_{p,fuel} \cdot m_{fuel}} \tag{3.13}$$

where $\dot{Q}_{SS}$, $c_{p,fuel}$, and m_{fuel} are the steady state core power in W, the fuel heat capacity, and mass of the fuel in the core. Adjusting this to a single fuel pin yields equation (3.14).

$$\Delta T_{DH} = \frac{(0.0825)t^{0.8}\dot{q}_{SS}}{c_{p,fuel} \cdot m_{fuel,pin}} \tag{3.14}$$

3.4.3.1 Comparing Oxide Reference Core to Hydride Cores

When comparing oxide fuel to hydride fuel over the same time period for the reference core geometry the steady state pin power is the same (74.58 kW), while the volumetric heat capacity (product of heat capacity and fuel mass) are different, as was shown in tables 3.2 and 3.7. The mass of the fuel is the product of the volume of the fuel and the fuel density, as shown in equation (3.15).

$$m_{fuel,pin} = \rho_{fuel} \cdot \frac{\pi}{4} \cdot D_{fo}^2 \cdot \Delta z \tag{3.15}$$

where D_{fo} and Δz are the fuel outer diameter and fuel height.

The fuel diameter and height is the same for the same geometry, leaving yielding the following proportionality for comparing oxide to hydride of the same geometry.

$$\Delta T_{DH} \alpha \frac{\dot{q}_{SS}}{c_{p,fuel} \cdot \rho_{fuel}} \tag{3.16}$$

With a slightly lower volumetric heat capacity the oxide fueled clad temperature will rise slightly faster due to decay than any hydride fueled clad with the same power and geometry. The initially time rate of change of the clad temperature due to decay heat for the oxide reference core and hydride reference core is shown in table 3.9.

Table 3.9: Initial Time Rate of Change of Clad Temperature, Oxide vs. Hydride

Parameter	Reference Oxide Core	Reference Hydride Core
$\frac{dT}{dt}_{DH}$	$5.52 \frac{^oF}{s}$	$4.84 \frac{^oF}{s}$

This difference is not great however, due to the similar values of the volumetric heat capacity. Therefore over the time period of interest the change in clad temperature due to decay heat will be similar, as shown in figure 3.32.

Figure 3.32: Reference Core Geometry Clad Temperature During LBLOCA

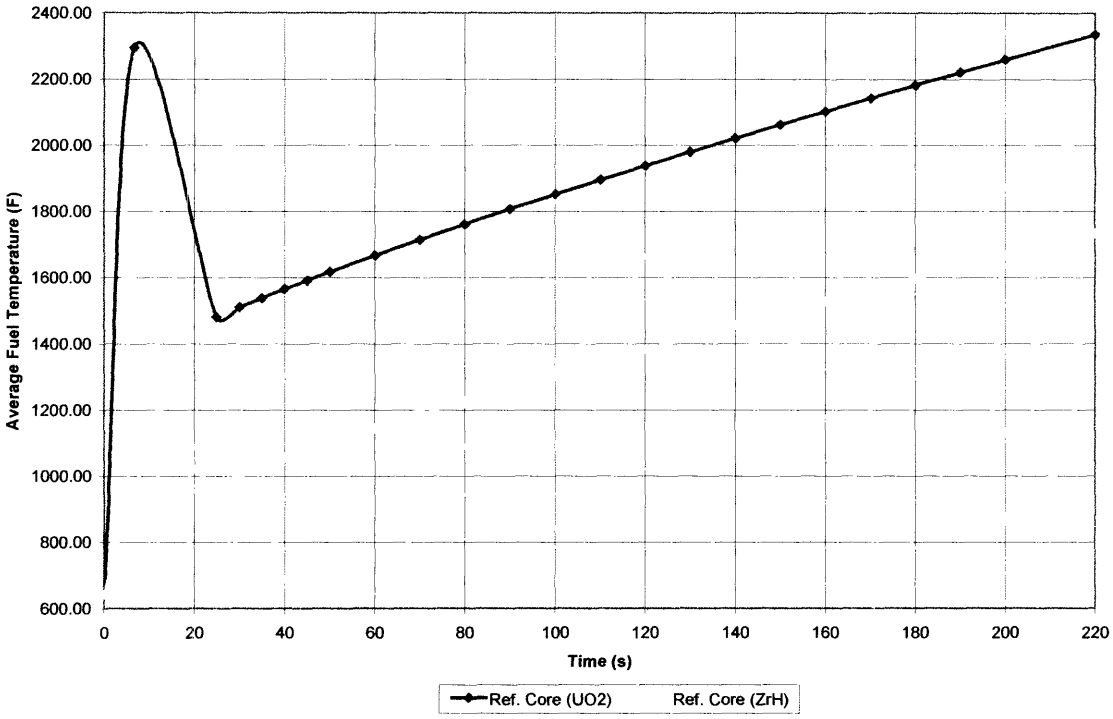

3.4.3.2 Variable Geometry

In order to compare cores with the same fuel but of differing geometry and power over the same time period, let's recall equation (3.14).

$$\Delta T_{DH} = \frac{(0.0825)t^{0.8}\dot{q}_{SS}}{c_{p,fuel} \cdot m_{fuel,pin}} \tag{3.14}$$

The heat capacity of the fuel is the same, leaving the initial steady state power and the mass of the fuel. As previously stated the mass of the fuel is a product of the fuel volume and density. The fuel density and the fuel height are the same. Thus the change in

temperature due to decay heat for cores of the same fuel type is proportional to the following.

$$\Delta T_{DH} \propto \frac{\dot{q}_{SS}}{D_{rod}^2} \tag{3.17}$$

Figures 3.33 and 3.34 show the initial time rate of change of clad temperature due to decay heat.

Figure 3.33: Initial Time Rate of Change of Clad Temperature Due to Decay Heat for Hydride Fuels, 60 psia pressure drop

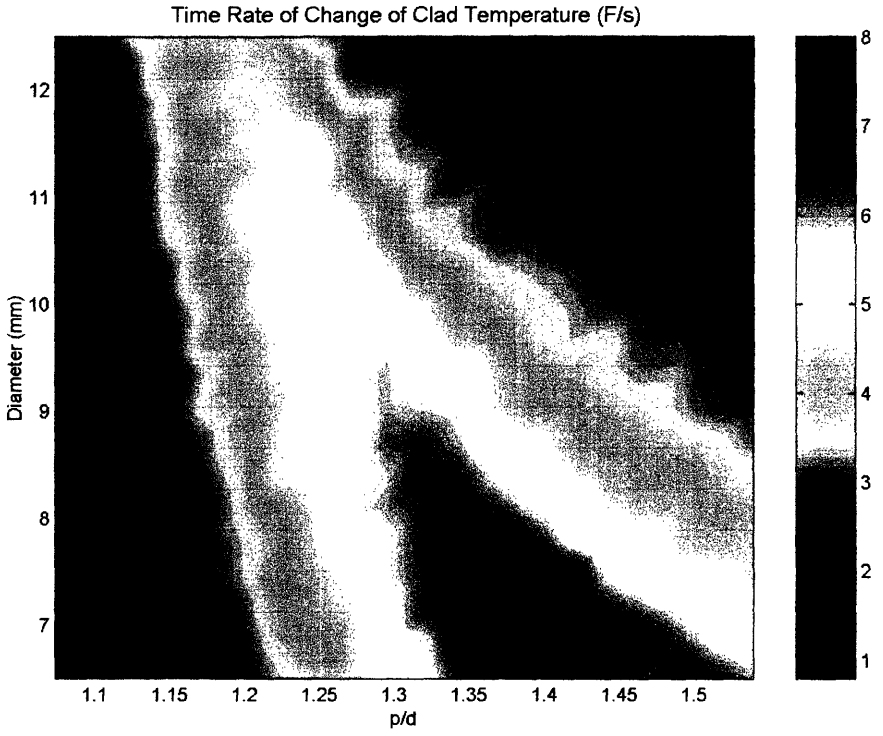

Figure 3.34: Initial Time Rate of Change of Clad Temperature Due to Decay Heat for Oxide Fuels, 60 psia pressure drop

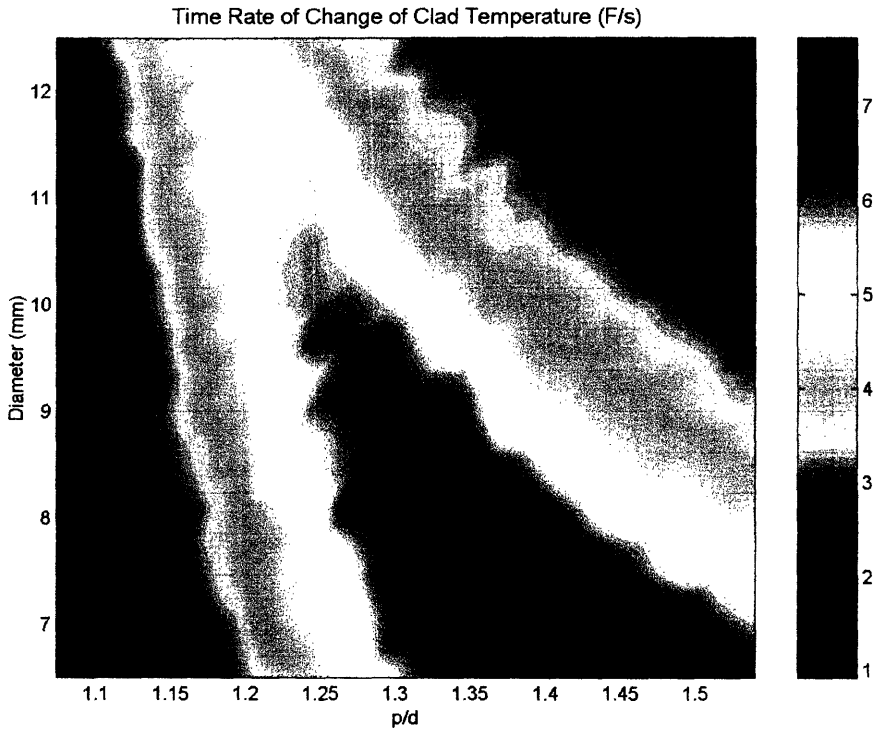

Recalling the shape of the linear heat rate with geometry as presented in figure 3.25, notice the curve of the time rate of change of the clad temperature due to decay heat is similar; however, the rods with lower diameters have higher time rate of changes in clad temperature than that of the rods with higher diameters, due to the greater weight placed upon the rod diameter term due to squaring it as shown in equation (3.17). The regions of the lowest linear heat rate, however, have low decay heat heat-up rates, regardless of rod diameter.

3.5 LOCA CONCLUSIONS

The rated power of the hydride fueled cores over the entire range of geometries is not limited by the LOCA transient. This is due to the higher thermal conductivity of the hydride fuel yielding lower initial temperatures from stored energy redistribution and

lower temperature increases over time from decay heat due to the higher volumetric heat capacity of hydride fuels. This is despite the less beneficial effects of blowdown cooling for hydride fuels. It must be noted, however, that while the hydride fuel is in no danger of melting, there does exist the potential for hydrogen to be released from the fuel. This may cause clad rupture and hence require a reduction in power. However, the added benefit of reflood would lower the fuel temperature since, as discussed previously, the temperatures presented here are used as an upper bound without the benefit of reflood and refill. This potential release during the LOCA should be analyzed more precisely for any final core design.

The rated power of certain oxide cores is limited. As with the hydride cores, the initial temperatures from stored energy redistribution is lower despite certain geometries having higher linear heat rates due to the use of liquid metal bonding vice a helium gap. However, the temperature increase of the oxide cladding due to decay heat is considerably higher for certain cores than for the reference oxide core. This is due to those particular oxide cores having higher linear heat rates and lower rod diameters than the reference core, yet without the beneficial effects of the higher thermal conductivity of the hydride fuel.

Due to the limitations on the power of the oxide cores for 60 psia pressure drop case the hydride core power map is higher. The high power geometry for the hydride cores (P/D of 1.42 with a rod diameter of 6.82 mm) yields a power of 5458.5 MW, while the high power geometry for the oxide fueled cores (P/D of 1.39 with a rod diameter of 6.5 mm) yields a power of 4990.0 MW. This gives the hydride fuels a 9.39% power increase over oxide fuels, for the 60 psia pressure drop case.

At the 29 psia pressure drop case, only the maximum power geometry (P/D of 1.49 with a rod diameter of 6.5 mm) oxide core is limited, and only by 1.6%. The maximum power hydride fueled core has a power of 4990 MW, while the maximum power oxide core has a power of 4203 MW.

4 OVERPOWER TRANSIENT

4.1 BACKGROUND

As outlined in the South Texas Project Electric Generating Station (STPEGS) Final Safety Analysis Report (FSAR) [3], there are two types of ANS Condition II overpower transients considered. These two transients consist of a main steam line break at power and a rod bank withdrawal at power.

The main steam line break overpower transient is constrained by the plants 22.45 kW/ft linear heat rate limit. The rod withdrawal transient is limited by the 18% overpower limit. This 18% overpower limit equates to a 16.03 kW/ft peak linear heat rate. Therefore, when considering a generic overpower transient, the 16.03 kW/ft limit will be breached prior to the 22.45 kW/ft limit. Therefore, the rod bank withdrawal will be covered here to encompass both overpower transients over the entire geometry range. The limiting condition for this transient will be defined as the MDNBR of the reference core during the overpower transient.

4.2 METHODOLOGY

As stated above the rod bank withdrawal at power is an MDNBR limiting transient. This means that the 18% overpower limit setpoint is based on maintaining the MDNBR above a specific value during the transient. However, as with the steady state MDNBR, the exact limit is proprietary. Thus, as outlined in the transient methodology section, the limiting MDNBR for this transient will be defined as the MDNBR of the reference oxide core during the overpower transient. According to South Texas, the overpower value of the reference oxide core at the limiting MDNBR is 17.267%. Notice that this is just below the limit setpoint of 18%. The MDNBR of the reference oxide core during this overpower transient is 1.58, at a power of 4456.1 MW_{th}. Referring to figure 4.1 these are the safety analysis limit MDNBR and power.

Figure 4.1: Separated Components of Margin for MDNBR, Overpower Transient

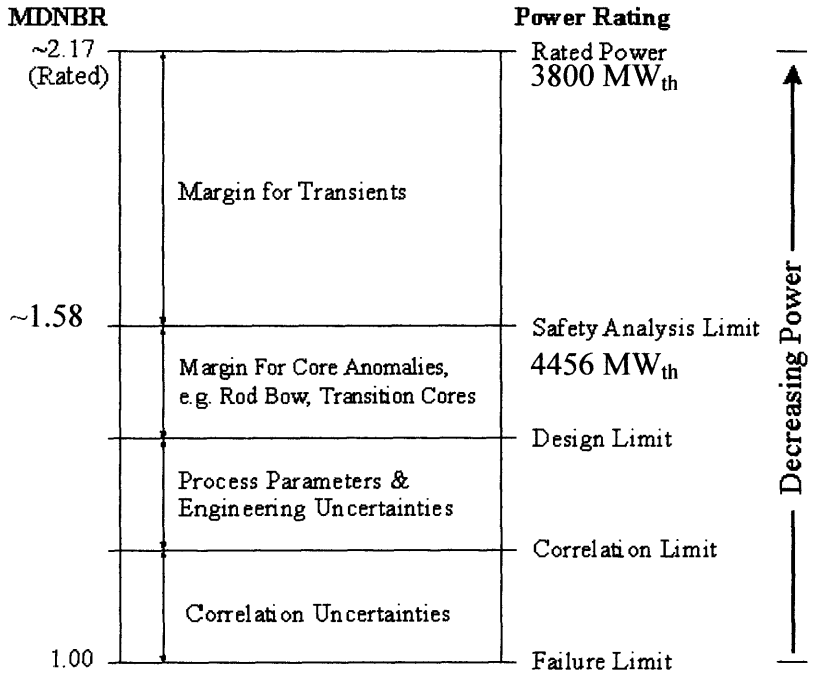

Besides the MDNBR limit, the steady state pressure drop, fuel centerline temperature, and flow velocity limits will also be applied. Table 4.1 shows the limiting criteria used during the overpower transient. All other conditions are taken from table 2.2

Table 4.1: Overpower Transient Limiting Conditions

Limiting Criteria	Value	Source
MDNBR	*1.58*	Overpower Limitations
Core Pressure Drop	*28.9 / 60 psia*	Steady State Ref. Core / Pump Limitations
Hydride Fuel Centerline Temperature / Oxide Average Fuel Temperature	*1382 °F / 2552 °F*	Hydride Fission Gas Release / Oxide Fission Gas Release
Flow Velocity	*8 m/s*	Team Judgement [2]

4.3 RESULTS

During steady state operations, the only limit difference between the oxide and hydride cores is the fuel temperature constraint. However, during steady state operations, this limit is not reached for either fuel. Therefore, the steady state power map is identical for each fuel type at each pressure drop limit. The fuel temperature limit is the only different criterion between the two fuel types for the overpower transient as well. Only at the locations where the fuel temperature criterion is reached will there be any difference between the two fuel types due to the overpower transient.

4.3.1 60 PSIA PRESSURE DROP CASE

The rated power of both the hydride and oxide cores for the 60 psia case are sharply limited at higher power regions due to the overpower transient. Figure 4.2 shows the ratio between the rated power of the hydride fueled cores given only the overpower constraints and the reference oxide core power of 3800 MW_{th}. Figure 4.3 shows the ratio between the linear heat rate and number of rods for hydride cores given only the overpower constraints and the linear heat rate and number of rods for the reference oxide core, respectively. In both figure 4.2 and 4.3 the solid black line represents where the ratio is equal to one.

Figure 4.2: Ratio of Hydride Core Rated Power Given Overpower Constraints to Reference Oxide Core Power, 60 psia Pressure Drop

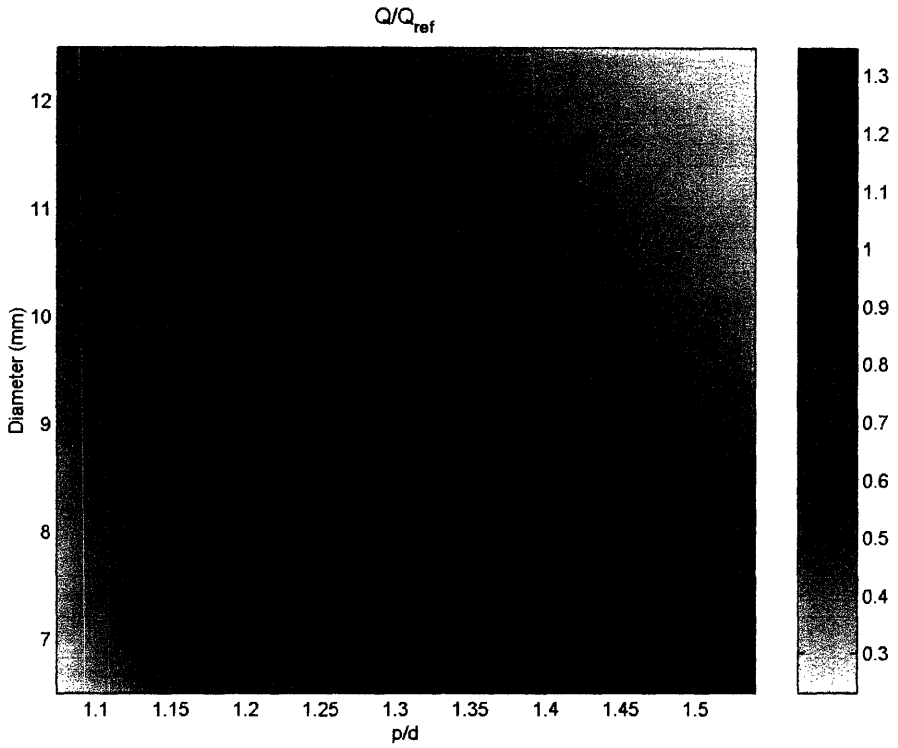

Figure 4.3: Ratio of Hydride Core Linear Heat Rate and Number of Rods Given Overpower Constraints to Reference Oxide Core, 60 psia Pressure Drop

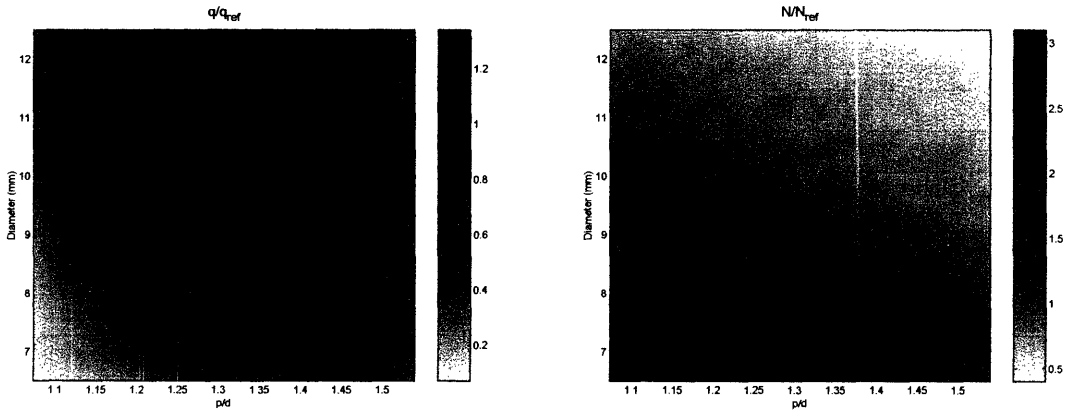

The maximum power hydride core given overpower constraints (5123.0 MW) occurs at a P/D of 1.39 with a rod diameter of 6.5 mm. This is also the maximum power oxide core for the 60 psia pressure drop case. This is due to the fact that only six hydride cores are limited by the hydride fuel centerline temperature constraint and none of the oxide cores are limited by the oxide average fuel temperature constraint. The six hydride cores

limited by fuel centerline temperature are in the high diameter, low P/D ratio region. Therefore, figures 4.2 and 4.3 are nearly identical for the oxide cores with only a small, lower power region being different, and will not be separately presented.

Figure 4.4 shows the four overpower constraints and the regions in which each criterion is limiting. In the region of maximum power, some cores are limited by velocity and others by MDNBR. However, the specific high power geometry mentioned above is velocity limited. This is a different maximum power geometry than at steady state. The steady state maximum power geometry (5458.5 MW) was at a rod diameter of 6.82 mm with a P/D of 1.42 and was MDNBR limited.

This geometry was also MDNBR limited for the overpower transient, however at a power of 5003.3 MW. This implies that during the overpower transient, the steady state MDNBR limited geometries were still MDNBR limited. However, the cores that had margin to the MDNBR limit were able to maintain a higher power for the overpower transient.

Figure 4.4: Hydride Fueled Core Limiting Criteria Given SS and Overpower Limits, 60 psia Pressure Drop

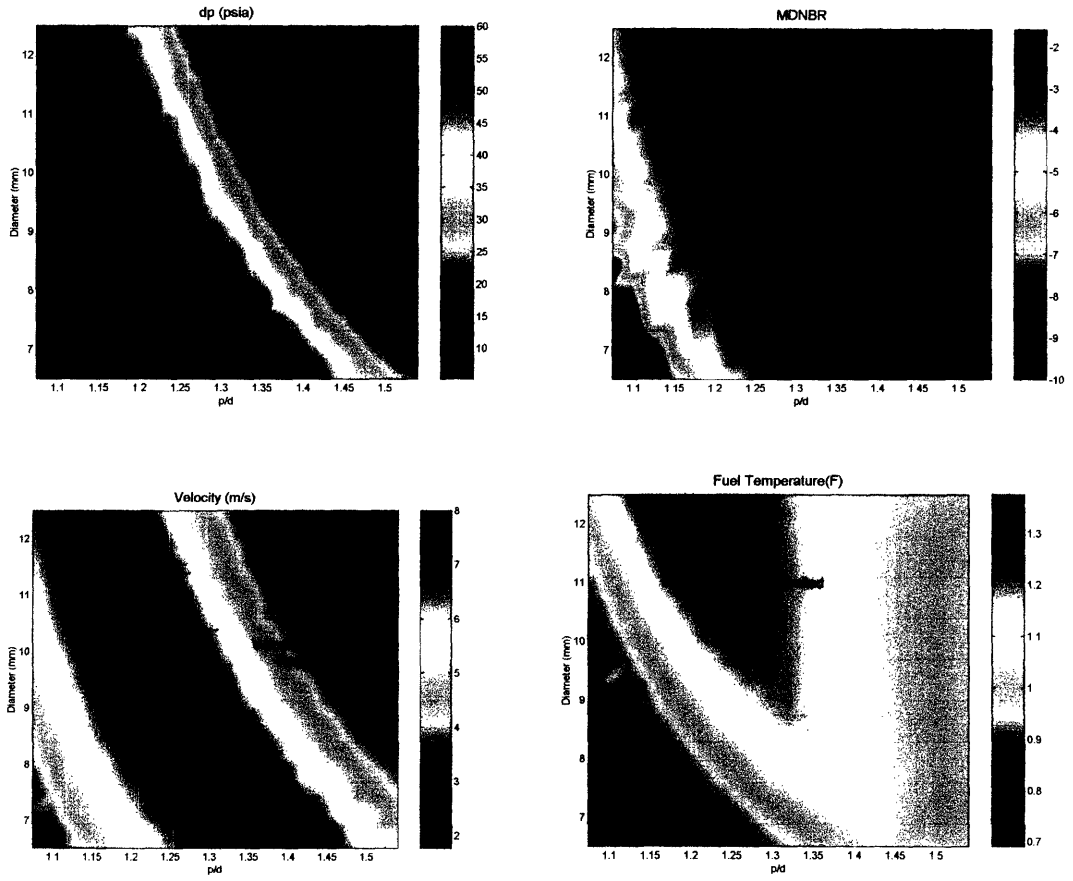

Figure 4.5 shows the regions where the maximum achievable power was limited by the overpower constraints. The purple regions are the overpower limited regions, while the light blue regions denote where the steady state constraints were either more limiting or as limiting as the overpower constraints. Recalling figures 4.2 and 4.3, notice the majority of the overpower limited regions are also the regions of highest power and linear heat rate. This is also the region where the velocity was the limiting constraint. However, due to the fact that this overpower transient is MDNBR limited, according to the STPEGS FSAR, a more thorough investigation into the velocity limits during the rod withdrawal transient could remove this velocity limit and allow for higher powers up to the MDNBR limit.

Figure 4.5: Overpower Limited Regions, 60 psia Pressure Drop

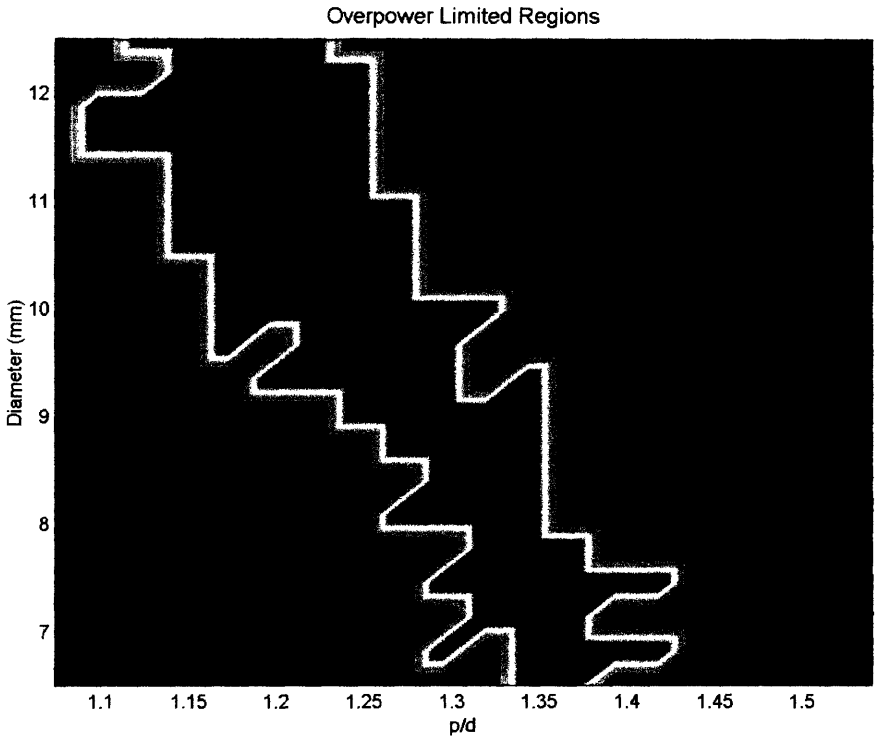

The final rated power given both overpower and steady state constraints is shown in figure 4.6, with the maximum power geometry being that which was outlined above for the overpower limited constraints alone.

Figure 4.6: Hydride Core Rated Power Given Steady State Overpower Constraints, 60 psia Pressure Drop

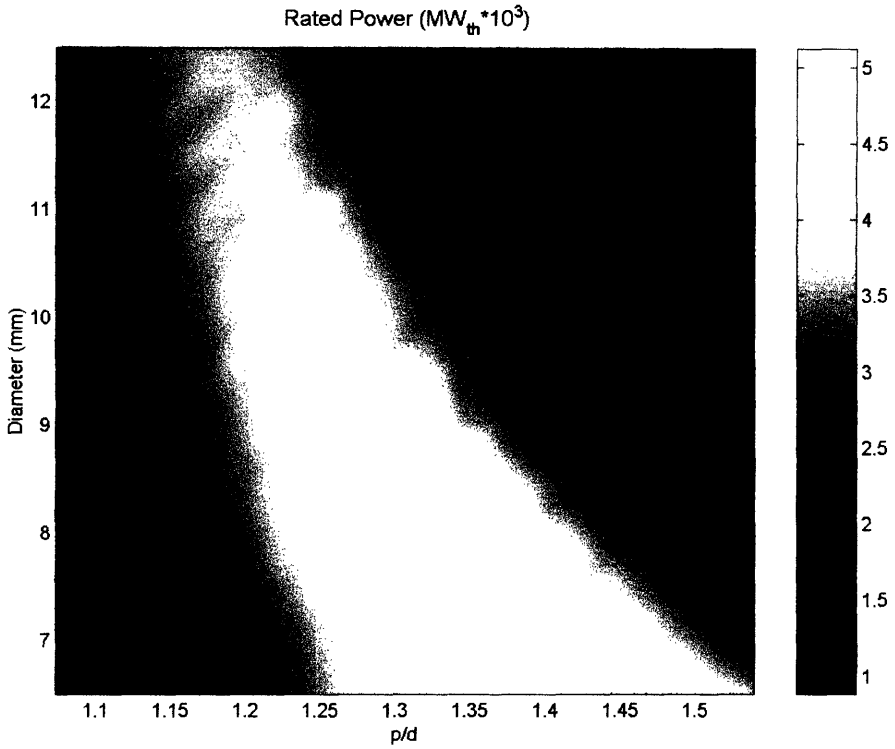

4.3.2 29 PSIA PRESSURE DROP CASE

The rated power of both the hydride and oxide cores for the 29 psia case are limited at higher power regions due to the overpower transient, but not as much as for the higher pressure drop case. Figure 4.7 shows the ratio between the rated power of the hydride fueled cores given only the overpower constraints and the reference oxide core power of 3800 MW_{th}. Figure 4.8 shows the ratio between the linear heat rate and number of rods for the hydride cores given only the overpower constraints and the linear heat rate and number of rods for the reference oxide core, respectively. In both figure 4.7 and 4.8 the solid black line represents where the ratio is equal to one.

Figure 4.7: Ratio of Hydride Core Rated Power Given Overpower Constraints to Reference Oxide Core Power, 29 psia Pressure Drop

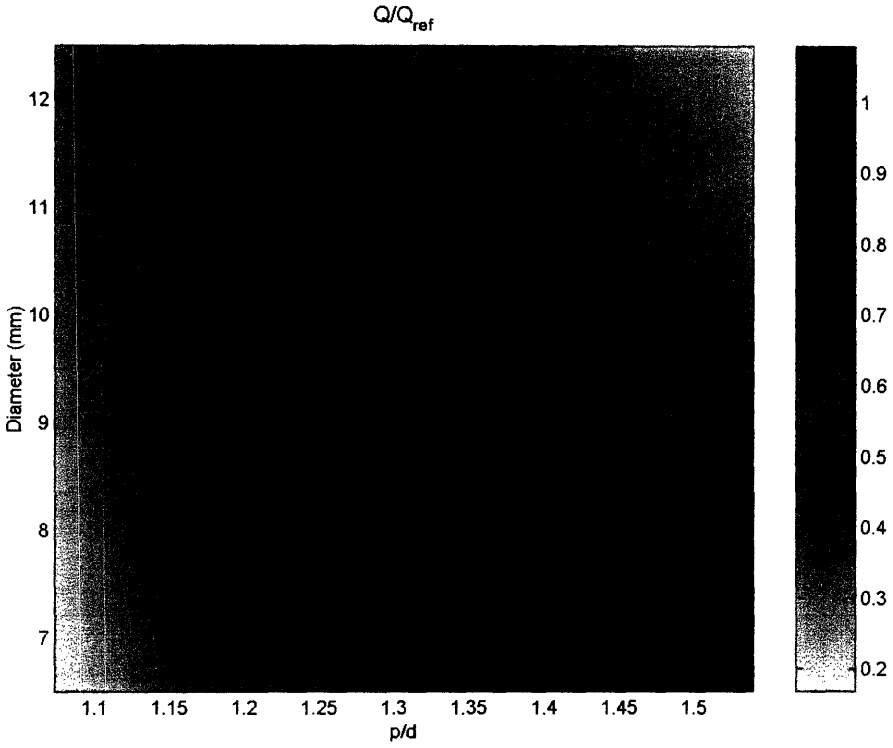

Figure 4.8: Ratio of Hydride Core Linear Heat Rate and Number of Rods Given Overpower Constraints to Reference Oxide Core, 29 psia Pressure Drop

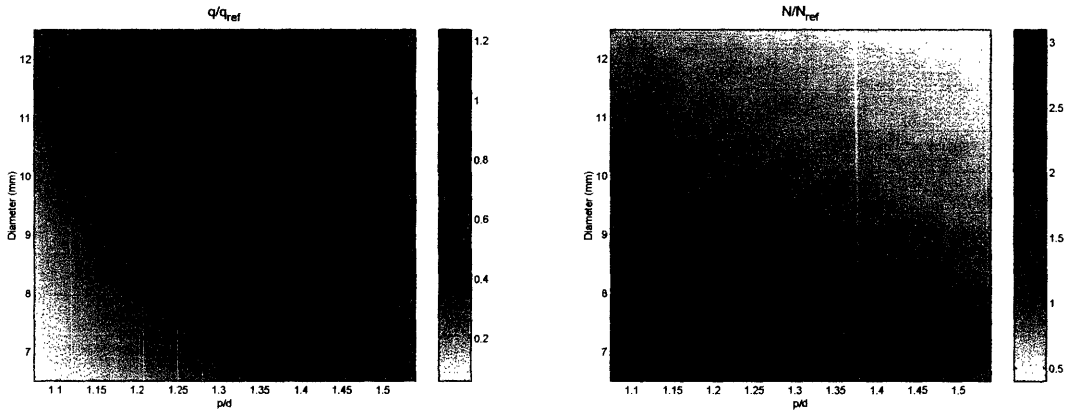

The maximum power hydride core given overpower constraints (4103.9 MW) occurs at a P/D of 1.49 with a rod diameter of 6.5 mm. This is also the maximum power oxide core for the 29 psia pressure drop case. The fuel temperature is not limiting for the overpower

transient at the 29 psia pressure drop limit and therefore the oxide and hydride behavior is identical.

Figure 4.9 shows the two overpower constraints that are limiting for the 29 psia pressure drop case and the regions in which each criterion is limiting. As with the steady state case, the limiting criterion for the maximum power core is the pressure drop constraint. This is also the same maximum power location as the steady state case; however, the power was reduced from the steady state value (4245.3 MW).

Figure 4.9: Limiting Criteria Given SS and Overpower Limits, 29 psia Pressure Drop

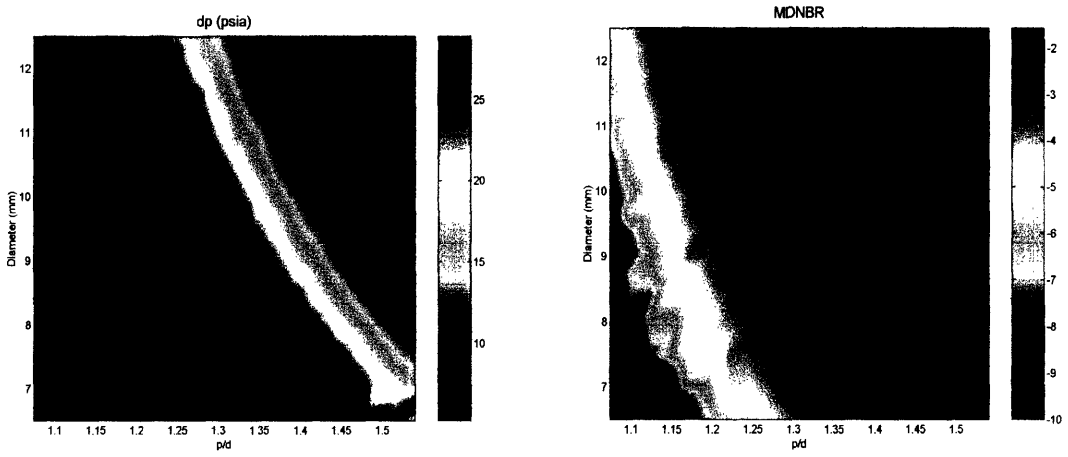

Figure 4.10 shows the regions where the maximum achievable power was limited by the overpower constraints. The purple regions are the overpower limited regions, while the light blue regions denote where the steady state constraints were either more limiting or as limiting as the overpower constraints. Recalling figure 4.8, notice the majority of the overpower limited regions are also the regions of highest linear heat rate.

Figure 4.10: Overpower Limited Regions, 29 psia Pressure Drop

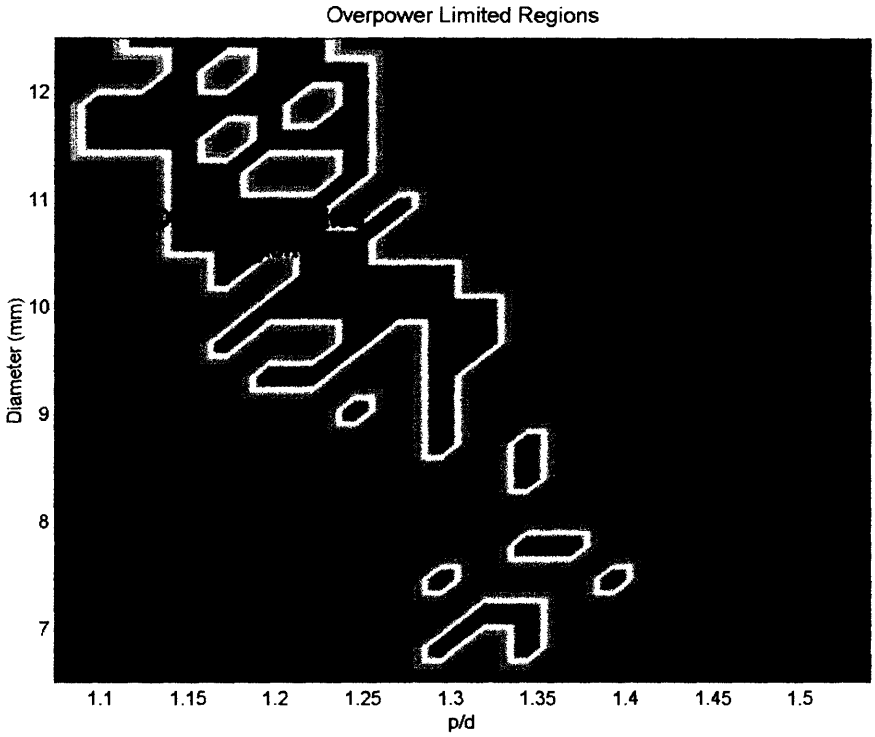

The final rated power given both overpower and steady state constraints is shown in figure 4.11, with the maximum power geometry being that which was outlined above for the overpower limited constraints alone.

Figure 4.11: Hydride Core Rated Power Given Steady State Overpower Constraints, 29 psia Pressure Drop

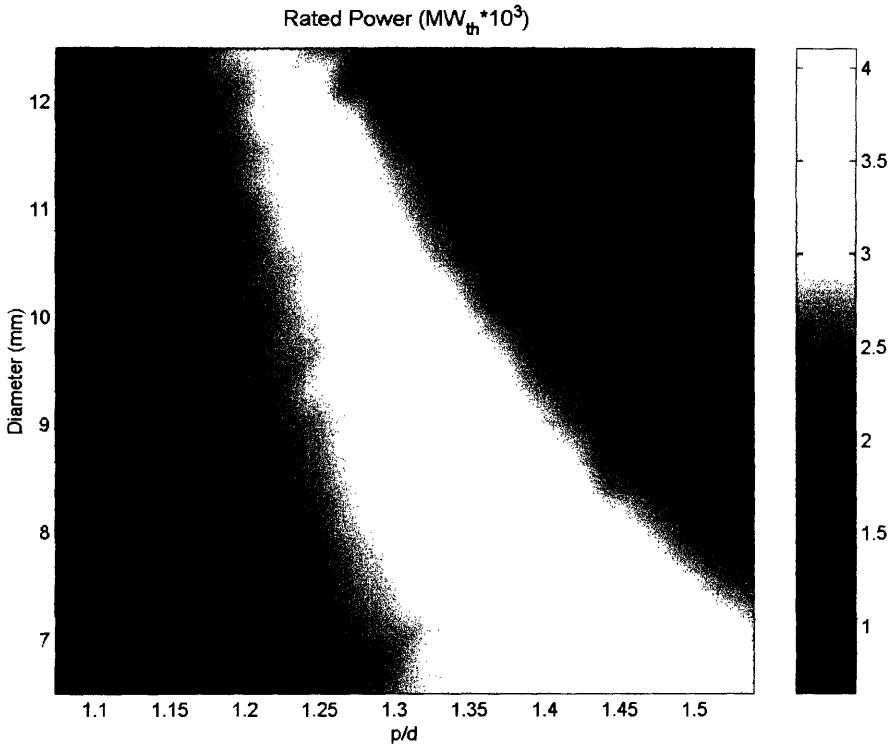

4.4 OVERPOWER CONCLUSIONS

The rated power of both the hydride fueled and oxide fueled cores for the 60 psia pressure drop case is sharply limited by the overpower transient in the regions of the highest linear heat rate and core power. The limiting criterion for the maximum power geometry during the transient is the velocity limit. A more thorough investigation into the velocity limits during the rod withdrawal transient could remove this velocity limit and allow for higher powers up to the MDNBR limit. This maximum power core considering overpower and steady state constraints (5123.0 MW) occurs at a P/D of 1.39 with a rod diameter of 6.5 mm for the 60 psia pressure drop case. This is a 6% decrease in maximum core power.

The rated power of both the hydride fueled and oxide fueled cores for the 29 psia pressure drop case is somewhat limited by the overpower transient in the regions of the highest linear heat rate. The limiting criterion for the maximum power geometry during

the transient is the pressure drop limit. The maximum power hydride core given overpower constraints (4103.9 MW) occurs at a P/D of 1.49 with a rod diameter of 6.5 mm for the 29 psia pressure drop case. This is a 3.3% decrease in maximum core power.

5 LOSS OF FLOW ACCIDENT

5.1 REGULATORY REQUIREMENTS

The complete loss of flow accident (CLOFA) is considered an ANS condition III incident (infrequent accident). However, the South Texas Project Electric Generating Station (STPEGS) Final Safety Analysis Report (FSAR) analyzed this event to ANS condition II criteria as part of the non-emergency AC event power event [3]. ANS condition II incidents are defined as faults of moderate frequency. Condition II faults are those that cause the reactor to trip, at worst, with the plant remaining capable of returning to operation. In addition these faults do not propagate to cause more serious faults.

The primary concern during a CLOFA is the rise in coolant temperature leading to a departure from nucleate boiling. As such, the MDNBR will be the limiting factor during this transient.

5.2 APPLYING LOFA TO RELAP AND VIPRE CODES

The LOFA is easily applied to the VIPRE code assuming the flow and power coastdown rates are known. Adjusting the values of linear heat rate and mass flux for each time step according to the coastdown rates and using those values as the inputs to VIPRE will yield the MDNBR of the core at each time step. The lowest MDNBR over all time steps is the actual MDNBR of the given core during the LOFA.

Acquiring the coastdown rates require use of a code such as RELAP. However, unlike VIPRE the RELAP code does not currently have the capability to be used in conjunction with MATLAB to efficiently cover the entire range of geometries.

As such, the LOFA will not be applied to the entire range of geometries. Instead it will be applied only to the high power cores and most economic core, as determined by C. Shuffler [4], in order to determine if they are limited by the LOFA.

Creating an input deck for RELAP for use with a specific core is both a lengthy process and involves the use of information not readily available. Also, RELAP will be used here for multiple core geometries. Due to these factors a generic RELAP input deck for a Westinghouse plant was used. However, this input deck was for a 12-foot core, like most Westinghouse cores. Due to the intricate nature of the code there exists no method for converting the input deck to a 14-foot core without extensive alterations to the input deck.

The rod worth curves used in the RELAP code were taken directly from the values used in the RETRAN computer code used for the FSAR. Therefore, this change in core height has no effect on the power coastdown curves. The flow coastdown curves are dependant upon the flow resistance of the core. In order to account for the difference in flow resistance between the 12-foot core used in the input deck and the reference 14-foot core a correction factor was used in the input deck.

This correction factor took the form of an extra grid spacer at the top of the core. The loss coefficient of this spacer was determined such that it would cause a pressure drop equal to the pressure drop of the last two feet of the reference core. This included gravity losses, friction losses, and spacer losses (for the grid spacers located in the last two feet of the core). The method used to determine these losses is identical to that presented later in this work is section 6.1 as well as in appendix D.

The pump information was also taken directly from the RETRAN computer code used for the FSAR. However, due to the increased potential pressure drop, the pump head had to be adjusted. However, these adjustments still cause the flow to coastdown faster than if the specific pump information for the higher pressure drop pumps were used. Therefore, the flow coastdown values obtained throughout this section are conservative.

5.3 Reference Core LOFA Analysis

The first core to be analyzed under the LOFA conditions will be the reference core (South Texas) with the geometry and operating conditions as previously shown in table 2.2. The initial steady state MDNBR of the reference core is 2.167.

Using RELAP to apply the LOFA to the reference core provides the inlet mass flow and reactor power curves. These values are normalized and are inputs to the VIPRE code. The normalized inlet mass flux is shown in figure 5.1 and the normalized reactor power is shown in figure 5.2.

Figure 5.1: Reference Oxide Core Inlet Mass Flow Rate vs Time for CLOFA

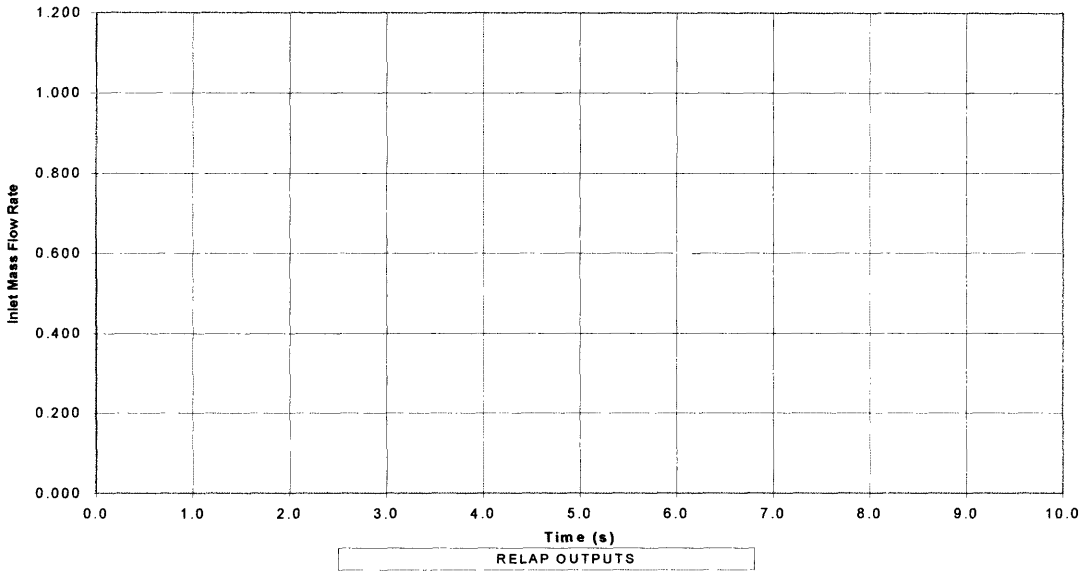

Figure 5.2: Reference Oxide Core Reactor Power vs Time for CLOFA

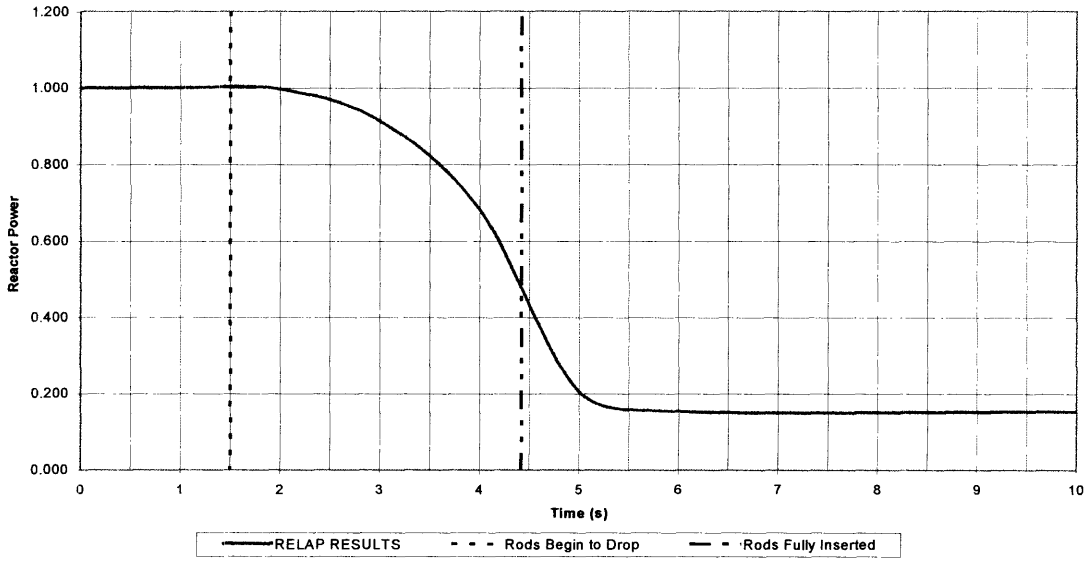

5.3.1 REFERENCE CORE CODE VALIDATION

In order to confirm these results, they were compared against the values derived in the STPEGS FSAR for the complete loss of flow accident. The comparative flow is shown in figure 5.3 and the comparative power is shown in figure 5.4.

Figure 5.3: Mass Flow Rate vs Time (Normalized) Reference Core Validation

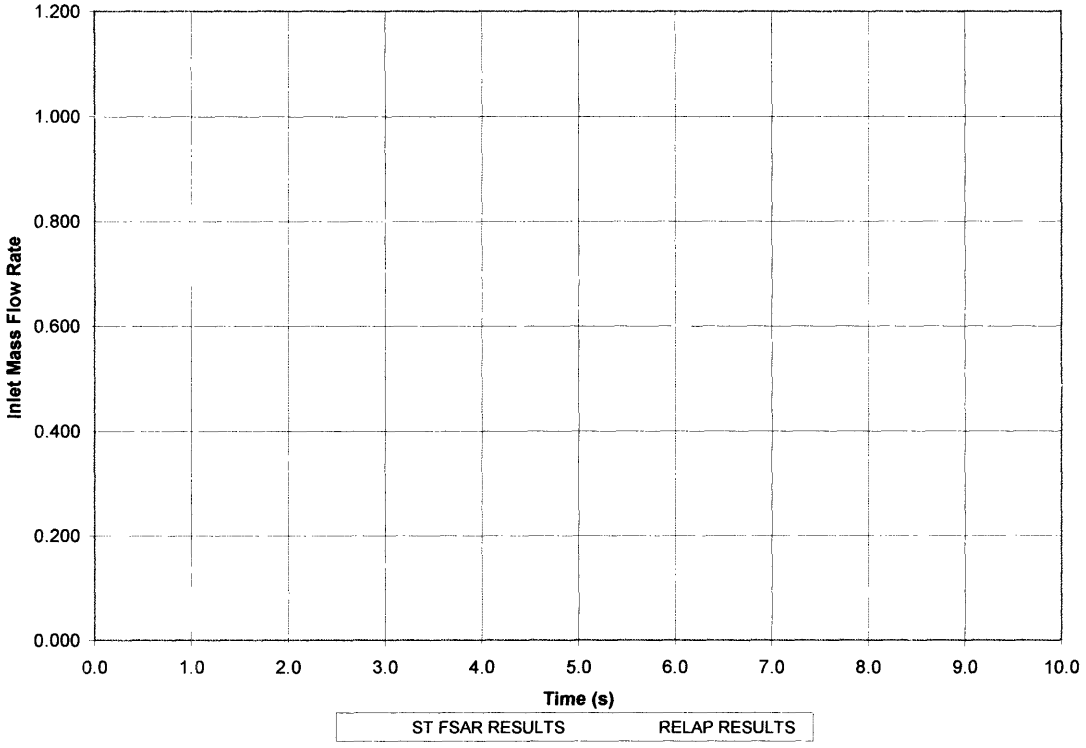

Figure 5.3 shows that the flow coast down provided by RELAP given a LOFA is similar to the flow coast down as provided by the FSAR for the same casualty. There is a slight discrepancy between the two values of approximately 10%. The pump momentum curves used in the RELAP code were taken directly from the RETRAN computer code used for the FSAR. However, the majority of the RELAP input uses a generic Westinghouse input deck. This discrepancy along with error factors inherent in the two different computer codes used (RETRAN and RELAP) explains the minor difference in

the two flow curves. In order to correct this error, a correction factor was applied to the flow coastdown curves supplied by RELAP to match them to the FSAR results.

Figure 5.4: Reactor Power vs Time (Normalized) Reference Core Validation

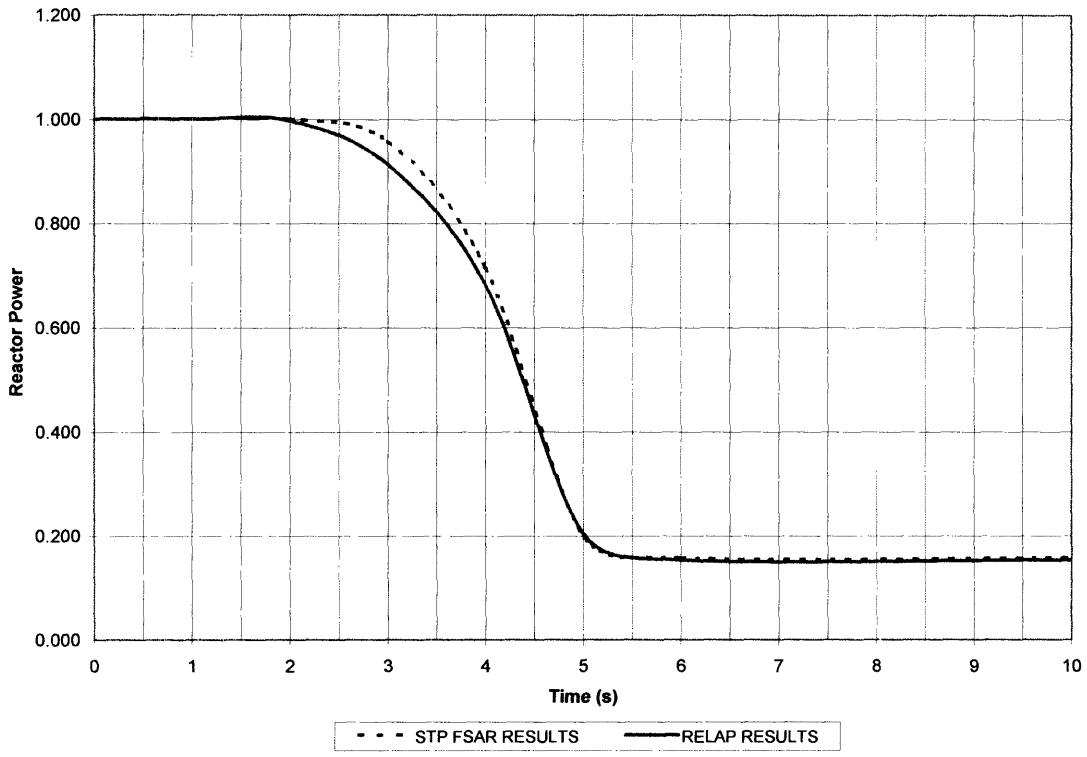

Figure 5.4 also shows that the reactor power curve provided by RELAP given a LOFA is very similar to the reactor power curve as provided by the FSAR for the same casualty. The greatest error of 4.7% occurs at 3.0 seconds. This error is down to 2.0% at 5.0 seconds remains at or below 2% thereafter. The rod worth curves used in the RELAP code were also taken directly from the values used in the RETRAN computer code used for the FSAR. As previously stated, however, most of the RELAP input is for a generic Westinghouse core. Thus, again, this discrepancy along with the inherent difference in RETRAN and RELAP explains the minor difference in the two power curves. A separate correction factor was applied to the power curve to match it identically to the reference core power curve from the FSAR.

The final MDNBR versus time curve for the reference core as provided by the VIPRE code using the corrected flow and power coastdown curves is shown in figure 5.5.

The Safety Analysis Limit MDNBR for the reference core ($MDNBR_{S.A.L., REF}$) was determined to be 1.33 and occurred 2.5 seconds into the transient. This value is the new baseline MDNBR value from which all final MDNBR values will be derived.

Figure 5.5: MDNBR vs Time (REF)

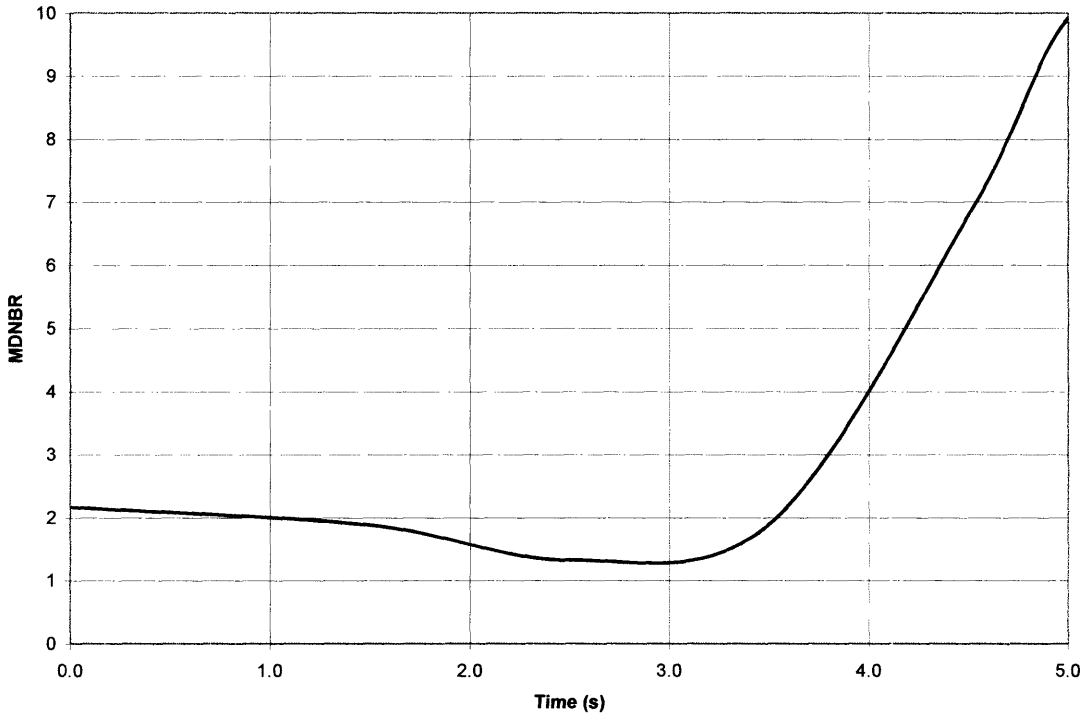

The MDNBR occurred 2.5 seconds into the transient due to the fact that the flow has been coasting down for the full 2.5 seconds; however, it takes 1.5 seconds for the rods to begin to drop once the scram signal has been initiated. Thus at 2.5 seconds into the transient the flow has dropped to approximately 83% of its initial value (for the reference core geometry only) while the power has only dropped to 99.5% of its nominal value. After this point, the rods continue to drop and are fully inserted 4.42 seconds into the transient. Once the rods begin to drop the power is driven down much faster than the flow coast down, and just before 4 seconds into the transient the normalized power is

below the normalized flow. This can be can be seen in figure 5.65 which shows both the corrected flow and power curves.

Figure 5.6: Inlet Mass Flow Rate & Reactor Power vs Time (REF)

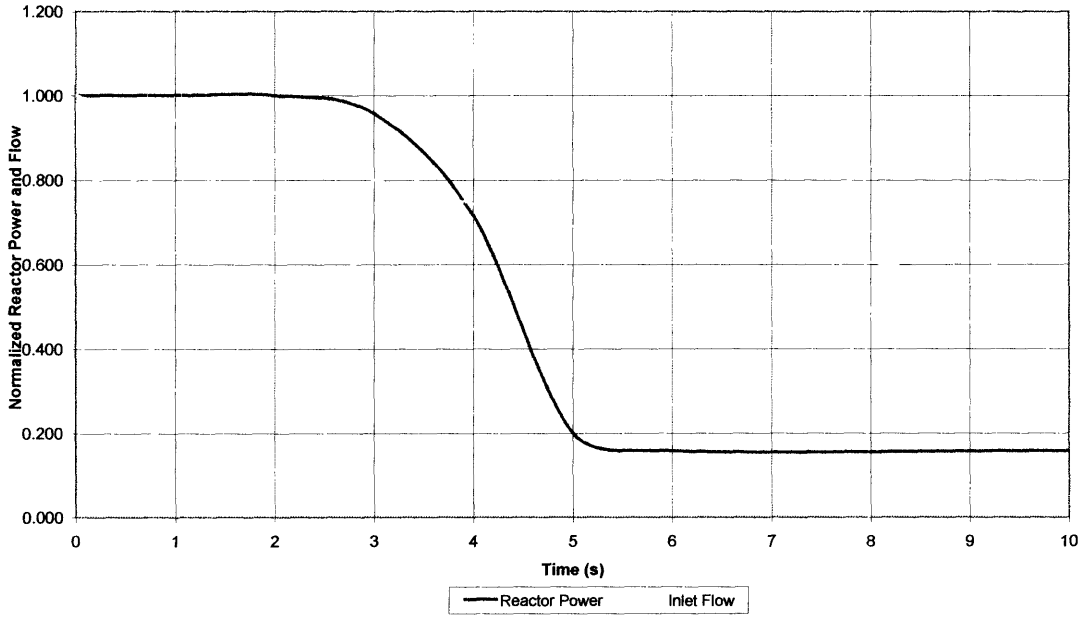

5.4 LOFA ANALYSIS

The LOFA was conducted for particular core geometries of interest. There were two criteria used for determining to which geometries this transient should be applied. The first was based solely on the maximum achievable power determined through the previous steady state and transient analyses. The second was based on which cores were the most economic [4].

5.4.1 MAXIMUM ACHIEVABLE POWER ANALYSIS

Based on the steady state, LOCA, and overpower conditions there were four particular hydride geometries of interest on the basis of maximum achievable power.

Table 5.1: Initial High Power Hydride Cores, 60 psia Pressure Drop

P/D	Diameter (mm)	Power (MW)	Mass Flow Rate (Mg/s)
1.39	6.5	5123.2	25.114
1.39	6.82	5063.2	24.820
1.42	6.82	5003.3	24.526
1.37	6.82	4883.4	23.938

Recall from section 2.2 and Appendix B that the flow coastdown rate of each core is dependant upon both the core geometry and the initial mass flow rate. The tighter the core geometry (lower P/D ratio) and the higher initial the mass flow rate the greater the flow coastdown rate. Each of the high power cores in table 5.1 is more open (higher P/D ratio) than the reference core but the power, and thus initial flow rate, is higher.

5.4.1.1 Results

Despite the fact that the lattices are more open (higher P/D ratio) than the reference core, the higher flow rates of these higher power geometries did increase the flow coastdown rates. The rated power of each of these cores was limited, as shown in table 5.2.

Table 5.2: Fianl High Power Hydride Cores, 60 psia Pressure Drop

P/D	Diameter (mm)	Power (MW)	Mass Flow Rate (Mg/s)
1.39	6.5	4820	23.63
1.39	6.82	4750	23.28
1.42	6.82	4750	23.28
1.37	6.82	4679	22.94

At each of these geometries, the final hydride fueled core maximum achievable power, and thus flow rate, is the same or higher than that of the oxide fuel core. Therefore, at each of these geometries the oxide fueled cores are limited to the same power as the hydride fuel based on the LOFA.

The higher power cores for the 29 psia pressure drop case have lower powers than those of the higher pressure drop case. They also occur at higher P/D ratios. This holds true for both fuel types for the lower pressure drop case. As expected, therefore, the LOFA does not limit the maximum achievable power of either fuel type for the 29 psia pressure drop case.

5.4.2 MOST ECONOMIC GEOMETRIES

Based on the steady state, LOCA, and overpower conditions there were two particular hydride fueled geometries of interest on the basis of economics [4].

Table 5.3: Most Economic Hydride Cores, 60 psia Pressure Drop

P/D	Diameter (mm)	Power (MW)	Mass Flow Rate (Mg/s)
1.22	9.0	3700	18.14
1.25	8.7	3800	18.63

Each of these economically advantageous cores in table 5.3 is tighter (lower P/D ratio) than the reference core but the power, and thus initial flow rate, are approximately the same.

5.4.2.1 Results

Despite the tighter core geometry (lower P/D ratio) the power, and thus flow, was at a value such that the power of these cores was not limited by the LOFA.

The most economic oxide cores had very similar power values (~ 3800 MW) but at a more open geometry (higher P/D ratio). Therefore, the maximum achievable powers of the most economic oxide cores were also not limited by the LOFA.

The lower pressure drop economic cores in the same region and have approximately the same power. These cores were also not limited by the LOFA.

The maximum achievable powers of the economically advantageous cores for both fuels and for both pressure drop cases are not limited by the LOFA.

6 HEXAGONAL WIRE WRAPPED CORES

This chapter will determine the maximum achievable power of hexagonal wire wrapped cores for steady state and selected transient conditions. This analysis will be performed for both oxide and hydride fuels for both pressure drop limited cases.

6.1 PRESSURE DROP: WIRE WRAP VS. GRID SPACERS

One of the benefits of going to a hexagonal lattice over a square lattice is the use of wire wraps vice grid spacers. In order to verify the lower pressure drop of the wire wraps for the region of interest, the pressure drop over a range of P/D values was compared for both grid spacers in a square lattice and for wire wraps in a hexagonal lattice. This initial pressure drop assessment inspects the range of P/D values at the reference pitch value of 1.26 cm by varying the rod diameter from the reference value of 0.95 cm upwards to 1.0, 1.05, 1.10, 1.15, and 1.20 cm and downwards to 0.9, 0.8, and 0.7 cm. The final analysis of the hexagonal array will include the entire range of geometries.

Using the reference core values as outlined by C. Shuffler [4] the P/D was varied as previously noted for both grid spacers in a square lattice and for wire wraps in a triangular lattice. In order to compare the hexagonal lattice to the square, the data is plotted against the hydrogen to heavy metal ratio (H/HM). The comparison between H/HM and P/D uses the method also outlined in the projects initial power and burnup analysis [2], in which both the clad thickness and gap were scaled over the entire range of diameters. For hydride fuels this range of rod diameters provides for a P/D of 1.05 to 1.80 and H/HM of 6.3 to 21.6 for the triangular lattice and 7.6 to 25.2 for the square lattice. The comparison between P/D and H/HM is shown in figure 6.1 for both oxide and hydride fuels. While this initial pressure drop assessment is for hydride fuels, the relationship between P/D and H/HM as well as all the information presented here is consistent for both oxide and hydride fuels.

Figure 6.1: P/D vs H/HM for Hydride Fuels

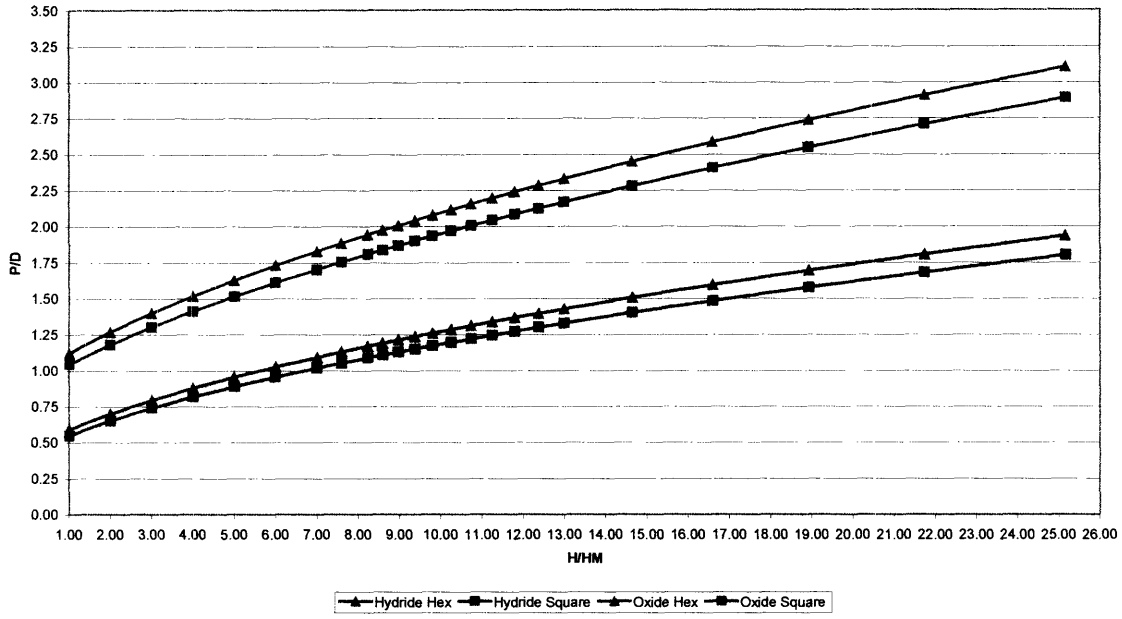

The wire wrap pressure loss was computed using the Cheng-Todreas correlation for turbulent flow wire wrap losses [8] over a range of wire wrap lead distances. The grid spacer losses were computed using the Cheng-Todreas correlation for bare rod friction losses for a square array [8] and the In et al. correlation losses for grid spacers both with and without mixing vanes [9]. Appendix D demonstrates the equations used in In et al. and compares them against the results of Rehme and DeStordeur and the manner in which these equations are used in VIPRE. The number of grids was also varied from the reference value of 2 non-mixing vane and 8 mixing vane grids up to 2 non-mixing vane and 14 mixing vane grids. Also, a range of H/D and wire lead/span lengths were compared at the reference P/D of 1.326 and 1.20.

Gravity and bundle entrance and exit effects were determined but are not shown in the current figures in order to focus upon the pressure loss difference due to the grids and wire wraps only. Table 6.1 shows the total pressure drop losses of the reference core, including gravity and bundle entrance and exit effects.

Table 6.1: Calculated Reference Oxide Core Pressure Drop

Bare Rod Losses	*8.66 psia*
Gravity Losses	*4.55 psia*
Entrance & Exit Losses	*2.25 psia*
Grid Spacer Losses	*15.44 psia*
Total Pressure Drop	*30.9 psia*

When these effects were included the square lattice reference losses were calculated to be 30.9 psia. This is very close to the value produced by VIPRE and outlined in reference [4] as 29.0 psia. The difference is due to the fact that VIPRE both continually updates the density and uses a more exact equation for the entrance and exit losses while the values used here were derived graphically.

6.1.1 RESULTS

Figure 6.2 is for the triangular lattice wire wrap pressure drop. It shows that for a given H/HM_{hex} and rod diameter as the wire wrap lead increases (i.e. H/D goes up for the given H/HM_{hex}) the pressure drop goes down. It must be noted that the H/D using the reference rod diameter of 0.95 cm and setting the lead equal to the spacing of the grids for the reference core gives an H/D of 54.8, which is outside the bounds of the Cheng-Todreas correlation which supports an H/D of 8 to 50. It must also be noted that the reference triangular lattice core has a P/D of 1.43 in order to provide an H/HM equal to that of the square lattice. At the reference case of H/HM_{hex} of 13.0, P/D of 1.43, and hence 0.881 cm rod diameter with a wire lead of 20.5 inches the triangular lattice pressure drop is 5.7 psia.

Figure 6.2: Triangular Lattice Wire Wrap Pressure Drop (P=1.26cm) (Dr=0.70cm - 1.20cm)

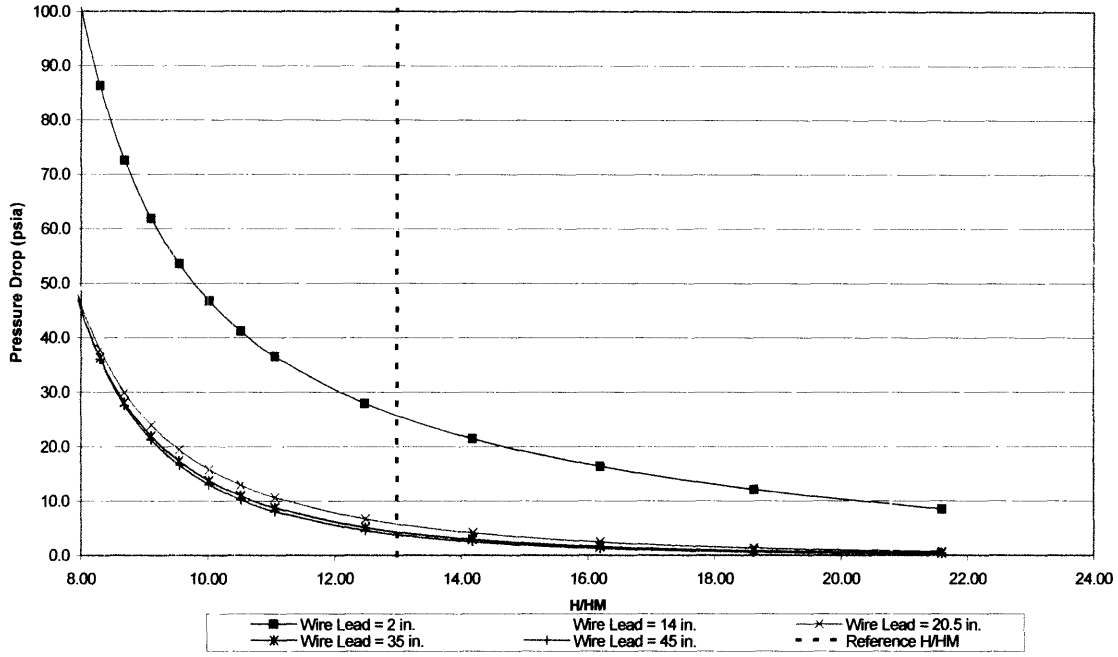

Figure 6.3 shows the square lattice grid spacer pressure drop. It shows the pressure losses as H/HM_{sq} increases and as the number of grid spacers is increased from the reference value of 10 grids (2 non-mixing vane, 8 mixing vane) up to 16 grids (2 non-mixing vane grids, 14 mixing vane grids). This shows that increasing the number of grid spacers (which corresponds to lowering the wire wrap lead in figure 6.1) does not have a significant effect on the pressure drop. Using 16 grids vice 10 raises the pressure drop by 9.5 psia (39%) at the reference H/HM_{sq}. This percentage increase roughly holds over the entire range of H/HM values. Thus, the actual pressure drop is significantly higher for tighter cores when more grids are added. At the reference case of 0.95 cm rod diameter, P/D of 1.326, H/HM_{sq} of 13.0, and 10 grids (2 non-mixing vane grids, 8 mixing vane grids) the pressure drop is 24.1 psia.

Figure 6.3: Square Lattice Grid Spacer Pressure Drop (P=1.26cm) (Dr =0.70cm – 1.20cm)

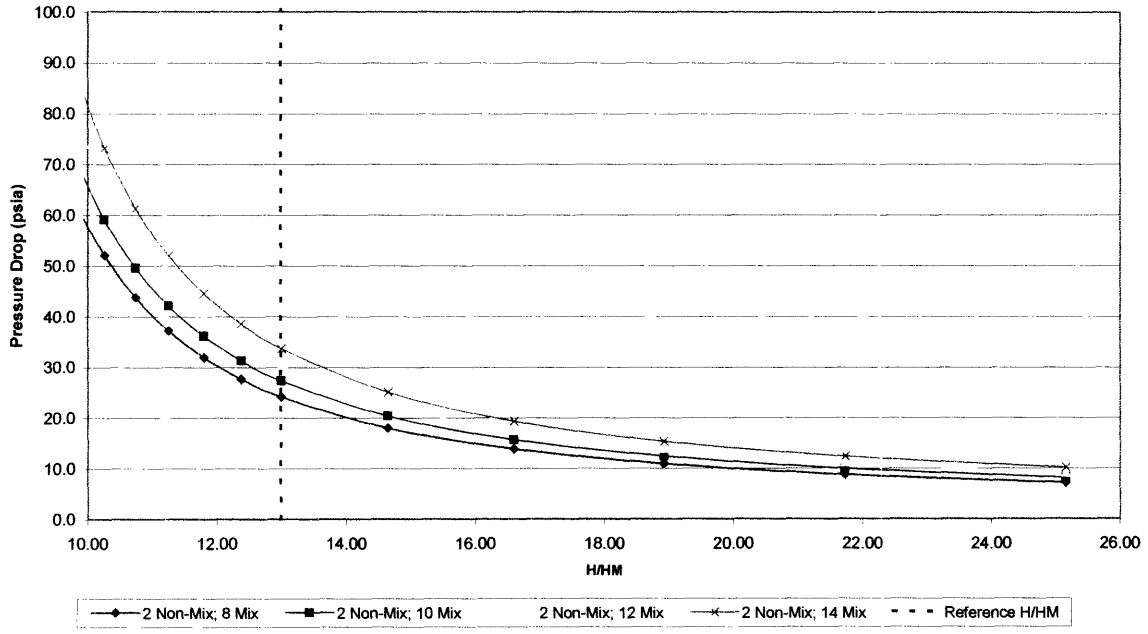

Figure 6.4 compares the pressure drop over the given H/HM range with the reference number of spacers and H/D value for the both the square lattice with grids and the triangular lattice with wire wrap, respectively. The wire wrap provides a lower pressure drop than the grid over the entire range. The pressure drop difference when comparing the two cases at the reference H/HM values is 18.4 psia (76%). While this percent difference remains fairly constant, the actual difference is even greater at lower H/HM ratios, for instance at an H/HM of 10.00 the grid loss is 36 psia higher (69%). The pressure drop difference increases as the H/HM ratio goes down, thus the wire wrap would provide the highest savings over grids at the tightest P/D ratios.

Figure 6.4: Wire Wrap (TRI) vs. Grid Spacer (SQ) Pressure Losses (Wire Lead = 20.5 in.) (10 Grids) (P=1.26cm) (Dr=0.70cm – 1.20cm)

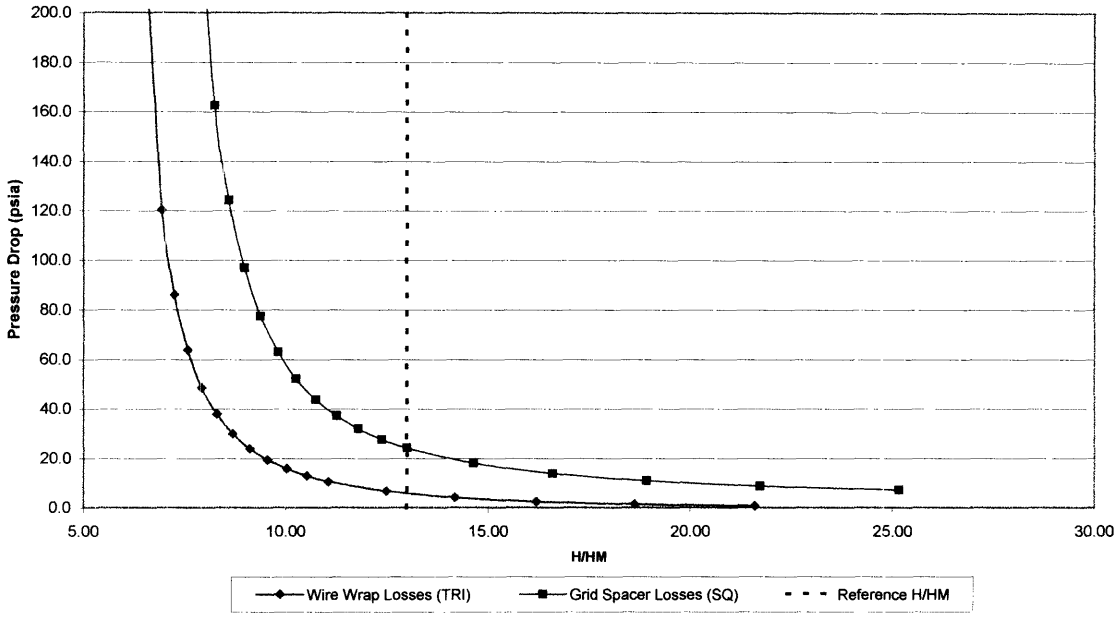

Figure 6.5 compares the pressure drop over the given H/HM range for the 15-grid case and a wire wrap with a corresponding lead of 14 inches. This case shows that at the reference H/HM values the grids give a pressure drop of 30.44 psia and the wire wrap gives a pressure drop of 8.0 psia. Thus, when more grids are added and the wire wrap lead is lowered both pressure drops increase. However, the wire wrap increase is smaller. In this case the pressure drop difference is also greatest for the wire wrap at the tighter P/D ratios.

Figure 6.5: Wire Wrap (HEX) vs. Grid Spacer (SQ) Pressure Losses (Wire Lead = 14 in.) (15 Grids) (P=1.26cm) (Dr=0.80cm – 1.15cm)

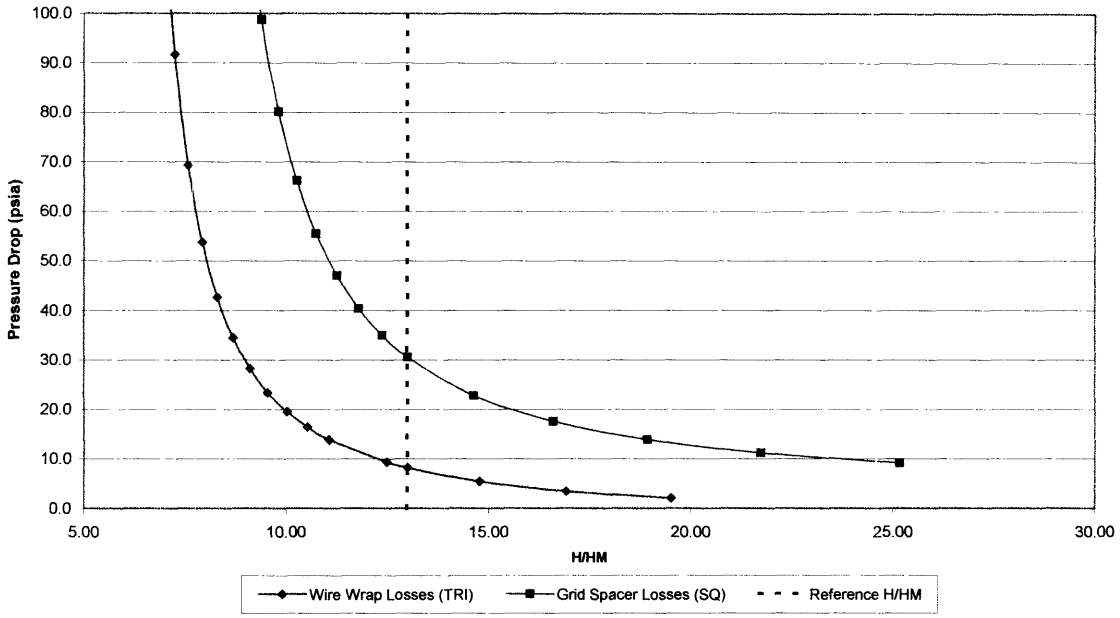

Figure 6.6 compares the pressure loss at two specific H/HM values of 13.0 (the reference value) and a tighter value of 10.3. The wire wrap lead/grid span length is varied from a value of 2 inches up to the reference value of 20.5 inches. Values greater than 20.5 inches were not tested because they would greatly exceed the range of the Cheng-Todreas wire wrap loss coefficient correlation. For both P/D values the wire wrap gives consistently lower pressure drops with the greatest savings being in the lower lead/span length region of 4 to 10 inches.

Figure 6.6: Pressure Losses vs Lead or Span Length (Constant P/D)

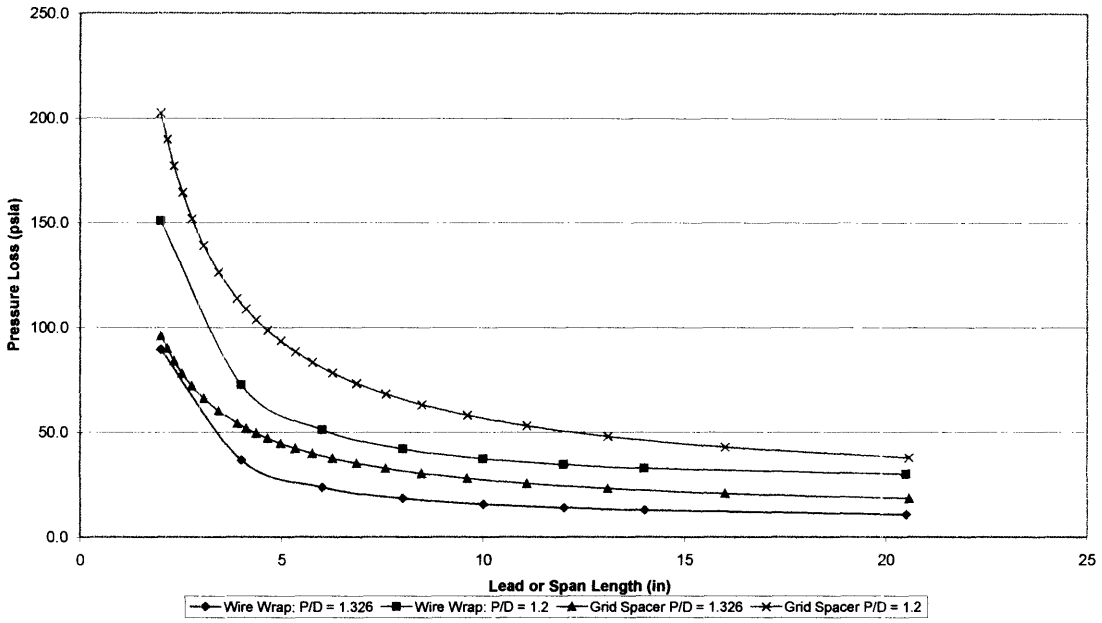

6.1.1.1 Pressure Loss Validation

In order to validate the grid spacer pressure loss coefficients the grid loss coefficients from the Comanche Peak OFA and SPC assemblies' were compared to the calculated grid loss coefficients using In et. al. The non-mixing vane grids loss values are very similar. The Comanche Peak OFA assembly non-mixing vane grids having a loss coefficient of 0.67 while the In et. al. correlation provides a loss coefficient of 0.73. The Comanche Peak OFA assembly mixing vane grids have a loss coefficient of 1.287 while the SPC assemblies mixing vane grids have a loss coefficient of 1.380. Both of these are at a P/D of 1.38. For a P/D of 1.38 the In et. al. correlation used here provides a loss coefficient of 0.87. The difference in the mixing vane values is due to the fact that mixing vanes are highly specific and proprietary and thus have a range of loss coefficients. While these values are different, they show that our grid losses are fairly consistent with industry losses. The coefficients calculated with the In et. al. correlations provide lower pressure losses than those used in Comanche Peak, and thus would show

the wire wraps to be less beneficial than if they were compared to Comanche Peak directly.

Figure 6.7 is similar to Figure 6.3 but uses the Comanche Peak loss coefficients. At each number of spacers and H/HM value the Comanche Peak losses are higher than the calculated square losses.

Figure 6.7: Square Lattice Grid Spacer Pressure Drop (COMANCHE PEAK GRID LOSSES) (P=1.26cm) (Dr =0.70cm – 1.20cm)

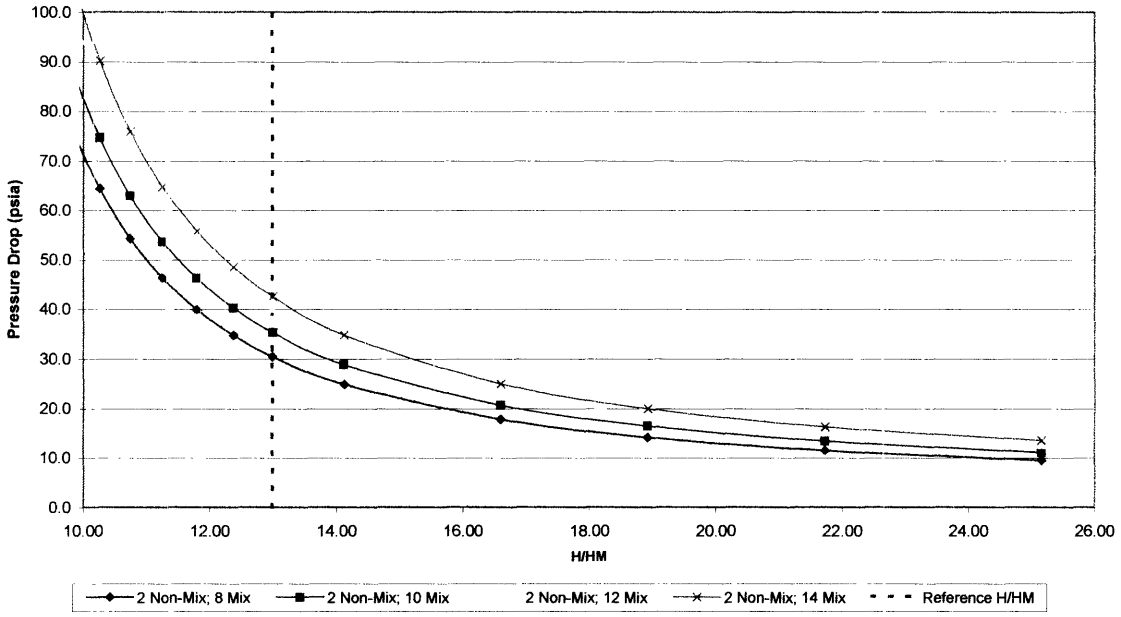

Figure 6.8 is similar to Figure 6.4 but with the Comanche Peak loss coefficients added for comparison at the reference case. This shows that the Comanche Peak loss coefficients provide a higher loss at all H/HM values than both the calculated grids and wire wrap losses.

Figure 6.8: Wire Wrap (HEX) vs. Grid Spacer (SQ) Pressure Losses (Incl. Camanche Peak Grids) (Wire Lead = 20.5 in.) (10 Grids) (P=1.26cm) (Dr=0.7cm – 1.20cm)

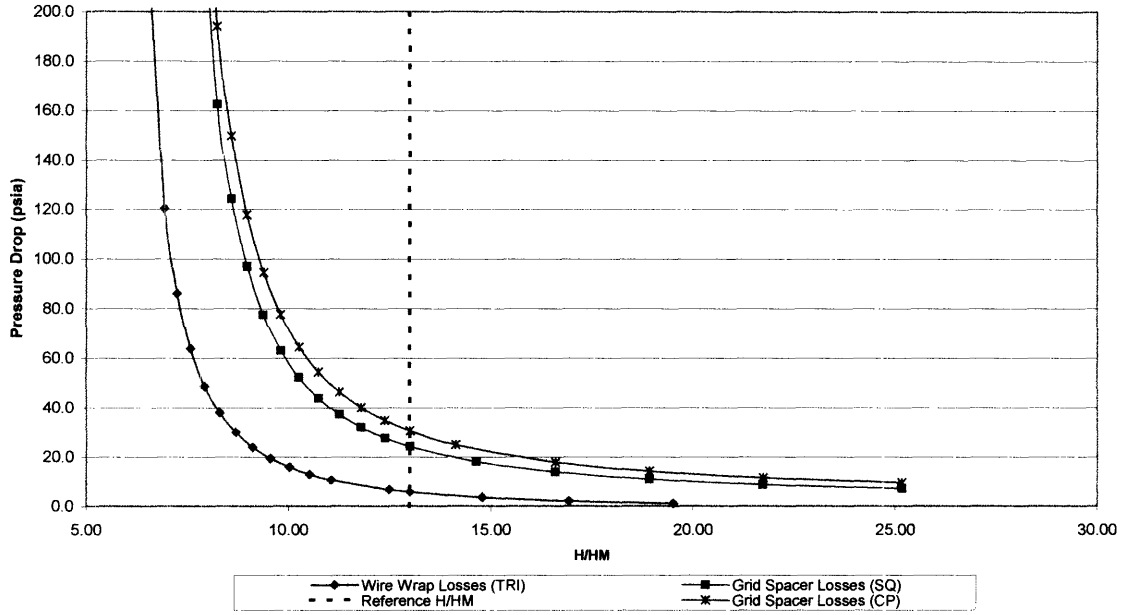

In conclusion, over the given H/HM range the wire wrap gives a consistently lower pressure drop than grid spacers for a matching grid spacer span length and wire wrap lead. These grid spacer losses are confirmed by the losses shown using the values from Comanche Peak. The greatest pressure drop savings is at the tighter P/D values (thus lower H/HM) while for the more open cores the difference in pressure drop is less significant.

6.2 WIRE WRAPPED HEXAGONAL CORE METHODOLOGY

As discussed above, in order to compare hexagonal arrays to square, it becomes necessary to use the hydrogen to heavy metal ratio (H/HM) vice pitch to diameter ratio (P/D). The comparison between H/HM and P/D uses the method also outlined in the initial power and burnup analysis [2], in which both the clad thickness and gap were scaled over the entire range of diameters.

Due to current coding limitations, it is not possible to determine the maximum power for hexagonal wire wrapped cores over the entire geometric range. However, at the same H/HM ratio and rod diameter a square and hexagonal core will have the same flow area,

heated perimeter, and wetted perimeter. Using these results, the maximum achievable power for hexagonal array cores will be equal to the square array, both using grid spacers, as demonstrated by C. Shuffler [4]. In this comparison of performance between the two geometric arrays, the wire lead in the hexagonal core was set equal to the average spacing between the grids of the square core (20.5 inches). However, the Cheng-Todreas correlation [9] used to determine the pressure loss of the wire wraps is limited to an H/D (wire wrap lead over rod diameter) of 50. At any geometry where the H/D would exceed 50 the wire lead was reduced until the value of H/D was equal to 50. For example, for the steady state maximum power geometry (P/D = 1.52, D_{rod} = 6.82 mm) a wire lead of 20.5 inches would yield an H/D = 76.5. Therefore the wire lead was set to 13.4 inches, yielding an H/D = 50.0. This reduction in wire lead will be conservative with respect to pressure loss in that it will increase the pressure loss compared to using the grid spacing value.

As discussed above, using wire wraps as opposed to grid spacers would lower the pressure drop of the hexagonal cores. In the regions where the steady state performance was limited by MDNBR, fuel temperature, or flow velocity, use of wire wraps would not change the maximum achievable power. Only in the pressure drop limited regions would the wire wrapped core maximum achievable power be different. It must be noted, however, that the MDNBR values would behave differently for a specific full core analysis of a hexagonal wire wrapped core due to differences in the MDNBR correlations.

A two-step process was used to determine the maximum achievable steady state power for hexagonal wire wrapped cores. First, an analysis was performed over the entire range of geometries using the previously outlined steady state constraints, with the exception of the pressure drop constraint. Second, the maximum flow was determined at each geometry for wire wrapped hexagonal cores in order to meet the relevant pressure drop constraint, 29 or 60 psia.

Since the enthalpy rise and inlet temperature are both constant, coolant flow is directly proportional to core power. Thus, the percent increase in flow to meet the pressure drop constraint also yielded the percent increase in both linear heat rate and core power. At each geometry, the maximum achievable power was compared for the two steps. If the

power yielded by the first step was lower, then that hexagonal wire wrapped core was limited by MDNBR, fuel temperature, or flow velocity and that power was used. If the power yielded by the second step was lower, then that hexagonal wire wrapped core was limited by pressure drop.

6.3 STEADY STATE MAXIMUM POWER

As with the square core steady state results, the steady state fuel temperature constraint was not limiting for either the hydride or the oxide fuel for the hexagonal wire wrapped cores for either pressure drop case. Therefore the maximum achievable power for the hydride and oxide fueled cores is identical over the range of geometries, for each pressure drop case.

6.3.1 60 PSIA PRESSURE DROP CASE

The steady state maximum achievable power of the hexagonal wire wrapped cores over the entire geometric range for the 60 psia pressure drop case is presented in figure 6.9. Figure 6.10 shows the ratio between the rated power shown in figure 6.9 and the reference oxide core power of 3800 MW_{th}. Figures 6.11 shows the ratio between the linear heat rate and number of rods for the rated power in figure 6.8 and the linear heat rate and number of rods for the reference oxide core, respectively. In both figure 6.10 and 6.11 the solid black line represents where the ratio is equal to one.

Figure 6.9: Hexagonal Wire Wrapped Steady State Core Rated Power, 60 psia pressure drop

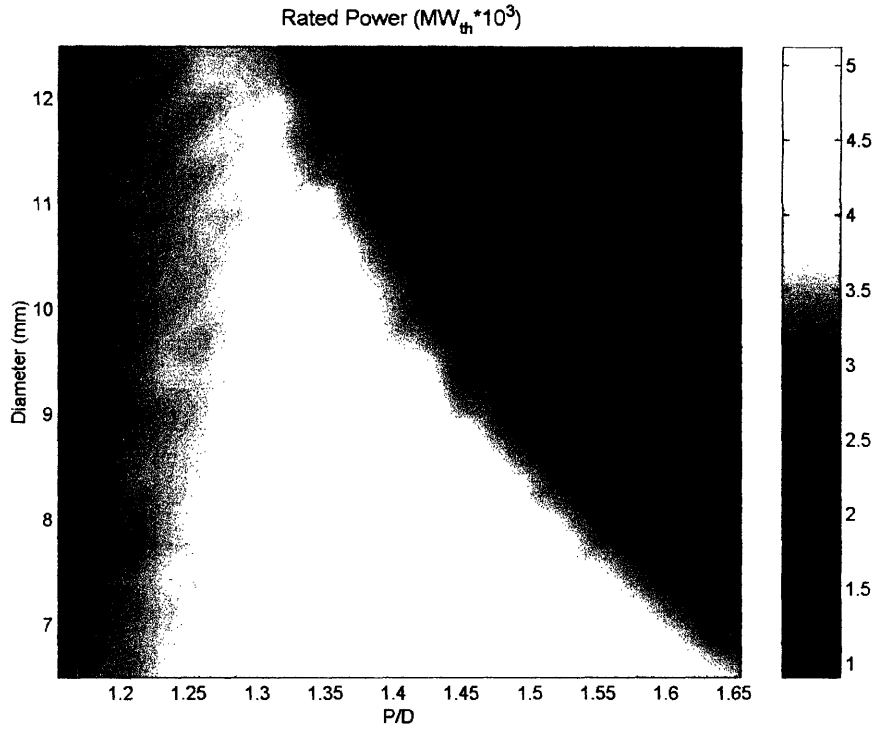

Figure 6.10: Ratio Hexagonal Wire Wrapped Steady State Core Rated Power to Reference Oxide Core Power, 60 psia pressure drop

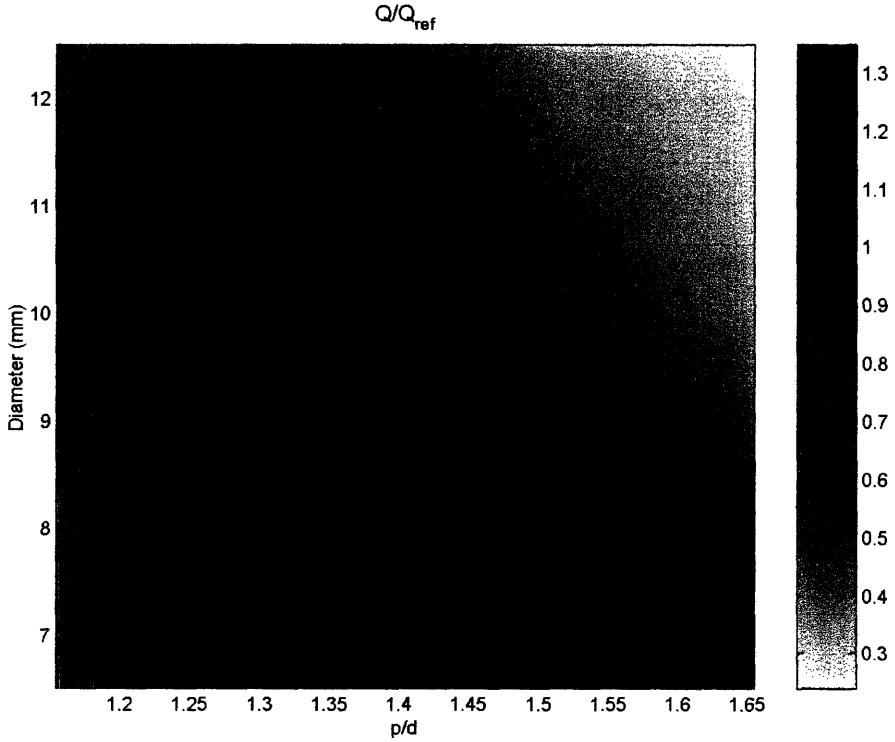

Figure 6.11: Ratio of Hexagonal Wire Wrapped Steady State Linear Heat Rate and Number of Rods to Reference Oxide Core, 60 psia pressure drop

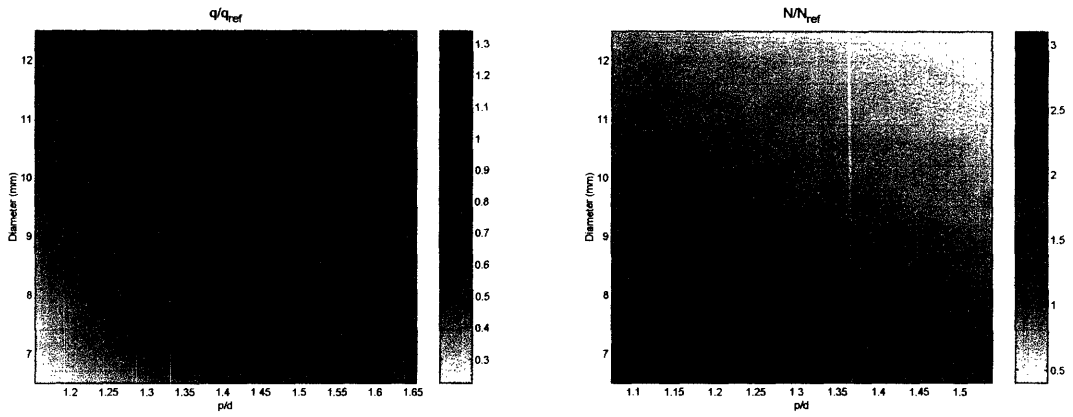

The maximum achievable steady state power using hexagonal array with wire wraps for the 60 psia pressure drop case (5458.5 MW) occurs at a P/D of 1.52 (H/HM of 15.04) with a rod diameter of 6.82 mm. This is the same H/HM and rod diameter as the maximum power square core, with the same maximum achievable power.

Figure 6.12 shows the limiting criteria and the regions in which each is limiting.

Figure 6.12: Hexagonal Wire Wrapped Steady State Limiting Criteria, 60 psia Pressure Drop

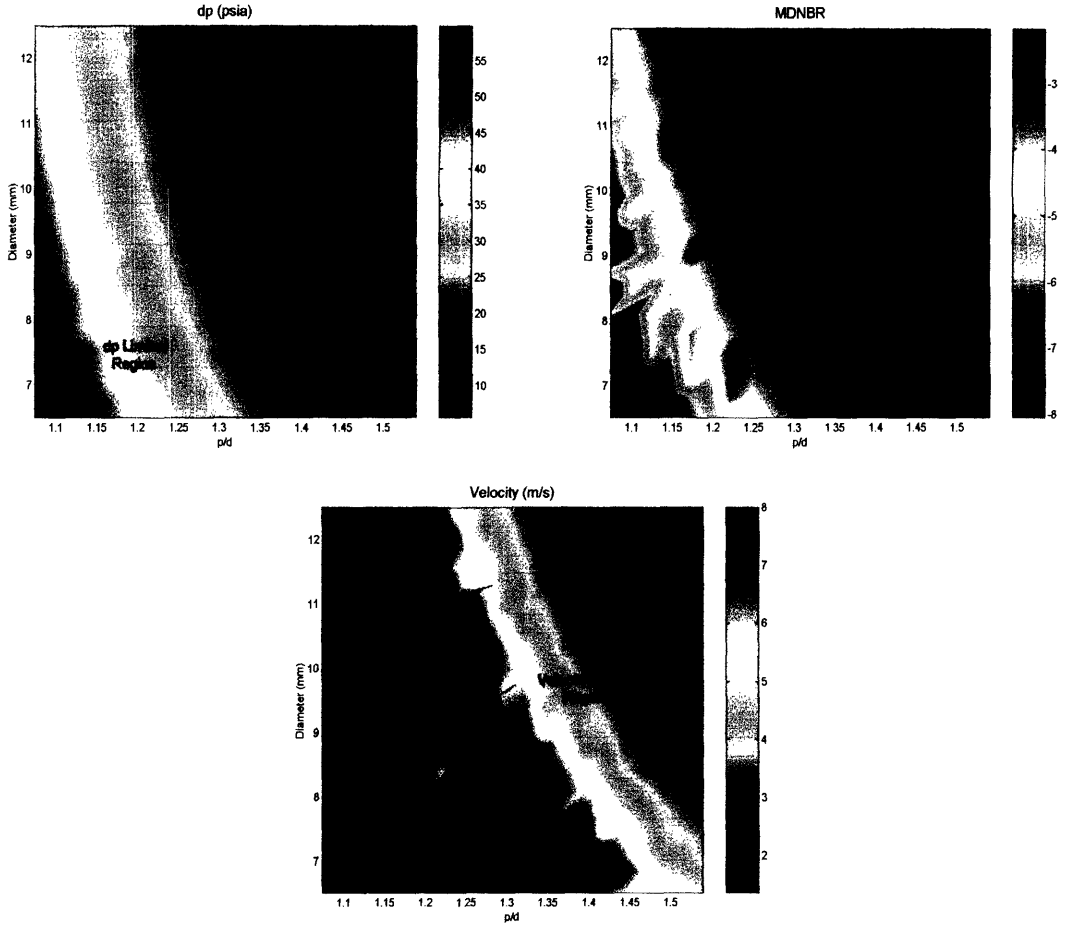

Notice, that using the wire wraps has reduced the pressure drop limited region to only the tightest cores with the smallest rod diameters. However, the velocity limit expanded to encompass the region that was previously pressure drop limited. All of the previously pressure drop limited cores did experience an increase in maximum power due to the use of wire wraps. This increase in power ranged from 300% to 5%. However, none of the power increases were enough to exceed the previous high power regions. Thus, for steady state conditions, the maximum achievable power was not affected by the use of hexagonal wire wrapped core arrays.

Unlike for the square array [4], no existing data on the vibration limits of wire wraps could be determined. If future work were to determine specific rod vibrations limits as opposed to the current flow velocity limit, these regions could possible attain a higher power, due to the effective removal of the pressure drop constraint. Also, the wire lead

was reduced for every rod diameter less than and including 10.29 mm. These smaller rod diameters encompass the majority of the velocity limited cases, specifically the higher power cases. The reduced wire lead would provide more protection against rod vibrations. Therefore, the velocity limited region most likely provides a conservative maximum power for the wire wrapped cores and the power could exceed the previous maximum achievable power given future work on wire wrap rod vibrations limits. This is further confirmed by results from the FFTF Driver Fuel [10]. After 825 effective full power days (EFPD), at 400 MW full power, with an H/D of 52.2 no wear was observed. Recalling our maximum H/D is set to a value of 50, our cores are more conservative with regards to rod vibrations and wear. This information as well as other wire wrapped vibrations results currently available are shown in Appendix E.

6.3.2 29 PSIA PRESSURE DROP CASE

The steady state maximum achievable power of the hexagonal wire wrapped cores over the entire geometric range for the 29 psia pressure drop case is presented in figure 6.13. Figure 6.14 shows the ratio between the rated power shown in figure 6.13 and the reference oxide core power of 3800 MW_{th}. Figures 6.15 shows the ratio between the linear heat rate and number of rods for the rated power in figure 6.13 and the linear heat rate and number of rods for the reference oxide core, respectively. In both figure 6.14 and 6.15 the solid black line represents where the ratio is equal to one.

Figure 6.13: Hexagonal Wire Wrapped Steady State Core Rated Power, 29 psia pressure drop

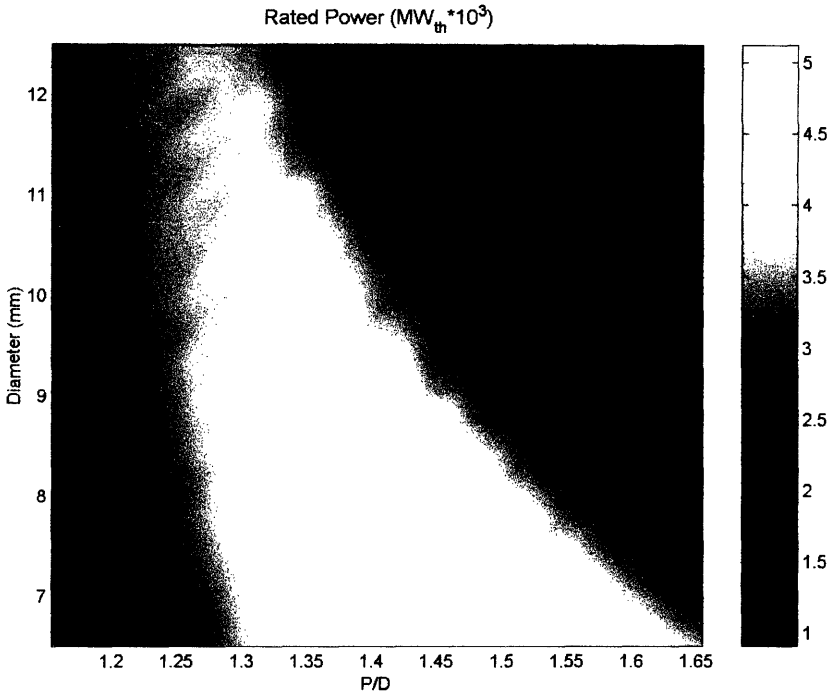

Figure 6.14: Ratio Hexagonal Wire Wrapped Steady State Core Rated Power to Reference Oxide Core Power, 29 psia pressure drop

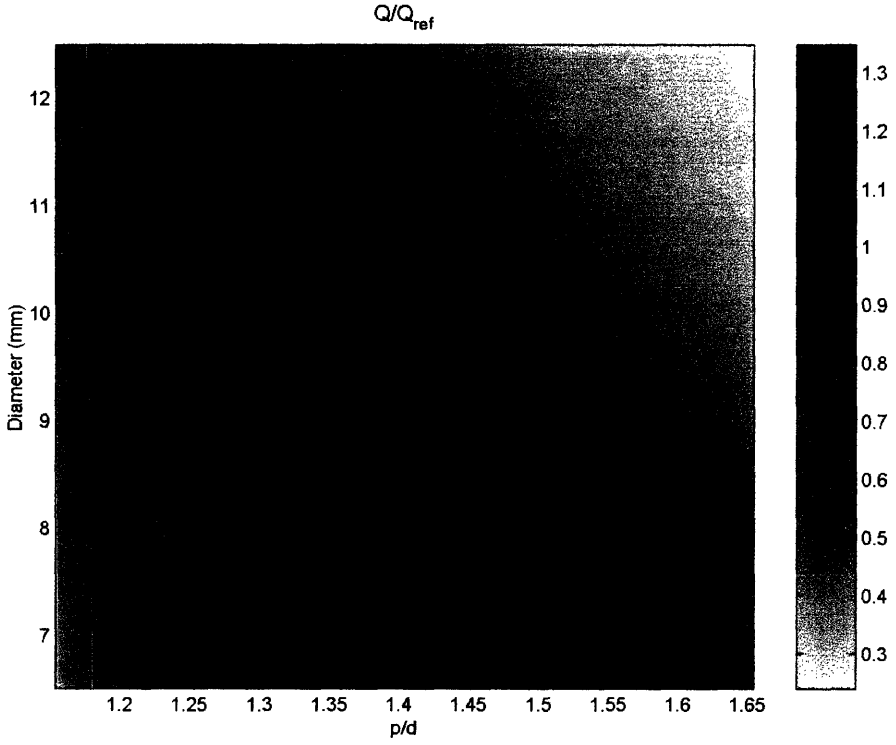

Figure 6.15: Ratio of Hexagonal Wire Wrapped Steady State Linear Heat Rate and Number of Rods to Reference Oxide Core, 29 psia pressure drop

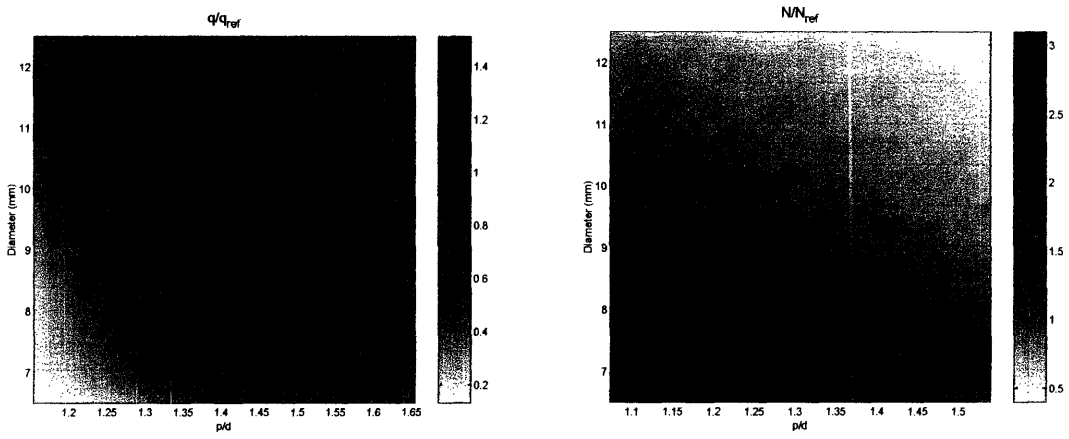

The maximum achievable steady state power using hexagonal array with wire wraps for the 29 psia pressure drop case (5458.5 MW) occurs at a P/D of 1.52 (H/HM of 15.04) with a rod diameter of 6.82 mm. This is the same H/HM (and P/D), rod diameter, and power as the 60 psia case. This is due to the lower pressure drop due to the wire wrap core. The limiting criteria at this geometry was the 29 psia pressure drop limit for the square array with grid spacers. However, for the wire wrapped hexagonal core the limiting criteria at this geometry is flow velocity.

Figure 6.16 shows the limiting criteria and the regions in which each is limiting.

Figure 6.16: Hexagonal Wire Wrapped Steady State Limiting Criteria, 29 psia Pressure Drop

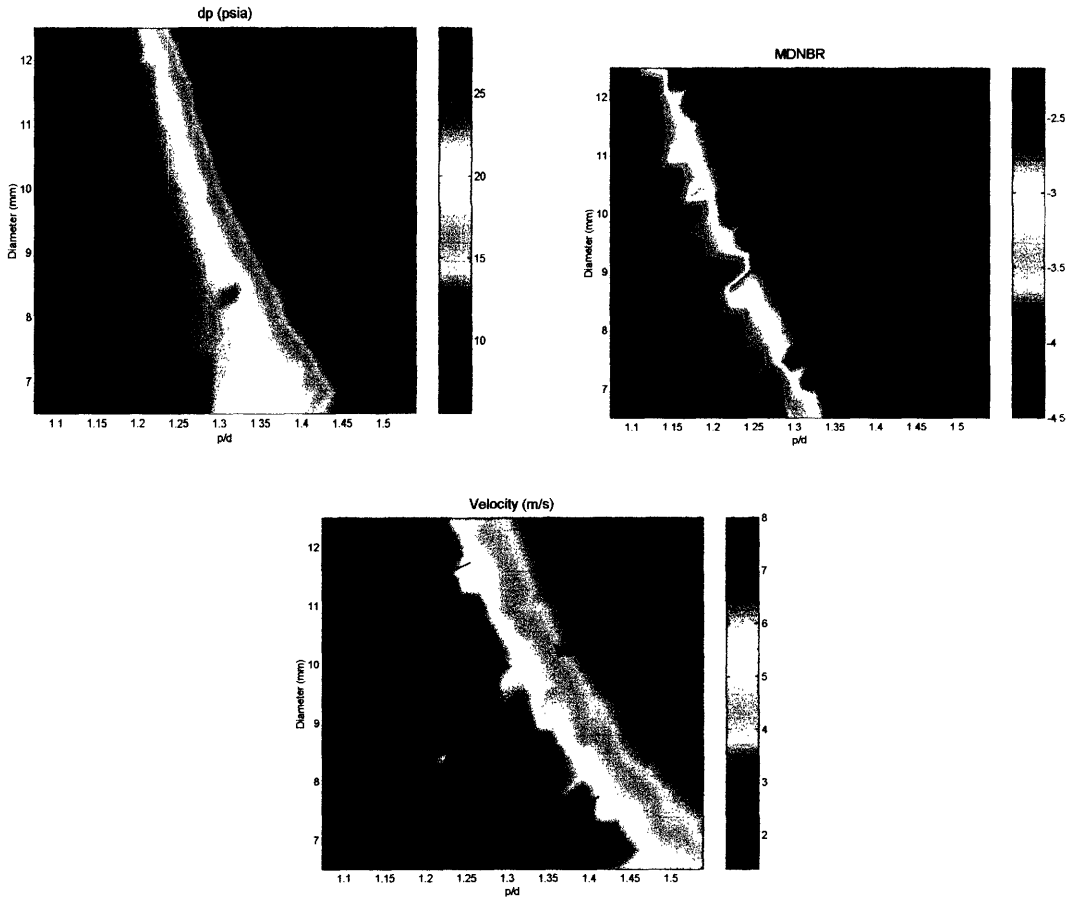

Notice, that using the wire wraps has reduced the pressure drop limited region. However, as with the 60 psia pressure drop case, the velocity limit expanded to encompass the region that was previously pressure drop limited. All of the previously pressure drop limited cores did experience an increase in maximum power due to the use of wire wraps. This increase in power was much more significant than with the 60 psia pressure drop case. Only in the region in which pressure drop is limiting will the maximum achievable power be different for the two pressure drop cases. Since the maximum power geometry is in the velocity limited region, it is now identical for each pressure drop case. Therefore, for steady state conditions for the 29 psia pressure drop case, the maximum achievable power increased by 22.2%.

As with the previous case, the maximum achievable power could be increased given future work in the area of rod vibrations for wire wrapped cores.

6.4 TRANSIENT ANALYSIS

Both the large break loss of coolant accident and overpower transient analysis were performed on the wire wrapped hexagonal cores at both pressure drop cases and for both the oxide and hydride fuel. However, the loss of flow accident analysis was not performed. At a given H/HM and rod diameter the hexagonal wire wrapped cores have lower pressure losses than the grid spacers and thus will produce less flow restriction. Given this fact and the results of the square core analysis the LOFA will not restrict the high power wire wrap hexagonal core geometries.

6.4.1 LOSS OF COOLANT ACCIDENT

6.4.1.1 Hydride Fueled Cores, 60 psia and 29 psia Pressure Drop Cases

As with the square core, the loss of coolant accident was not limiting for the hydride fueled cores for either pressure drop case. Therefore, the power map will identical to the steady state case and will not be presented here. The maximum achievable power given steady state and LOCA constraints for hydride fuel using the hexagonal array with wire wraps for the both the 60 psia and 29 psia pressure drop case (5458.5 MW) occurred at a P/D of 1.52 ($H/HM_{hydride}$ of 15.04) with a rod diameter of 6.82 mm.

6.4.1.2 Oxide Fueled Cores, 60 psia and 29 psia Pressure Drop Cases

The oxide fueled core behavior for the hexagonal wire wrapped cores was also similar to the square core behavior. There were 43 oxide fueled cores limited by the LOCA for both pressure drop cases. Each of these limited cases occurred in the regions that were MDNBR or flow velocity limited during steady state operations, which includes the high power region. Therefore each of the geometries limited by the LOCA were identical between the two cases. Only in the region in which the steady state power was pressure drop limited will the maximum achievable power be different between the two cases

given both steady state and LOCA constraints. In this region the power will be identical to the steady state power for each case. The maximum achievable power given steady state and LOCA constraints for hydride fuel using the hexagonal array with wire wraps for the both the 60 psia and 29 psia pressure drop case (4996.1 MW) occurred at a P/D of 1.42 (H/HM_{oxide} of 3.18) with a rod diameter of 6.5 mm.

6.4.2 Overpower Transient

The overpower transient limits the high power regions for the wire wrap hexagonal array in a similar manner as it did for the square array. Again, only a small region outside the high power region was limited by the fuel temperature constraint. Therefore, the power map will be nearly identical between the two fuel cases. Also, as with the LOCA analysis, the power map will only be different between the two pressure drop cases in the region where the steady state power was pressure drop limited. For both fuel types this was a small region outside the high power region. Therefore, the high power region will also be identical between the two pressure drop cases. The maximum achievable power given steady state and overpower constraints for both fuels using the hexagonal array with wire wraps for both the 60 psia and 29 psia pressure drop cases (5123.2 MW) occurred at a P/D of 1.50 ($H/HM_{hydride}$ of 14.48; H/HM_{oxide} of 3.84) with a rod diameter of 6.5 mm.

6.5 Hexagonal Versus Square Array

6.5.1 60 psia Pressure Drop Case

The use of wire wrapped hexagonal array core had a significant effect on the overall maximum achievable power map for both fuel types. The increase in power occurred in the pressure drop limited region and the new limiting criterion was the velocity limit. However, the power increase was not significant enough to surpass the single maximum power geometry for either fuel type. Therefore, the maximum achievable power for both fuel types is the same for both the square array with grid spacer and the wire wrapped hexagonal array. This maximum achievable power appears conservative based on available wire wrap rod vibrations and could be increased given future work in this area.

6.5.2 29 PSIA PRESSURE DROP CASE

Both the maximum achievable power map as a whole and the single maximum achievable power geometry increased for the lower pressure drop case for both fuel types. Due to the decreased pressure drop, the high power region was no longer pressure drop limited for the hexagonal wire wrapped core as it was for the square array. Therefore, the entire previously pressure drop limited region increased in power. The maximum achievable power for the wire wrapped hexagonal arrayed cores for the lower pressure drop case was the same as that of the higher pressure drop case for each fuel type, respectively.

7 CONCLUSIONS

There are two potential uses for the hydride fueled cores with respect to current industry practices. The first involves a minor backfit of existing cores. The minor backfit of existing LWRs seeks to limit the plant modifications required for conversion to hydride fuel use by maintaining the existing fuel assembly and control rod configurations within the pressure vessel (i.e., maintaining the same pitch and rod number in the core). In this case, upgrades to the steam generators and high pressure turbine will be required to accommodate higher powers.

The major backfit of existing LWRs does not limit the design space. The layout of hydride fuel in the core can therefore assume any combination of lattice pitch, rod diameter, and channel shape, further referred to throughout this report as a design or geometry. Note that in addition to upgrades of components on the steam side of the plant, modifications to the reactor vessel head and core internals will also be necessary.

The final results for both pressure drop cases will be shown here for these two backfit conditions, where the single highest power hydride fueled core is compared to the single highest power oxide fueled core for each backfit condition. In this specific work each of these analyses will be compared on the basis of maximum achievable power. These analyses will be presented here for both square arrays with grid spacers and hexagonal arrays with wire wraps. However, the final conclusions for the project as a whole will be made on the basis of fuel cycle cost and the cost of electricity.

7.1 MAXIMUM POWER ANALYSIS

7.1.1 MINOR BACKFIT (MAINTAIN ROD PITCH), SQUARE ARRAY

The final results for all steady state and transient constraints are identical for both fuel types for each pressure drop constraint for all P/D ratios given the reference core pitch. The steady state results are independent of fuel type since the fuel temperature constraint was not limiting. Also the overpower and LOFA results are dependant upon only the

core geometry and initial steady state power. As such they too are independent of fuel type. Only the LOCA is dependent upon fuel type.

At the reference pitch the LOCA did limit some of the oxide fueled cores for the higher pressure drop case. However, the overpower transient was more limiting than the LOCA transient at each of the geometries. The limiting constraints for the overpower transient were pressure drop, MDNBR, and flow velocity for both fuel types. At the lower pressure drop limit, the overpower was more limiting for both fuel types. Thus, the final rated power of both the oxide and hydride fuels given all steady state and transient constraints for both pressure drop cases is identical. As an example, the highest power hydride and oxide cores for the 60 psia pressure drop case are shown in tables 7.1 and 7.2.

Table 7.1 Hydride Fueled Minor Backfit Maximum Power Geometry, 60 psia Pressure Drop

Condition	P/D	Diameter (mm)	Power (MW)	Q/Q_{ref}
Steady State	1.27	9.9	4642.5	1.22
LOCA	1.27	9.9	4642.5	1.22
Overpower	1.27	9.9	4238.2	1.12
SS, LOCA, OP	1.27	9.9	4238.2	1.12

Table 7.2 Oxide Fueled Minor Backfit Maximum Power Geometry, 60 psia Pressure Drop

Condition	P/D	Diameter (mm)	Power (MW)	Q/Q_{ref}
Steady State	1.27	9.9	4642.5	1.22
LOCA	1.27	9.9	4556.9	1.20
Overpower	1.27	9.9	4238.2	1.12
SS, LOCA, OP	1.27	9.9	4238.2	1.12

Figure 7.1 shows these results in graphical form

Figure 7.1: Minor Backfit Rated Power, 60 psia Pressure Drop

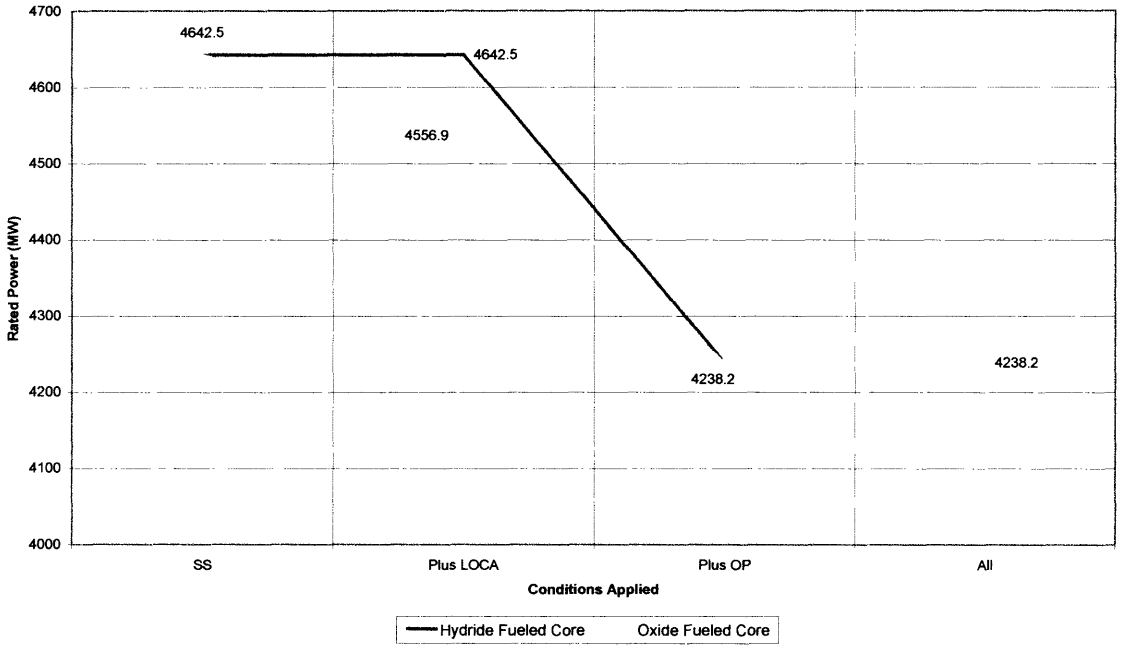

7.1.2 MAJOR BACKFIT (MAINTAIN VESSEL ENVELOPE), SQUARE ARRAY

7.1.2.1 60 psia Pressure Drop Case

The single best oxide and hydride cores both occurred at the same core geometry for the 60 psia pressure drop case (P/D = 1.39; D_{rod} = 6.5 mm). Prior to applying the LOFA, the hydride fueled core was limited by the overpower transient while the oxide fueled core was limited by the LOCA. However, after applying the LOFA, the high power cores were limited to a power below that of both the overpower and LOCA limits for both fuel types.

Tables 7.3 and 7.4 show the maximum power core geometry, power, and ratio of power to reference power for each fuel type.

Table 7.3 Hydride Fueled Maximum Power Geometry, 60 psia Pressure Drop

Condition	P/D	Diameter (mm)	Power (MW)	Q/Q_{ref}
Steady State	1.39	6.5	5308.7	1.40
LOCA	1.39	6.5	5308.7	1.40
Overpower	1.39	6.5	5123.2	1.35
LOFA	1.39	6.5	4820.0	1.27
SS, LOCA, OP, & LOFA	1.39	6.5	4820.0	1.27

Table 7.4 Oxide Fueled Maximum Power Geometry, 60 psia Pressure Drop

Condition	P/D	Diameter (mm)	Power (MW)	Q/Q_{ref}
Steady State	1.39	6.5	5308.7	1.40
LOCA	1.39	6.5	4990.2	1.31
Overpower	1.39	6.5	5123.2	1.35
LOFA	1.39	6.5	4820.0	1.27
SS, LOCA, OP, & LOFA	1.39	6.5	4820.0	1.27

Table 7.5 shows the ratio of the single highest maximum achievable power hydride fueled core against the single highest maximum achievable power oxide fueled core given all steady state and transient constraints.

Table 7.5: Comparative Power at the Maximum Achievable Power Geometry, 60 psia Pressure Drop

P/D	Diameter (mm)	Q_{hyd} / Q_{ox}
1.39	6.5	1.00

The highest maximum achievable power hydride fueled core provided no increase in power over the highest maximum achievable power oxide fueled core.

Figure 7.2 shows these results in graphical form. The dotted line represents the actual power limit of the oxide core for the overpower transient, while the solid line represents the maximum power given all transient to that point.

Figure 7.2: Major Backfit Rated Power, 60 psia Pressure Drop

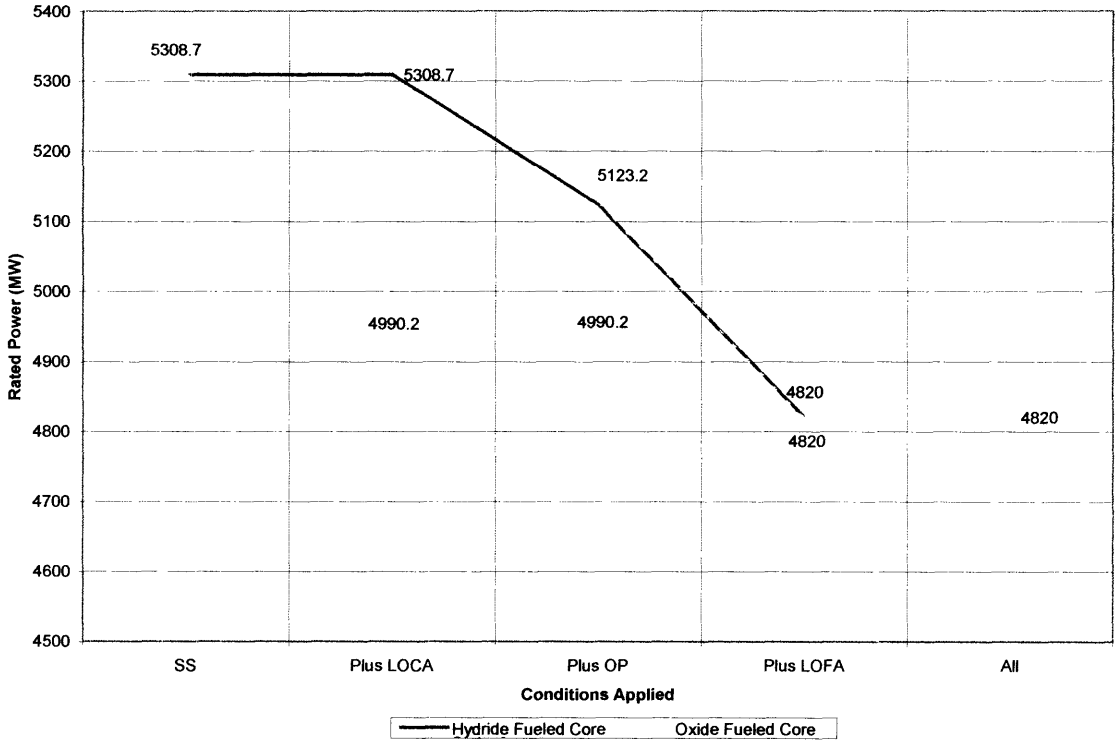

7.1.2.2 29 psia Pressure Drop Case

Considering the steady state limits and each transient event, both the hydride and oxide fueled cores yield identical power maps. Again, this is due to the fact that the overpower transient is the most limiting transient for both fuel types. The maximum power hydride and oxide core given all previously outlined steady state and transient constraints (4103.9 MW) occurs at a P/D of 1.49 with a rod diameter of 6.5 mm for the 29 psia pressure drop case.

Tables 7.6 and 7.7 show the maximum power core geometry, power, and ratio of power to reference power for each fuel type for the 29 psia pressure drop case.

Table 7.6 Hydride Fueled Maximum Power Geometry, 29 psia Pressure Drop

Condition	P/D	Diameter (mm)	Power (MW)	Q/Q_{ref}
Steady State	1.49	6.5	4245.0	1.18
LOCA	1.49	6.5	4245.0	1.18
Overpower	1.49	6.5	4103.9	1.08
LOFA	1.49	6.5	4103.9	1.08
SS, LOCA, OP, & LOFA	1.49	6.5	4103.9	1.08

Table 7.7 Oxide Fueled Maximum Power Geometry, 29 psia Pressure Drop

Condition	P/D	Diameter (mm)	Power (MW)	Q/Q_{ref}
Steady State	1.49	6.5	4245.0	1.18
LOCA	1.49	6.5	4202.8	1.11
Overpower	1.49	6.5	4103.9	1.08
LOFA	1.49	6.5	4103.9	1.08
SS, LOCA, OP, & LOFA	1.49	6.5	4103.9	1.08

Figure 7.3 shows these results in graphical form.

Figure 7.3: Major Backfit Rated Power, 29 psia Pressure Drop

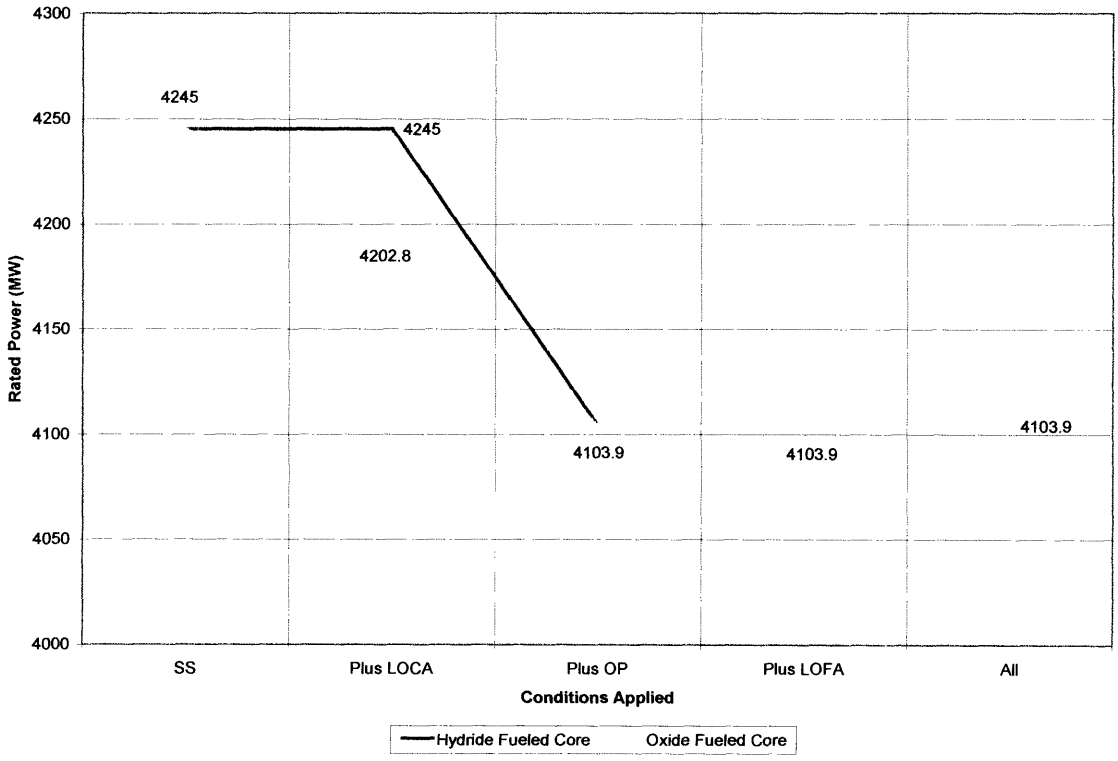

7.1.3 MINOR BACKFIT (MAINTAIN ROD PITCH), HEXAGONAL ARRAY

As with the square core, the overpower transient is the most limiting transient for both fuel types and for both pressure drop cases for all P/D ratios given the reference core pitch. Also, the oxide fueled maximum power geometry for the minor backfit was not limited by the LOCA therefore the maximum achievable power of for each fuel type for the minor backfit is identical through all cases, as is shown in table 7.8.

Table 7.8 Hydride & Oxide Minor Backfit Maximum Power Geometry, Hex Array

Condition	P/D	Diameter (mm)	Power (MW)	Q/Q_{ref}
Steady State	1.37	9.2	4684	1.23
LOCA	1.37	9.2	4684	1.23
Overpower	1.37	9.2	4254	1.12
SS, LOCA, OP	1.37	9.2	4254	1.12

Figure 7.4 shows these results in graphical form.

Figure 7.4: Minor Backfit Rated Power, Hex Array

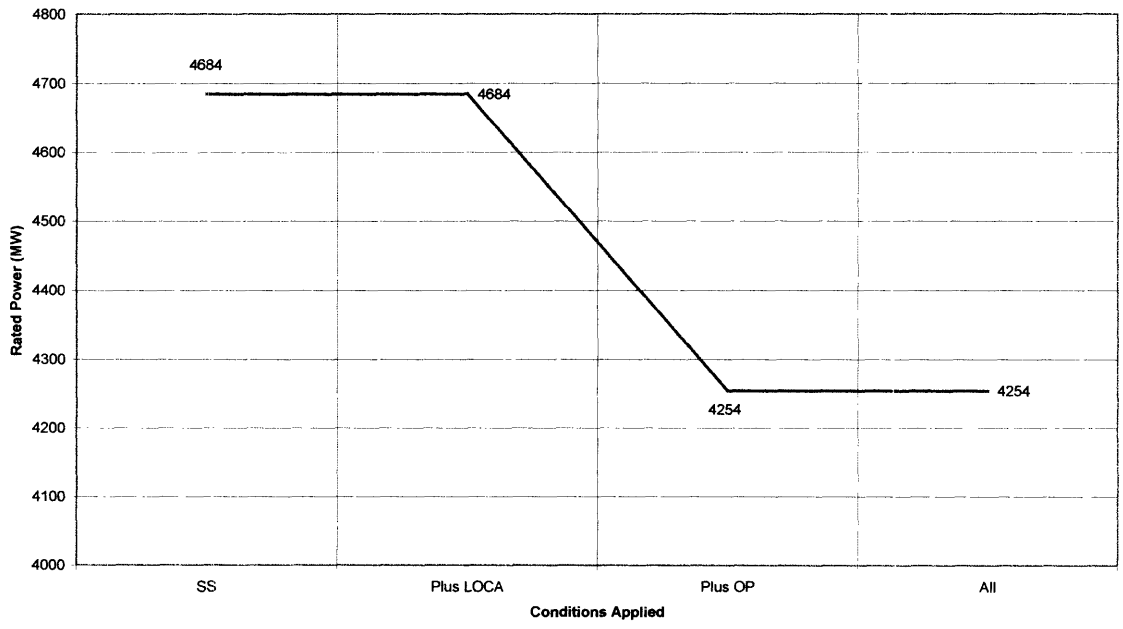

7.1.4 MAJOR BACKFIT (MAINTAIN VESSEL ENVELOPE), HEXAGONAL ARRAY

Due to the lower pressure drop performance of the wire wrap versus the grid spacers, the pressure drop criterion was only limiting in a small, lower power region. As such, the majority of the power map, specifically the high power region, is identical for a given fuel for both pressure drop cases.

Tables 7.9 and 7.10 show the single highest maximum power core geometry, power, and ratio of power to reference power for each fuel type for each condition. Recall that these values apply for both pressure drop cases.

Table 7. 9 Hydride Fueled Maximum Power Geometry, Hex Array

Condition	P/D	Diameter (mm)	Power (MW)	Q/Q_{ref}
Steady State	1.52	6.82	5458.5	1.44
LOCA	1.52	6.82	5458.5	1.44
Overpower	1.50	6.5	5123.2	1.35
SS, LOCA, OP	1.50	6.5	5123.2	1.35

Table 7.10 Oxide Fueled Maximum Power Geometry, Hex Array

Condition	P/D	Diameter (mm)	Power (MW)	Q/Q_{ref}
Steady State	1.52	6.82	5458.5	1.44
LOCA	1.42	6.5	4996.1	1.32
Overpower	1.50	6.5	5123.2	1.35
SS, LOCA, OP	1.42	6.5	4996.1	1.32

Table 7.11 shows the ratio of the single highest maximum achievable power hydride fueled core against the single highest maximum achievable power oxide fueled core given all previously outlined steady state and transient constraints for the wire wrapped hexagonal array cores.

Table 7.11 Comparative Power at the Maximum Achievable Power Geometry, Hex Array

P/D (Hyd/OX)	Diameter (mm)	Q_{hyd} / Q_{ox}
1.50 /1.42	6.5	1.025

The highest maximum achievable power hydride fueled core provides for a 2.5% increase in power over the highest maximum achievable power oxide fueled core for the hexagonal wire wrapped cores.

Figure 7.5 shows these results in graphical form. The dotted line represents the actual power limit of the oxide core for the overpower transient, while the solid line represents the maximum power given all transient to that point.

Figure 7.5: Major Backfit Rated Power, Hex Array

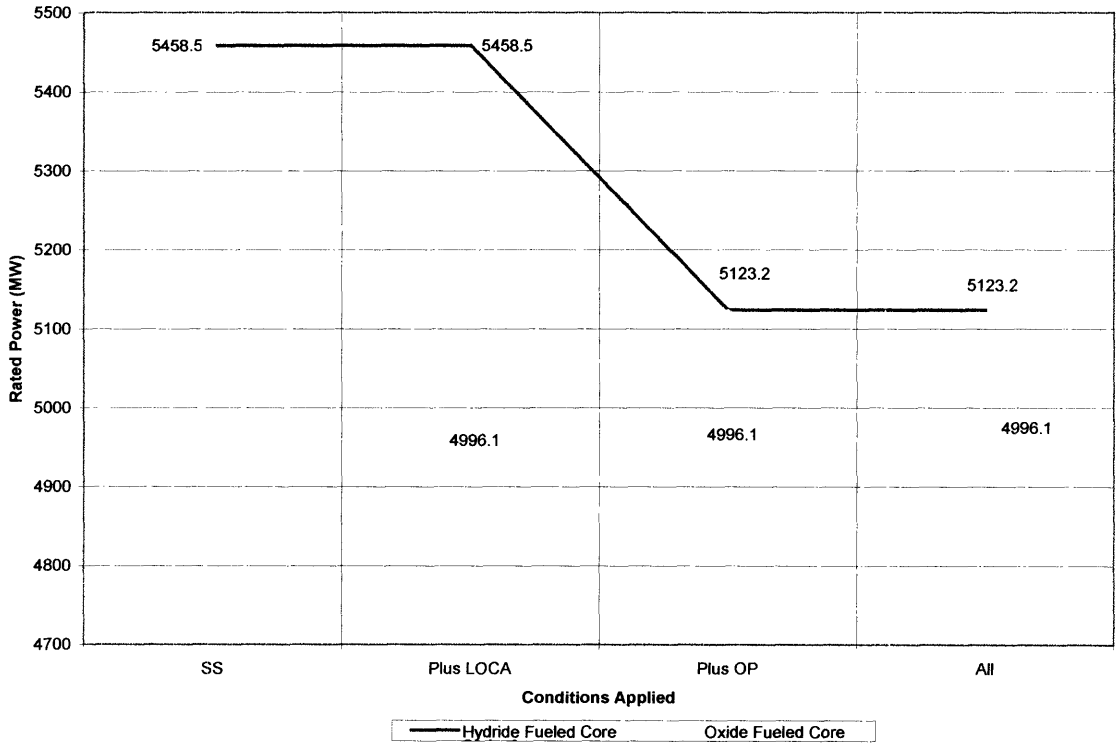

Recall, however, that given futher work in the field of wire wrapped rod vibrations, the maximum achievable power in the velocity limited region could increase. Recall the most detrimental effect on the oxide fueled cores for the LOCA came from increase in

clad temperature and that the increase in clad temperature due to decay heat was proportional to linear heat rate and inversely proportional the square of the rod diameter. The high power region that was velocity limited for the hexagonal array cores was also the lower diameter region. Therefore, potential increases in power in that region would be limited for the oxide fueled cores due to the LOCA constraints, but not for the hydride fuels.

7.2 ECONOMIC ANALYSIS

Following the steady state, LOCA, and overpower analysis, C. Shuffler completed an economic analysis [4] for each fuel type and pressure drop condition. The most economic cores were determined and the LOFA was performed on these geometries as well as the maximum power geometries.

The maximum achievable power of the economically advantageous hydride and oxide fueled cores for the 60 psia pressure drop case were not limited by the LOFA. The power for each fuel type for the lower pressure drop case is equal to or less than that of the higher pressure drop case. Therefore, the most economically viable hydride and oxide cores for the lower pressure drop case were also not limited by the LOFA.

The final economic results are presented by C. Shuffler [4].

8 FUTURE WORK

The future work for the hydride project that emerged from the work done for this thesis is listed in this chapter.

8.1 VIBRATIONS ANALYSIS FOR WIRE WRAPPED HEXAGONAL CORE GEOMETRIES

As demonstrated in chapter 6, wire wrapped hexagonal cores provide for higher power cores, specifically for tighter cores, due to the lower pressure drop. However, the best judgement flow velocity used in this work for the wire wrapped cores appears to be too conservative. A more detailed vibrations analysis similar to the one performed for the cores that utilize grid spacers [4] may allow for an increase in maximum achievable power. Also, this region is more restrictive for the oxide fuel due to LOCA constraints than for the hydride fuel and may increase the ratio of maximum hydride to oxide achievable power.

8.2 ADDITIONAL HYDRIDE FUEL TYPES

Due to fuel cycle lengths the hydride fuel is not as economically as viable as the oxide fuel. This is due primarily to the lower heavy metal loading of the $UZrH_{1.6}$ used in this work. The potential list of potential fuels includes $PuZrH_{1.6}$, PuH_2-ThH_2, UH_2-ThH_2, $UZrH_{1.6}$-ThH_2, and $PuZrH_{1.6}$-ThH_2. Based on the specific heat, density, and thermal conductivity of each fuel type the steady state, overpower, and particularly the LOFA conditions could yield different maximum achievable power values for each fuel type.

8.3 SPECIFIC TRANSIENT ANALYSIS

Specific and comprehensive transient analyses of any final core geometry must be performed. This should include a specific LOCA analyses using codes such as RELAP,

specific pump information for the higher pressure drop case, and a full core analyses for the wire wrapped hexagonal cores.

9 BIBLIOGRAPHY

This bibliography includes general references as well as those directly sited in the text.

9.1 REFERENCES CITED IN THE TEXT

[1] E. Geenspan, *"Use of Solid Hydride Fuel for Improved Long-Life LWR Core Designs,"* NERI Proposal In response to solicitation DE-PS03-02SF22467

[2] NERI02-189-TM4 (MIT-NFC-TR-062) J. A. Malen, N. E. Todreas and A. Romano, "Thermal Hydraulic Design of Hydride Fueled Pressurized Water Reactor Cores", MIT Department of Nuclear Engineering Internal Report, March 2004. 165 pages.

[3] South Texas Project Electric Generating Station Final Safety Analysis Report, Revision 12

[4] C. Shuffler, " Optimization of Hydride Fueled Pressurized Water Reactor Cores", MS Thesis, Nuclear Engineering, MIT, August 2004.

[5] I. Catton, et. al., "Quantifying Reactor Safety Margins Part 6: Physically Based Method of Estimating PWR Large Break Loss of Coolant Accident PCT", Nuclear Engineering and Design 119, pg 109-117 (1990)

[6] Feng.D, Hejzlar P., and Kazimi M.S., Thermal Hydraulic Design of High Power Density Fuel for Next Generation PWRs, The 10th International Topical Meeting on Nuclear Reactor Thermal Hydraulics (NURETH-10) Seoul, Korea, October 5-9, 2003.

[7] "Acceptance Criteria for Emergency Core Cooling Systems for Light Water Cooled Nuclear Power Reactors", 10CFR50.46 Appendix K of 10CFR50.

[8] S. K. Cheng, N. E. Todreas, "Hydrodynamic Models and Correlations for Wire-wrapped LMFBR Bundles and Subchannel Friction Factors and Mixing Parameters," Nuclear Engineering Design 92:227, 1985.

[9] W.K. In, D.S. Oh, and T.H. Chun, "Empirical and Computational Pressure Drop Correlations for Pressurized Water Reactor Fuel Spacer Grids", Nucl. Technol., Vol. 139, pg. 72 (2002)

[10] D.F. Washburn, J.W. Weber, "FFTF Driver Fuel Experience", Proc. ANS International Conf. on Reliable Fuels for Liquid Metal Reactors, September 7-11, 1986

[11] M. S. Kazimi, N. E. Todreas, "Nuclear Systems I, Thermal Hydraulic Fundamentals", Taylor & Francis, (1993).

[12] P.J. Levine, G.W. Schulze, T.P. Soffa, A. Boltax, " Grid-Spaced and Wire-Wrapped Fuel Assembly Tests in FFTF", Proc. ANS International Conf. on Reliable Fuels for Liquid Metal Reactors, September 7-11, 1986

[13] S. BLAIR, "Thermal Hydraulic Performance Analysis of a Small Integral PWR Core," Engineers Thesis , MIT, Department of Nuclear Engineering (Sept. 2003)

9.2 GENERAL REFERENCES

Schmidt, Henderson, Wolgemuth, "Introduction to Thermal Sciences: Thermodynamics, Fluid Dynamics, Heat Transfer, Second Edition", John Wiley & Sons, inc, NY, NY, 1993

M. S. Kazimi, N. E. Todreas, "Nuclear Systems II, Elements of Thermal Hydraulic Design", Taylor & Francis, (1993).

J.G.B. Saccheri, "A Tight Lattice Epithermal Core Design for the Integral PWR", Ph.D. Thesis, MIT, Department of Nuclear Engineering (Sept. 2003).

APPENDICES TABLE OF CONTENTS

LIST OF FIGURES

LIST OF TABLES

A NOMENCLATURE

A.1 GENERAL NOTATION

A: *Area*
C_d: *Grid Loss Coefficient*
c_p: *Specific Heat*
D: *Diameter*
f: *Friction Factor*
F_{axial}: *Axial Peaking Factor*
$F_{q'}$: *Pin Radial Peaking Factor*
g: *Gravitational Constant*
G: *Mass Flux*
h: *Heat Transfer Coefficient*
$\bar{h}$: *Average Heat Transfer Coefficient*
Δh: *Enthalpy Rise*
H: *Grid Height*
H/D: *Wire Lead to Rod Diameter Ratio*
H/HM: *Hydrogen to Heavy Metal Ratio*
k: *Thermal Conductivity*
K: *Total Form Loss Coefficient*
L_{act}: *Active Fuel Length*
L_{ass}: *Assembly Length*
L_t: *Developing Length*
m: *Mass*
$\dot{m}$: *Mass Flow Rate*
N: *Number of Rods*
p: *Pressure*
Δp: *Pressure Drop*
P: *Array Pitch*
Power
P/D: *Pitch to Diameter Ratio*
q': *Linear Heat Rate*
$\bar{q}'$: *Average Linear Heat Rate*
q'': *Heat Flux*
$\dot{q}$: *Specific Power*
Q: *Energy*
$\dot{Q}$: *Core Thermal Power*
t: *Thickness*
Time
T: *Temperature*
$\bar{T}$: *Average Temperature*
ΔT: *Change in Temperature*

U_R^n: *Reflood Rate*
v: *Velocity*
V: *Volume*
z: *Axial Position*
ε: *Plugging Factor*
ρ: *Density*

A.2 SUBSCRIPTS

BD: *Blowdown*
ci: *Cladding Inner*
clad: *Cladding*
co: *Cladding Outer*
cool: *Coolant*
Des: *DeStordeur Correlation*
DH: *Decay Heat*
f: *Grid Location*
fo: *Fuel Outer*
fuel: *Fuel Meat*
gap: *Fuel Gap*
grid: *Grid Spacer*
hex: *Hexagonal Array*
hyd: *Hydride Fuel*
i: *Initial*
Inetal.: *In et al. Correlation*
MCT: *Minimum Clad Temperature*
mv: *Mixing Vane*
OP: *Overpower*
ox: *Oxide Fuel*
PCT: *Peak Clad Temperature*
pin: *Single Pin*
r: *Refill*
ref: *Reference Core*
rod: *Fuel Rod*
Rh: *Rehme Correlation*
RP: *Rated Power*
s: *Grid Spacer Region*
Saturation Properties
Shutdown
SAL: *Safety Analysis Limit*
sq: *Square Array*
SS: *Steady State*
sub: *Subchannel*
surf: *Surface*
th: *Thermal*
v: *Average Bundle Value*

B FLOW COASTDOWN RATE

During analysis of the LOFA transient it was necessary to iterate between the flow coastdown rate determined from the RELAP code and the mass flow rate determined from the maximum achievable power from the VIPRE code. This is caused by the dependence of the flow coastdown rate on the initial mass flow rate.

It was expected that the flow coastdown rate, and thus the maximum achievable power would be dependant upon core geometry. In order to verify this and explain the observed dependence upon initial mass flow rate, we must look at the Bernoulli equation.

B.1 FLOW COASTDOWN RELATIONSHIP

The Bernoulli equation assumes the flow is incompressible, steady, there is negligible viscosity, no shaft work, and no heat transfer. For this analysis the assumptions that the flow is steady and has negligible viscosity are removed and the flow is considered unsteady and viscous. The initial Bernoulli equation adjusted to account for unsteady and viscous flow is given in equation (B.1).

$$0=\left(\frac{\ell}{A}\right)_T \frac{d\dot{m}}{dt}+p_{out}-p_{in}+\rho g(z_{out}-z_{in})+\frac{\dot{m}^2}{2\rho}\left(\frac{1}{A_{out}^2}-\frac{1}{A_{in}^2}\right)+f\frac{L}{D}\left(\rho\frac{v^2}{2}\right)+K\left(\rho\frac{v^2}{2}\right) \qquad \textbf{(B.1)}$$

Rearranging the equation to isolate the flow coastdown rate, $\frac{d\dot{m}}{dt}$, and converting the velocity term to mass flow rate yields equation (B.2).

$$\left(\frac{\ell}{A}\right)_T \frac{d\dot{m}}{dt}=\Delta p+\Delta p_{gravity}+\frac{\dot{m}^2}{2\rho}\left(\frac{1}{A_{iin}^2}-\frac{1}{A_{iout}^2}\right)-f\frac{L}{D}\left(\frac{\rho}{2}\frac{\dot{m}^2}{A^2\rho^2}\right)-K\left(\frac{\rho}{2}\frac{\dot{m}^2}{A^2\rho^2}\right) \qquad \textbf{(B.2)}$$

Further simplifications lead to equation (B.3).

$$\left(\frac{\ell}{A}\right)_T \frac{d\dot{m}}{dt}=\Delta p+\Delta p_{gravity}+\frac{\dot{m}^2}{2\rho}\left[\left(\frac{1}{A_{iin}^2}-\frac{1}{A_{iout}^2}\right)-f\frac{L}{D}\left(\frac{1}{A^2}\right)-K\left(\frac{1}{A^2}\right)\right] \qquad \textbf{(B.3)}$$

However, for a loop over the entire primary, z_{in} equals z_{out} and p_{in} equals p_{out}, thus $\Delta p_{gravity}$ and Δp are both equal to zero. The first term is also defined as follows.

$$\left(\frac{\ell}{A}\right)_T \equiv \sum_{n=1}^{N} \frac{\ell_n}{A_n} \tag{B.4}$$

As core geometry changes only A_{RX} changes and it is also larger than all the other core flow areas and thus $\left(\frac{\ell}{A}\right)_T$ is effectively constant.

The friction and form losses are summations over the primary loop as follows.

$$f\frac{L}{D}\left(\frac{1}{A^2}\right) \equiv \sum_i f\frac{L_i}{D_i}\left(\frac{1}{A_i^2}\right) \tag{B.5}$$

$$K\left(\frac{1}{A^2}\right) \equiv \sum_i K_i\left(\frac{1}{A_i^2}\right) \tag{B.6}$$

Replacing equations (B.4), (B.5), and (B.6) into equation (B.3) yields the final proportionality shown in equation (B.7).

$$\frac{d\dot{m}}{dt} \propto -\dot{m}^2\left[\sum_i\left(f\frac{L_i}{D_i \cdot A_i^2} + \frac{K_i}{A_i^2}\right)\right] \tag{B.7}$$

The terms A_i, L_i, D_i, and K_i are dependant upon geometry and f is dependant upon mass flowrate. Thus the flow coastdown rate, $\frac{d\dot{m}}{dt}$, is dependant upon both geometry and mass flow rate.

Looking at two cases with the same geometry and different initial mass flow rates, the flow coastdown rate is dependent only upon the respective flow rates.

$$\frac{dm}{dt} \propto -\dot{m}^2 \tag{B.8}$$

Therefore, since the initial mass flow rate of case two is higher than case one the flow coastdown rate of case two will be greater (more negative) than case one.

$$\dot{m}_1 < \dot{m}_2 \tag{B.9}$$

Figure B.1: Mass Flow Rate and Flow Coastdown Rate

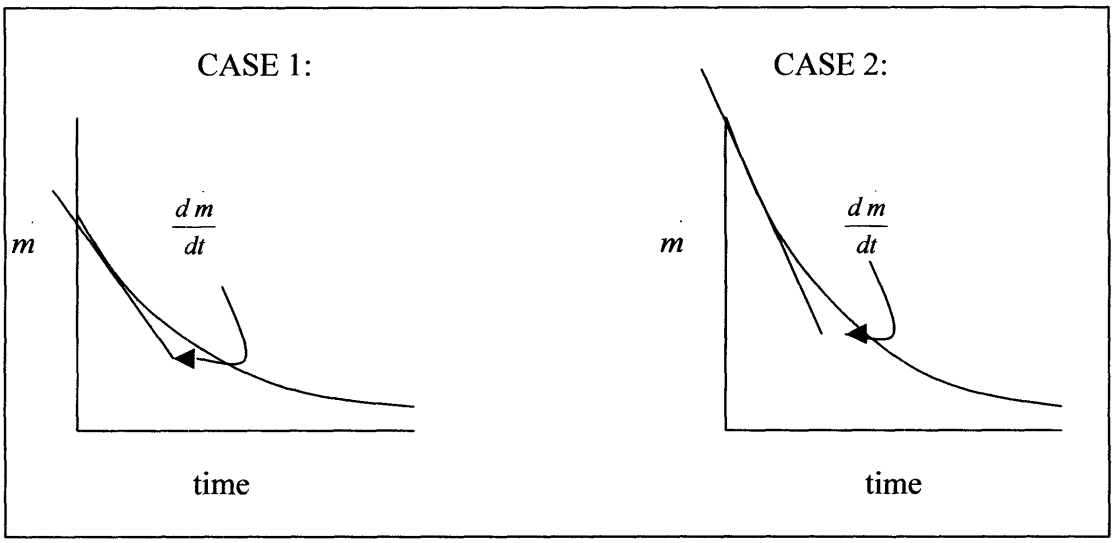

As is shown by figure B.1, the higher initial mass flow rate of the second case causes a higher initial flow coastdown rate for the second case. This, in turn, causes the mass flow rate in case two to drop faster.

C LOCA DERIVATIONS

C.1 STORED ENERGY REDISTRIBUTION

The average fuel temperature for a solid pellet is given by the following [11]:

$$\overline{T}_{fuel} = T_{fo} + \frac{q'}{8 \cdot \pi \cdot k_{fuel}} \tag{C.1}$$

However, the outer surface fuel temperature varies over the range of geometries. Due to the constant inlet coolant temperature and enthalpy rise, the coolant temperature is constant for all core geometries, and is known. Also, the difference between the coolant temperature and fuel outer temperature can be found.

$$\overline{T}_{fuel} = \frac{q'}{8 \cdot \pi \cdot k_{fuel}} + \left(T_{fo} - T_{cool}\right) + T_{cool} \tag{C.2}$$

$$\frac{q'}{\pi} = D_{rod} h_{cool} \left(T_{co} - T_{cool}\right) = D_{clad} \frac{k_{clad}}{t_{clad}} \left(T_{ci} - T_{co}\right) = D_{gap} h_{gap} \left(T_{fo} - T_{ci}\right) \tag{C.3}$$

where D_{clad} and D_{gap} are defined as the mean clad diameter and mean gap diameter. Solving for the difference between the fuel outer and coolant temperature yields:

$$T_{fo} - T_{cool} = \frac{q'}{\pi} \left[\frac{1}{D_{gap} \cdot h_{gap}} + \frac{t_{clad}}{D_{clad} \cdot k_{clad}} + \frac{1}{D_{rod} \cdot h_{cool}} \right] \tag{C.4}$$

Combining equations (C.4) and (C.2) yields the average fuel temperature (C.5).

$$\overline{T}_{fuel} = \frac{q'}{\pi} \left(\frac{1}{8 \cdot k_{fuel}} + \frac{1}{D_{gap} \cdot h_{gap}} + \frac{t_{clad}}{D_{clad} \cdot k_{clad}} + \frac{1}{D_{rod} \cdot h_{cool}} \right) + T_{cool} \tag{C.5}$$

C.2 BLOWDOWN COOLING

The decay heat power may be expressed in terms of a fraction of the constant steady state operating power prior to shutdown [11].

$$\frac{P}{P_o} = 0.066\left[t_s^{-0.2} - \left(t_s - \tau_s\right)^{-0.2}\right] \qquad \textbf{(C.6)}$$

where P, Po, ts, and τ_s are the power at time t, the steady state operating power, the time after shutdown (in seconds), and the operating time prior to shutdown (in seconds). Integrating the equation over time will yield the energy deposited. Equation (C.7) assumes the plant was operated at power, P_o, for at least one year prior to shutdown.

$$\int_o^t \frac{P}{P_o} dt_s = \int_o^t \left\{0.066\left[t_s^{-0.2} - \left(t_s - \infty\right)^{-0.2}\right]\right\} dt_s \qquad \textbf{(C.7)}$$

$$\int_o^t \frac{P}{P_o} dt_s = 0.0825 t^{0.8} \qquad \textbf{(C.8)}$$

$$Q = 0.0825 t^{0.8} \cdot P_o \qquad \textbf{(C.8)}$$

where t and Q are the time since shutdown and the energy deposited in that time. Converting the energy deposited in the fuel to the change in fuel temperature yields equation (C.10).

$$Q = m_{fuel} \cdot c_{p,fuel} \cdot \Delta T_{fuel} \qquad \textbf{(C.10)}$$

Solving for the change in fuel temperature and combining equations (C.9) and (C.10) yields the following:

$$\Delta T_{DH} = \frac{0.0825t^{0.8} \cdot P_o}{c_{p,fuel} \cdot m_{fuel}} \tag{C.11}$$

C.3 FINAL LOCA CLAD HEAT UP EQUATION

Combining equations (C.5) and (C.11) with the blowdown cooling equation [5], yields the complete clad heat up equation due to the LBLOCA.

$$T_{clad,final} - T_{clad,initial} = aq' - \left(T_{PCT,BD} - \overline{T_S}\right)\left(1 - \frac{1}{1.09 + 0.9 \cdot m \cdot \tau}\right) + \Delta T_{DH} \tag{C.12}$$

Which, in terms of the above equations, yields:

$$T_{clad,final} - T_{clad,initial} = \left\{\frac{q'}{\pi}\left(\frac{1}{8 \cdot k_{fuel}} + \frac{1}{D_{gap} \cdot h_{gap}} + \frac{t_{clad}}{D_{clad} \cdot k_{clad}} + \frac{1}{D_{rod} \cdot h_{cool}}\right) + T_{cool}\right\}$$
$$+\left(T_{PCT,BD} - \overline{T_S}\right)\left(1 - \frac{1}{1.09 + 0.9 \cdot m \cdot \tau}\right) + \frac{0.0825t^{0.8} \cdot P_o}{c_{p,fuel} \cdot m_{fuel}} \tag{C.13}$$

D GRID SPACER PRESSURE LOSS IN VIPRE

D.1 REHME VS DESTORDEUR

In order to provide the best pressure loss output from VIPRE it is desirable to determine which spacer pressure loss correlation, either Rehme or DeStordeur, is best suited for use in this study. The model used by VIPRE to solve for the pressure loss across a spacer is as follows (from VIPRE-01 manual pg. 2-188):

$$\Delta P = \frac{C_d * G_v^{\ 2}}{2 * \rho} \qquad \textbf{(D.1)}$$

In this equation mass flux (G_v) is a function of average bundle fluid velocity and the loss coefficient (C_d) is the input variable to VIPRE obtained from either the Rehme or DeStordeur correlation.

The Rehme correlation [1] is as follows:

$$\Delta P = \frac{C_v * \left(\frac{A_s}{A_v}\right)^2 * G_v^2}{2 * \rho} \qquad \textbf{(D.2)}$$

Where A_s is defined as the projected frontal area of the spacer; A_v is defined as the unrestricted flow area away from the grid or spacer; and C_v is defined as the modified drag coefficient. This yields the following for $C_{d,Rh}$, where the relative plugging ε is defined as the A_s/A_v:

$$C_{d,Rh} = C_v * \varepsilon^2 \qquad \textbf{(D.3)}$$

The Rehme equation is based on the average bundle, unrestricted area mass flux and the associated Reynolds number.

The DeStordeur correlation [1] for pressure loss is:

$$\Delta P_{Des} = \frac{C_s * \varepsilon * G_s^2}{2 * \rho} \quad \textbf{(D.4)}$$

The subscript s denotes that the DeStordeur equation is based on the mass flux in the spacer region, as opposed to the average bundle mass flux as in the Rehme equation and the VIPRE model. In order to modify the DeStordeur equation for use in the VIPRE model a ratio between the two mass fluxes must be used. Hence:

$$C_{d,Des} = C_s * \varepsilon * \left(\frac{G_s^2}{G_v^2}\right) \quad \textbf{(D.5)}$$

Therefore, to more easily compare the correlation C_d values, $C_{d,Des}$ must be transformed to convert the mass flux ratio to an area ratio. Thus for a constant flow rate where A_f is defined as the flow area at the grid or spacer location:

$$G_v * A_v = G_s * A_f \quad \textbf{(D.6)}$$

$$\left(\frac{G_s}{G_v}\right)^2 = \left(\frac{A_v}{A_f}\right)^2 \quad \textbf{(D.7)}$$

$$C_{d,Des} = C_s * \frac{(A_s * A_v)}{A_f^2} \quad \textbf{(D.8)}$$

Using the a standard PWR with input values and properties as shown in Table D.1 the Reynolds number is obtained both away from the spacer and locally at the spacer using

the respective mass flux and fluid viscosity. The area ratios and Reynolds numbers are derived as follow:

Table D.1 Standard PWR Core Values

INITIAL DATA	
Pitch **(in)**	0.4959
Diameter **(in)**	0.4629
Strap Thickness **(in)**	0.0197
H (Strap Height) **(in)**	1.5
D_h **(in)**	0.462
G_v **(kg/s-m^2)**	4086.5
G_s **(kg/s-m^2)**	4755.7
V_v **(m/s)**	6.647
V_s **(m/s)**	7.736
FLUID PROPERTIES	
Pressure **(bar)**	155.1
ρ_{avg} **(kg/m^3)**	614.8
μ_f **(N-s/m^2)**	9.274 E-5
L_t (developing length) **(m)**	6.81 E-4
DERIVED DATA	
A_s (projected frontal area of the spacer) **(in^2)**	0.0358
A_v (unrestricted flow area away from the grid or spacer) **(in^2)**	0.136
A_f (flow area locally at the grid or spacer) **(in^2)**	0.1002
A_{grid} (wetted area of the grid) **(in^2)**	3.00
A_{rod} (wetted area of the rod) **(in^2)**	1.85
ε (relative plugging)	0.263
ε^2	0.0692
ε_{mv}	0.13
$(A_s*A_v)/(A_f)^2$	0.484
f (Darcy friction factor)	1.32 E-2
Re_v	5.18 E5
Re_s	7.03 E5
Re_L	1.73 E6

The results for C_v and C_s determined from *Nuclear Systems I* figure 9-27 and 9-26, respectively [1], and the VIPRE input value C_d for both the Rheme and DeStordeur correlations from equations (D.3) and (D.8) are shown in table D.2.

Table D.2: Rehme vs DeStordeur

RESULTS	
C_v	6.5
C_s	1.65
(D.3) $C_{d,Rh} = C_v*(A_s/A_v)^2$	0.450
(D.8) $C_{d,Des} = C_s*(A_s*A_v)/(A_f)^2$	0.799

This suggests that the pressure loss for DeStordeur is slightly less than two times larger than for Rehme. Rehme stated that the effect of the relative plugging, ε, was more pronounced than in DeStordeur [1], and thus by observation the Rehme correlation should produce lower pressure losses than DeStordeur. This expected result did occur.

D.2 Literature Survey: "Empirical and Computational Pressure Drop Correlations for Pressurized Water Reactor Fuel Spacer Grids", W.K. In, D.S. Oh, and T.H. Chun

D.2.1 Grid Losses

Beyond the work of Rehme, there is a more recent empirical correlation by W.K. In, D.S. Oh, and T.H. Chun that includes not only the grid form loss, as in Rehme, but also the frictional losses of the grid and the rod as well as a coefficient for the loss due to two different types of mixing vanes. The base equation to solve for the VIPRE loss coefficient ($C_{d,In\ et\ al.}$) is as follows [2]:

$$C_{d,Inetal.} = \frac{C_{d,o} * \varepsilon}{(1-\varepsilon)^2} + \frac{C_{d,f,grid} * \left(\frac{A_{grid}}{A_v}\right)}{(1-\varepsilon)^2} + \frac{C_{d,f,rod} * \left(\frac{A_{rod}}{A_v}\right)}{(1-\varepsilon)^2} \qquad \textbf{(D.9)}$$

Where $C_{d,o}$ is defined as the form drag coefficient for the grid, $C_{d,f,grid}$ is defined as the frictional drag coefficient for the grid, $C_{d,f,rod}$ is defined as the frictional drag coefficient for the rod, A_{grid} is defined as the wetted area of the grid, and A_{rod} is defined as the wetted area of the rod.

In et. al solved for the drag coefficients using the following six equations [2]:

$$C_{d,o} = 2.75 - 0.27 * \log_{10}(\mathrm{Re}_v) \quad \textbf{(D.10)}$$

$$C_{d,f,grid} = C_{d,f,lam} * \frac{L_t}{H} + C_{d,f,turb} * \frac{H - L_t}{H} \quad \textbf{(D.11)}$$

$$C_{d,f,lam} = 1.328 * \mathrm{Re}_L^{-0.5} \quad \textbf{(D.12)}$$

$$C_{d,f,turb} = \frac{0.523}{\ln^2 0.06 * \mathrm{Re}_L} \quad \textbf{(D.13)}$$

$$C_{d,f,rod} * \left(\frac{A_{rod}}{A_v}\right) = f * \frac{H}{D_h} \quad \textbf{(D.14)}$$

$$f = 0.184 * \mathrm{Re}_v^{-0.2} \quad \textbf{(D.15)}$$

where L_t is defined as the developing length based on a Reynolds number of 30000, H is defined as the strap height, Re_L is defined as the Reynolds number based on the characteristic length of H-Lt, and f is defined as the Darcy friction factor solved for using the McAdams correlation.

Using the standard PWR values as used previously from table D.1 and applying these values to equations (D.9) through (D.14) yields the following results for the spacer pressure loss.

Table D.3: In et al. (Without Mixing Vanes)

RESULTS	
(D.10) $C_{d,o}$	1.21
(D.11) $C_{d,f,grid}$	3.92 E-3
(D.12) $C_{d,f,lam}$	1.01 E-3
(D.13) $C_{d,f,turb}$	3.92 E-3
(D.14) $C_{d,f,rod}$	4.51 E-2
(D.9) $C_{d,In\ et\ al.}$	0.827

D.2.2 MIXING VANE LOSSES

The VIPRE loss coefficient for mixing vanes ($C_{d,mv}$) from the In et al. paper is added directly to the base loss coefficient ($C_{d,In\ et\ al.}$). The value for the mixing vane coefficient is derived for as follows [2]:

$$C_{d,mv} = C_{plug,mv} * \frac{\varepsilon_{mv}}{(1-\varepsilon_{mv})^2} \qquad \textbf{(D.16)}$$

where $C_{plug,mv}$ is defined as the empirical drag coefficient and ε_{mv} is defined as the relative plugging of the mixing vane. In et al. showed that the drag coefficient is not dependant on Reynolds number but has a small variance of 0.6 to 0.8, with an assumed proper value of 0.72. Using split vanes with vane cutout the relative plugging has a value of 0.13 [2]. The value for the mixing vane loss coefficient and the total loss coefficient is as follows from table D.4.

Table D.4: In et al. (With Mixing Vanes)

RESULTS	
$C_{plug,mv}$	0.72
(D.16) $C_{d,mv}$	0.1237
(D.9) $C_{d,In\ et\ al.}$	0.827
$C_{d,total}$ **[(D.9) + (D.16)]**	0.950

D.3 COMPARATIVE RESULTS: REHME, DESTORDEUR, & IN ET AL.

The first look at pressure drop due to grid spacers made by Destrordeur was limited in scope, providing a final value for this example of $C_{d,Des} = 0.799$. However, Rehme has since provided a more accurate correlation that covered a broader scope. The Rehme paper found that the effect of the plugging ratio was more pronounced and thus lowered the total loss by nearly half, providing $C_{d,Rh} = 0.450$.

However, in 2002 W.K. In, D.S. Oh, and T.H. Chun did further research into the pressure losses due to grid spacers using previous empirical results and formulated a more comprehensive correlation. Unlike the previous two correlations, In et al. included not only the form loss due to the relative plugging of the grid, but also the friction losses from the grid and the rod. This gave a higher loss than either Rheme or DeStordeur, but also a more accurate result over a wider range of Reynolds numbers.

Furthermore, In et al. provided a correlation for the losses due to mixing vanes which neither Rehme nor DeStordeur provided. The results for In et al. are $C_{d,In\ et\ al.} = 0.827$ without the mixing vane and $C_{d,total} = 0.950$ with the mixing vane. The final results for the loss coefficient for use in VIPRE using the Rehme, DeStordeur, and In et al. correlations are shown in table D.5.

Table D.5: Comparative Results: Rehme, DeStordeur, & In et al.

RESULTS	
(D.3) $C_{d,Rh} = C_v*(A_s/A_v)^2$	0.450
(D.8) $C_{d,Des} = C_s*(A_s*A_v)/(A_f)^2$	0.799
$C_{d,total}$ **[(D.9) + (D.16)]**	0.950

E VIBRATIONS INFORMATION FOR WIRE WRAPPED ARRAYS

Table E.1 shows all vibrations data obtained with regards to wire wrapped cores. Additional information will be obtained in future work.

Table E.1: Wire Wrapped Vibrations Data

	Average Velocity / Flow Rate	Burnup	Residence Time	Wire Lead	Rod Diameter	Array Pitch	Number of Rods
FFTF Driver Fuel	6.7 m/s (7.6 m/s peak)	> 80 *MWd/kg*	825 *EFPD*	305 *mm*	5.842 *mm*	*	*
FFTF Fuel Assembly Tests [12]	1500 *l/min*	70-113 *MWd/kg*	*	*	*	*	*

***To be provided by Ron Baker: Ronald_B_Ron_Baker@rl.gov; 509-946-0123**

At flow rates similar to the limits imposed for this analysis but with a wider wire lead the FFTF driver fuel experienced no wear. No wear results wear results were specifically measured for the test assemblies, but they were noted to have performed satisfactorily for the given burnup condition.

F COMPUTER CODES

Throughout this work four specific computer programs were used. The first is Microsoft Excel. This program was used for simple data manipulation and storage and certain mathematical calculations, such as the wire wrap pressure drop and LOCA. VIPRE-01 was used for all other thermal-hydraulic calculations along with the MATLAB scripts created by Stuart Blair [13] and Jon Malen [2] to automate the VIPRE code and apply it to a large range of geometries. Lastly, RELAP5 Mod 3b was used to perform the initial LOFA calculations. Each of these computer codes along with example input and output decks is on a computer disc retained by the Nuclear Engineering Department at M.I.T.